Fall 2022

# Optimizing the Fluorescent Quantum Yield of Carbon Dots

Megan B. Prado
*Missouri State University*, Prado248@live.missouristate.edu

# OPTIMIZING THE FLUORESCENT QUANTUM YIELD OF CARBON DOTS

A Master's Thesis

Presented to

The Graduate College of

Missouri State University

In Partial Fulfillment

Of the Requirements for the Degree

Master of Science, Chemistry

By

Megan Bethany Prado

December 2022

**OPTIMIZING THE FLUORESCENT QUANTUM YIELD OF CARBON DOTS**

Chemistry

Missouri State University, December 2022

Master of Science

Megan Bethany Prado

## ABSTRACT

Carbon dots (CDs) are a subclass of carbon nanomaterials that exhibit unique properties of fluorescence, photostability, low toxicity, and biocompatibility. These unique properties have enabled numerous applications including biosensing, heavy-metal detection, and pH-sensing, among others. Their optical properties can be modified via doping to produce increasingly fluorescent CDs after appropriate purification. Herein, doped CDs were synthesized in four bottom-up methods for comparison using sucrose or citric acid as carbon precursors. Varying hetero-atom dopants (N, S, B) were used in differing molar ratios. The pH-dependent fluorescence and fluorescent quantum yield (QY) were measured for each sample. Characterization was conducted using Fourier-Transform Infrared Spectroscopy (FT-IR) for functional group identification, Scanning Electron Microscopy (SEM) and Transmission Electron Microscopy (TEM) for sizing, and Ultraviolet-visible Spectroscopy (UV-vis) and fluorescence spectroscopy for optical properties. The digestive microwave method was determined to be the best performing, with nitrogen as the hetero-atom dopant which produced the highest fluorescing CDs. All nitrogen-doped carbon dots (NCDs) demonstrated pH-dependent fluorescence with increased fluorescence from pH 7-13. Overall, citric acid-based nitrogen-doped carbon dots (NCD-ca) with a carbon-to-dopant molar ratio of 1:6 demonstrated the highest QY of 19% in pH 11. Therefore, NCDs, as prepared, may serve as cost-effective fluorescent pH sensors.

**KEYWORDS**: carbon dots, doping, nanoparticles, pH-sensing, fluorescence, nanomaterials, quantum yield

**OPTIMIZING THE FLUORESCENT QUANTUM YIELD OF CARBON DOTS**

By

Megan Bethany Prado

A Master's Thesis
Submitted to the Graduate College
Of Missouri State University
In Partial Fulfillment of the Requirements
For the Degree of Master of Science, Chemistry

December 2022

Approved:

Adam K. Wanekaya, Ph.D., Thesis Committee Chair

Keiichi Yoshimatsu, Ph.D., Committee Member

Gautam Bhattacharyya, Ph.D., Committee Member

Kartik Ghosh, Ph.D., Committee Member

Julie Masterson, Ph.D., Dean of the Graduate College

## ACKNOWLEDGEMENTS

I want to thank everyone who has supported me throughout my academic endeavors. I would not have made it this far without each of you. To my family and close friends: your love and support are immeasurable. I would like to thank my parents, Bobby and Robin Prado, my best friend, Ariel Prugger, and my twin sister, Becca Prado, for listening and offering comfort when needed. Most of all, I want to thank God for blessing me with endurance and flexibility to finish this thesis despite hurdles. His love endures forever.

I especially want to express my appreciation to Dr. Adam Wanekaya for welcoming me to his lab which has been my home these last five years. His wonderful tutelage and kindness have supported my growth as a chemist. Thank you. I would also like to thank my thesis committee members, Dr. Keiichi Yoshimatsu, Dr. Gautam Bhattacharyya, and Dr. Kartik Ghosh, for their support of this project. For aiding with SEM, thank you Dr. Ridwan Sakidja and Zia Mahmud. I am also appreciative of all the faculty and staff who have guided me over the years, especially Linda Allen, Dr. Gary Meints, Dr. Rich Biagioni, and Dr. Nikolay Gerasimchuk.

Additionally, I would like to thank my fellow students who have encouraged me, particularly Megan Westwood, Giselle Campos, and Colin Johnson, as well as fellow researchers Alli Trammell, Fantasia Critchfield, and Joe Truong. And to my American Chemical Society-Student Affiliates crew over the years, thank you! Finally, this thesis could not have been completed without support from the MSU Graduate College, the MSU Department of Chemistry and Biochemistry, and the Harthcock Chemistry Fellowship.

I dedicate this thesis to my parents: Bobby and Robin Prado.

## TABLE OF CONTENTS

## ABBREVIATIONS

**BCD-ca**: Boron-doped carbon dots, citric acid-based

**BCD-su**: Boron-doped carbon dots, sucrose-based

**Ca**: Citric acid

**CD**: Carbon dot

**CNDs**: Carbon nanodots

**EDS**: Energy dispersive X-ray spectroscopy

**FT-IR**: Fourier transform infrared spectroscopy

**GQD**: Graphene quantum dots

**HPPT**: 4-hydroxy-1H-pyrrolo[3,4-c]pyridine-1,3,6(2H,5H)-trione

**IPCA**: imidazo[1,2-a]pyridine-7-carboxylic acid

**MWCO**: Molecular weight cut-off

**NCD-ca**: Nitrogen-doped carbon dots, citric acid-based

**NCD-su**: Nitrogen-doped carbon dots, sucrose-based

**PDs**: Polymer dots

**QY**: Quantum yield

**SCD-sc**: Sulfur-doped carbon dots, sodium citrate-based

**SCD-su:** Sulfur-doped carbon dots, sucrose-based

**SEM**: Scanning electron microscopy

**TEM**: Transmission electron microscopy

**UV-vis**: Ultraviolet-visible spectroscopy

**XPS**: X-ray photoelectron spectroscopy

## LIST OF TABLES

## LIST OF FIGURES

# CHAPTER 1: INTRODUCTION

## 1.1 Introduction to Nanoparticles

Nanoparticles are nano-sized ($1x10^{-9}$ m) particles with at least one 1-100 nm sized dimension.[1] They exist in a variety of morphologies including sheets, cages, tubes, spheres, platelets, etc. depending on nanoparticle type.[1,2] Nanoparticles' small size gives them a substantial surface area to volume ratio and allows them to exhibit quantum effects.[1] This property significantly alters their physicochemical properties in contrast to bulk material counterparts.[2] Their possible reactivity is then greatly increased as many reactions take place on molecular surfaces. A grouping of nanoparticles, therefore, have immensely more reactive potential than a larger sized particle with the same combined volume. Consequently, nanoparticles have myriad potential applications in biomedicine, commercial goods, electronics, sensing, and energy storage, among others.[1]

Nanoparticles vary widely based on composition, morphology, physiochemical properties, and application. Broadly speaking, they can be classed as carbon-based (fullerenes, nanotubes, carbon dots, etc.), organic-based (micelles, liposomes, etc.), or inorganic-based (metal, metal oxide, etc.).[2] Nanoparticles' properties can be tuned for various specific applications through surface functionalization.[1] Therefore, diverse nanoparticle types exist, making their application of increasing interest for researchers globally.

## 1.2 Introduction to Carbon Dots

Carbon dots (CDs) are a sub-class of carbon nanoparticles with zero-dimensionality.[3] Known for their fluorescence, low-cost, biocompatibility, and tunable optical properties, CDs are attractive for numerous potential applications, including fluorescent pH sensing,[4,5] wearable

optoelectronics,[6] security labeling,[6] bioimaging,[7] biosensing,[7] and drug delivery.[8] Their fluorescence has made them the subject of increased interest in chemical sensing, particularly in lieu of traditional fluorescent dye probes.[9] CDs also lack disadvantages that other traditional fluorescent materials possess like low stability, high toxicity, or fast photobleaching, making CDs more desirable alternatives.[9]

Carbon dots were first discovered by accident in 2004 when Xu et al. synthesized soot-based single-walled carbon nanotubes, producing fluorescent byproducts.[10] These byproducts were later named "carbon dots" in 2006 by Sun et al.[11] Having an average size of less than 10 nm, these fluorescent nanoparticles were heralded for their "quantum-size."[11] It was not until later that two distinct synthetic categories emerged apart from the initial pathway utilized by Xu et al and Sun et al. They had created carbon dots in what is now known as a "top-down" synthesis route starting from pure carbon. Top-down synthesis of carbon dots (often aptly called graphene quantum dots) involves the transformation of graphitic material—namely graphite or graphene in structures like carbon nanotubes—into lateral nanostructures.[12] Several substantial methods prevailed including arc-discharge (initial discovery method), laser ablation, chemical exfoliation, and electrochemical oxidation.[9,13]

The other major synthetic route is a "bottom-up" synthesis because it carbonizes and polymerizes small organic precursors like citric acid upon heating to form carbon dots.[9] Bottom-up syntheses are far more popular in current research because of their facile synthesis and low-cost in comparison to top-down synthetic methods. Some major methods for bottom-up syntheses include pyrolysis, microwave-assisted pyrolysis, thermal decomposition methods, or the use of hydrothermal or oil-bath medias.[9] This project details four bottom-up synthetic methods which are discussed in detail in later sections.

The nomenclature for CDs varies widely between major synthetic routes as well as by chemical choice. Essner et. al. presented a list of inconsistencies in literature of carbon dots, where articles reported acronyms like FCDs (fluorescent carbon dots),[14] C-dots (carbon dots),[15] CQDs (carbon quantum dots),[16] GQD (graphene quantum dots),[13] etc. all used inter-changeably.[14] Because of the relatively recent discovery by Xu, et. al. in 2004, no set standard has been agreed upon.[10,14] Nomenclature specific to this project will be discussed in later sections.

**1.2.1 Doping**. The optical properties of carbon dots, namely their fluorescence, can be tuned through functionalization, surface passivation, or doping.[4,17] This project focuses on the effects of doping.

Altering the surface through surface passivation or functionalization often occurs by attaching chemical species to the surface by chemical reaction or through oxidation of the surface by acid.[17] Surface oxidation results in increased carboxylic (-COOH) and hydroxyl (-OH) surface functional groups.[17] Alternatively, passivation is performed to reduce the reactivity of nanoparticles by coating or altering the surface.[1] Both surface passivation and functionalization occur after the synthesis of CDs, leaving the core intact, whereas doping introduces dopants into the synthesis to alter the carbon core.

Doping is a powerful method to alter the optical properties of CDs. Ideally, heteroatom elements to carbon, such as nitrogen, boron, sulfur, and phosphorous, are utilized as dopant impurities because of their similar atomic sizes and number of electrons to carbon. It is considered p-type doping with B (3 electrons) and n-type doping with N and S (5 electrons). Doping into the carbon core with these elements produces changes in the CD's electronic structure, altering the surface structure for increased fluorescence.[4] Doping with nitrogen

additionally forms amine (-$NH_2$) functional groups on the surface which contribute to pH-dependent optical properties.

**1.2.2 Carbon Dot Structure**. Though the exact structure of carbon dots is not yet understood fully, recent efforts to elucidate CD composition and fluorescence have yielded important considerations. Namely, efforts to understand the nature of CD fluorescence have called into question whether researcher's reports of fluorescence are due to CDs themselves or largely due to groupings of oligomeric or monomeric fluorophore byproducts.[14] Therefore, careful consideration of synthesis parameters and proper purification are vital in CD formation.

There are three main types of carbon dots (see Figure 1): graphene quantum dots (GQDs), carbon nanodots (CNDs), and polymer dots (PDs).[18] GQDs are synthesized in top-down approaches, while CNDs and PDs are largely products of bottom-up syntheses. While the exact mechanism of CNDs and PDs syntheses are not yet well known, they are considered to form through polymerization and carbonization of carbon and dopant precursors, leading to a combination of products dependent on reaction time and temperature (see Figure 2).[19]

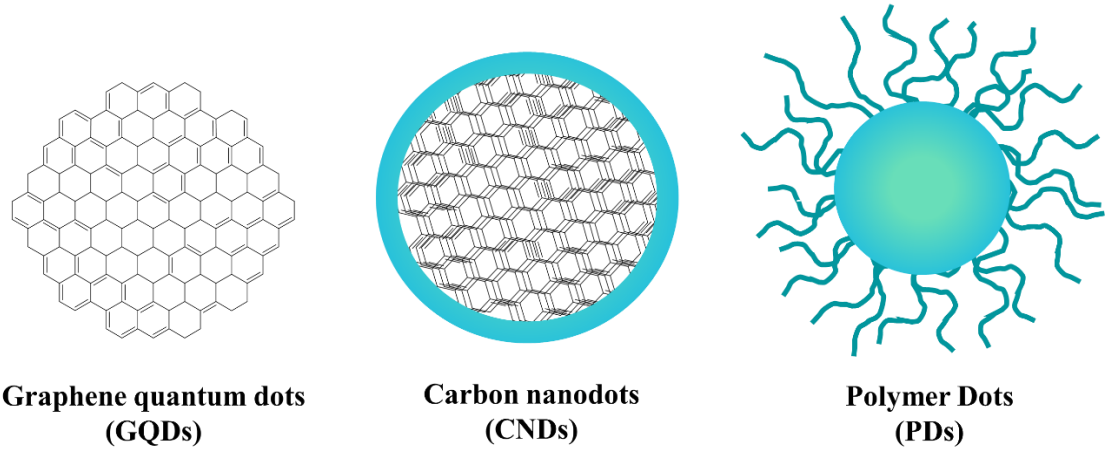


Figure 1. Three types of carbon dots**:** graphene quantum dots, left, carbon nanodots, middle, and polymer dots, right.

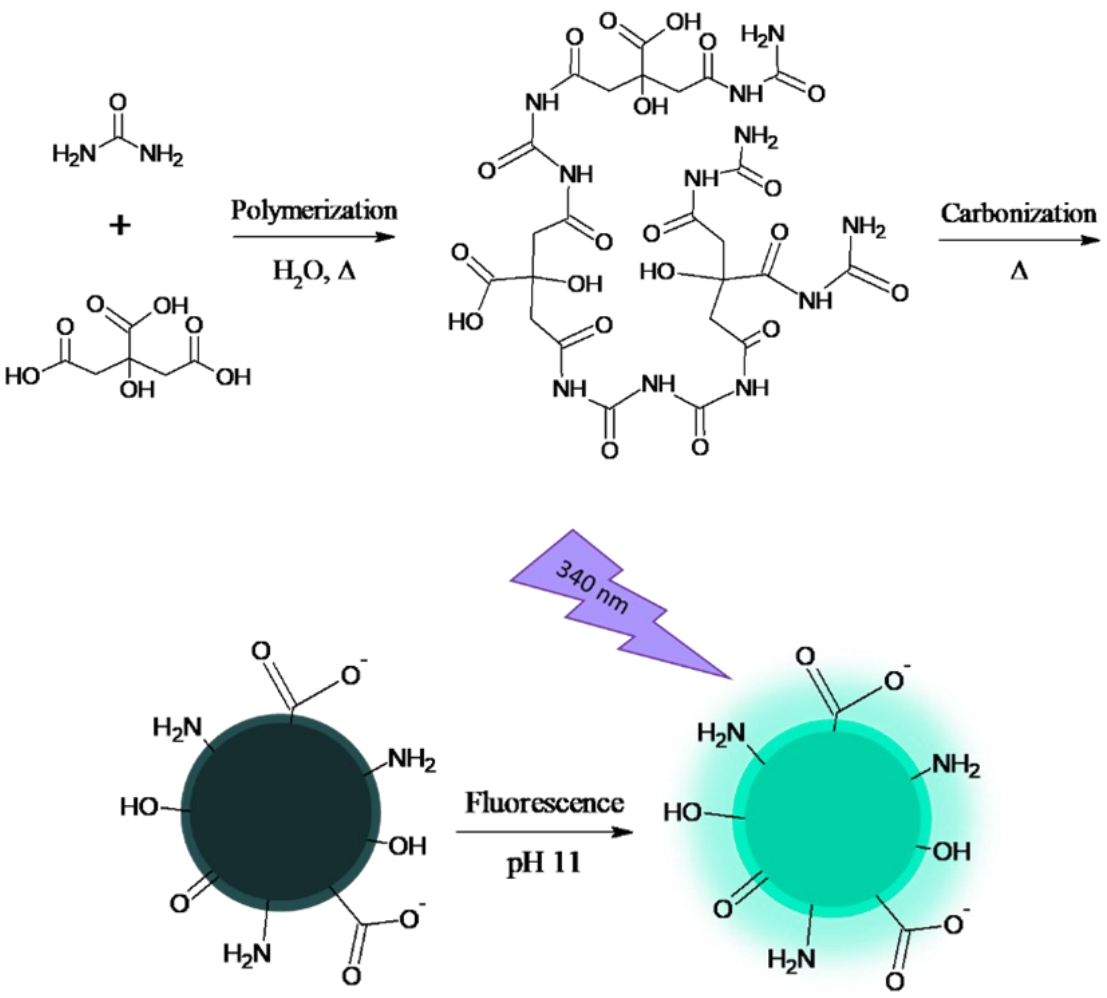


Figure 2. Proposed synthesis mechanism for NCD-ca showing precursors undergoing polymerization and carbonization in a hydrothermal pyrolysis to form carbon dots with pH-sensitive functional groups on their surface. The carbon dots fluoresce blue under 340 nm light.

The temperature of CD syntheses determines the degree of carbonization of products and CD composition. Song et al. found that for a hydrothermal synthesis using citric acid and ethylene diamine in an autoclave reactor for 10 hours, that increased temperatures from 200-300 °C, termed "carbon core state" produced a higher degree of carbonaceous products and carbon nanodots.[19] However, temperatures below 150 °C, termed "molecular state," produced a larger percentage of polymeric products including polymer dots and an isolated fluorophore, imidazo[1,2-a]pyridine-7-carboxylic acid (IPCA).[19] Additionally, reaction time influences the

CD composition. Longer reaction times, usually several hours, produces more CND-like composition, while shorter reaction times, usually minutes, produces more PD-like composition.[20] Lin et al. found that increased cooking time in a microwave led to larger CD sizes, where 5 minutes produced no visible CDs, but 10 minutes produced 3-4 nm sized CDs.[21] This trend is most likely due to the larger time allowed for carbonization and polymerization. In this study, reaction temperatures between 200-250 °C and times at 5-10 min or 3.5 hours were chosen.

**1.2.3 Purification**. Another important consideration in CD synthesis is proper purification. Due to the exponential growth of research into fluorescent CDs over the past 20 years, unification in nomenclature, synthetic method, and purification techniques has not yet occurred, leading to inconsistent results between researchers.[14] This is especially prevalent in reported QYs, where the integrity of results is dependent on properly isolating CDs from other fluorophore byproducts. Essner et al. showed that over half of reported procedures in CD literature up to 2018 had inadequate purifications, with 12% having no purification techniques at all and that filtering with a 0.2 μm filter alone was wholly inadequate to purify CD products.[14] They concluded that researchers should perform dialyses with a 5 kDa or higher molecular weight cut-off (MWCO) membrane with at least a 24-hour cycle and multiple replacements of exchange water in order to prevent contamination from fluorophore byproducts.[14] The MWCO is the lowest molecular weight in which more than 90% of solute with that weight are retained by the membrane.[22] Even then, they found that dialysis with a <50 kDa MWCO may be insufficient at separating CDs from small oligomeric or polymeric fluorophores, as both the retentate and dialysate fractions still produced thin organic films in TEM obscuring CDs.[14] In this study, pre-

filtering with a paper filter, followed by 0.2 μm filtration and dialysis with a 3.5 kDa membrane were performed. In future, a larger MWCO should be employed.

In order to prevent falsely attributing a high QY to CDs when other polymeric fluorophores are present, additional purification via column chromatography could be done. After dialysis with 3.5 kDa MWCO membrane, Song et al. found that a high QY fluorophore was present in both dialysate and retentate, prompting them to perform column chromatography to isolate the fluorophore species. They found that in addition to carbon core CDs, an IPCA fluorophore with quantum yield (QY) 85.84% was present, as well as oligomers of citric acid and ethylene diamine.[19] They theorized that some of the fluorescence of the isolated CDs could be attributed to the high QY of IPCA attached to the CD surface or within the carbon core.[19] Similarly, Strauss et al. reacted citric acid and urea in a non-hydrothermal microwave pyrolysis, forming three distinct fractions in column chromatography: a non-water soluble carbonaceous species, a 4-hydroxy-1H-pyrrolo[3,4-c]pyridine-1,3,6(2H,5H)-trione (HPPT) fluorophore fraction, and a fluorescent fraction contributed to conjugated oligomeric ureas.[23] However, their synthesis did not use any prior purification, therefore it is imperative for researchers to use dialysis in CD formation in addition to column chromatography for proper qualification of their results. Though column chromatography was not performed in this study, it would be an important future step to improve the synthetic method.

**1.2.4 Fluorescence and Quantum Yield**. The term "fluorophore" is used to describe compounds which exhibit fluorescence emission when excited by light.[24] Fluorescence is observed when a fluorophore first absorbs a photon of light becoming energetically exited, then relaxes to its ground state (see Figure 3).[24] This relaxation is prominently expressed as

fluorescence, though the emission is redshifted to longer wavelengths, as some energy is lost to heat or vibrational relaxation.

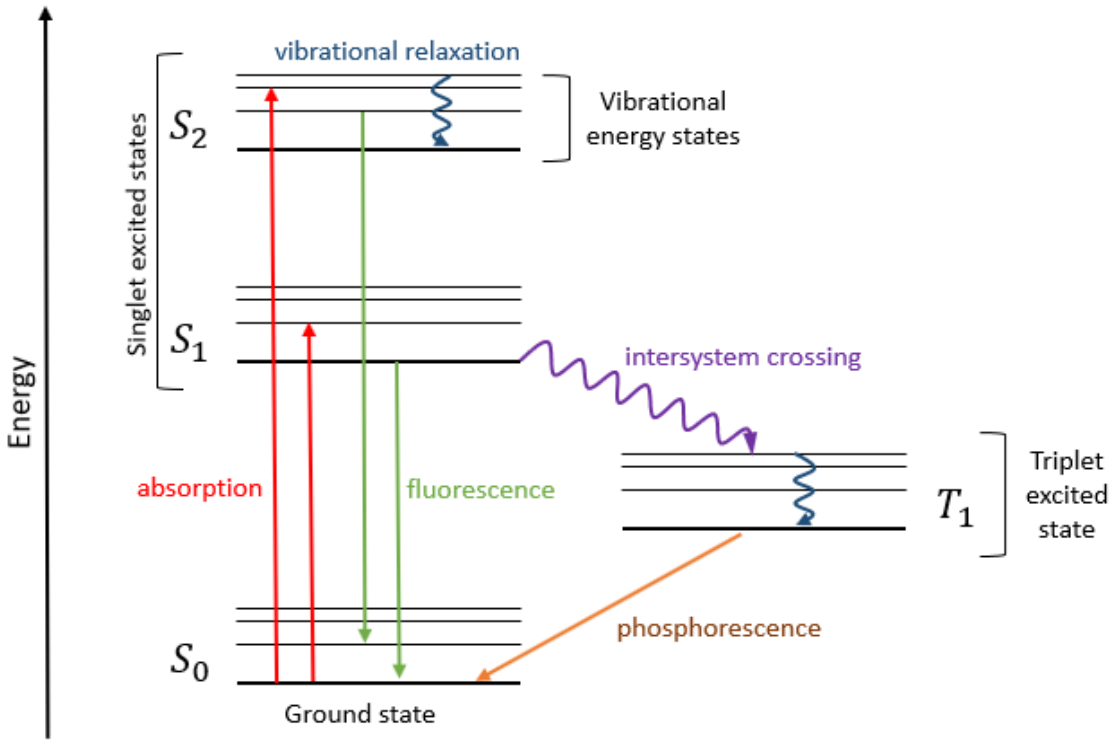


Figure 3. Jablonski energy diagram depicting transitions between electronic and vibrational energy levels for singlet ground state ($S_0$), first ($S_1$) and second ($S_2$) excited singlet states, and triplet excited state ($T_1$). Lines depict energy transitions: absorption (red), fluorescence (green), vibrational relaxation (blue), intersystem crossing (purple), and phosphorescence (orange).

Fluorophores are characterized by the extent of fluorescence, measured as a quantum yield (QY).[24] The QY offers a comparative value of fluorescence between fluorophores.[24] Calculated with Equation 1 shown below, the QY is based on the slopes derived from integrated fluorescence intensity vs. absorbance (*Grad*), the refractive indexes ($\eta$), and the standard's literature QY ($\Phi$); *X* and *ST* denote the sample and standard, respectively.[24]

Equation 1 $$\Phi_X = \Phi_{ST}\left(\frac{Grad_X}{Grad_{ST}}\right)\left(\frac{\eta^2{}_X}{\eta^2{}_{ST}}\right)$$

In order to choose a proper fluorescent standard, the emission ranges of the standard and sample should partially overlap.[24] Otherwise, the sample and standard will not be comparable once the fluorescence spectra are integrated within the sample range. For the prepared CD samples which emit between 300-500 nm, quinine sulfate (QY: 0.54, emission range: 400-600 nm) and 2-aminopyridine (QY: 0.60, emission range: 315-480 nm) were chosen.[24]

As is, the fluorescence mechanism for CDs is not well understood as their structure is relatively complicated and their fluorescence is pH dependent. To further complicate matters, researchers have no unified theory on the fluorescence mechanism as different precursors create CDs with quite varied pH-dependent fluorescence trends.[25] Therefore, each varied composition should be treated separately, as their mechanism could vary wildly.[25] It's a well-accepted theory that the deprotonation and protonation of surface functional groups alters the energy levels of CDs.[25] However, exactly what mechanism occurs is highly debated. In basic pHs, for example, increased fluorescence could be attributed to deprotonation of carboxyl groups which leads to a protective shell formed on the CD surface from delocalized π electrons.[4,25] This would theoretically help prevent energy loss due to non-radiative recombination, where the emitted fluorescence would otherwise be lowered due to energy loss to heat or vibrational relaxation.[4,25]

**1.2.5 Cytotoxicity and Biocompatibility**. Carbon dots prepared from bottom-up syntheses are derived from organic precursors which make them innately more biocompatible than other fluorescent species like cadmium sulfide quantum dots.[15] Many researches have even used more natural carbon sources available such as lemon juice[26]**,** bee pollen[27]**,** cellulose[28]**,** or plant leaves[29] in attempts to make the most biocompatible CDs. Though the drawback to some of these precursors are the lengthy syntheses they require and potentially low QYs. The biocompatibility of CDs is verified by cytotoxicity tests. Liu et al. tested their sucrose-based

nitrogen-doped CDs on HeLa cells, finding even when exposed to up to 1 mg $mL^{-1}$ NCD for 24 hours, cell viability was above 98.5%.[4] Wang et al. likewise concluded that their graphitic CDs did not pose any risk to mice populations even after multiple doses, suggesting potential application *in vivo* for bioimaging purposes.[8]

### 1.3 Synthetic Methods in Literature

Traditionally, CDs are produced through one of two major synthetic pathways which depend on the application of the synthesized CDs and the starting carbon material. As previously discussed in the introduction, top-down syntheses are the pathways transforming large graphitic material into lateral nano structures.[12] Bottom-up syntheses, practiced in this study, carbonize and polymerize small organic precursors upon heating to form CDs.[9] These bottom-up CDs are amorphous and not as ordered as CDs derived from graphitic material.

Methods to synthesize CDs in bottom-up ways vary greatly in literature. However, a facile approach is the one-step hydrothermal method, conducted using pressurized reactors, microwaves, or simple hot plates. Similarly, the oil-bath method employed by Liu et. al. utilizes a one-pot method, replacing water with reusable oil during synthesis, followed by separation with water and filtration.[1]

For carbon precursors, CDs can be prepared from almost limitless sources including orange juice[30], sucrose[4], bee pollen[27], glycerol[31], citric acid[32], ascorbic acid[33], etc. Although increased fluorescence is noted in sources with higher carboxyl group quantities, sucrose and citric acid are often used because of their low-cost as carbon precursors despite lower QY.[34] Other quantum dots using different base structures, like cadmium sulfide, can achieve QYs up to

69%.[35] However, such heavy metal-based nanoparticles lack the biocompatible properties that CDs have which allow for safer and more widespread applications.[4]

For CD dopant choice, small molecules containing heteroatom dopants are preferred. For N, popular choices include urea[36], ethylene diamine[19], ethanolamine[37], etc. For B as a dopant, boracic acid[38], boric acid[33,39], and sodium tetraborate[40], among others are present in literature. Additionally, for S as a dopant, thiocarbamide[38] or sodium thiosulfate[41] are present in literature.

### 1.4 Current Applications in Literature

CDs' unique properties of photostability, biocompatibility, tunable fluorescence, non-toxicity, etc., allow for diverse applications in literature. Increasingly, CDs have biomedical application as bioimaging agents. Yue et al. used red-emissive carbon dots containing ruthenium to bioimage zebra fish.[42] Likewise, the potential of nitrogen-doped carbon dots (NCDs) as bioimaging agents was demonstrated from Khan et al. in 2018 with their NCDs exhibiting green emission in HeLa cell membranes.[43] CDs have further applicability as chemical sensors, such as in the detection of metal ions where sensing is based on fluorescence quenching. Song et al. had success in using NCDs to detect $Fe^{3+}$ in living cells.[44] Due to the pH-dependent fluorescence of some CDs, they can also serve as pH sensors like Liu et al. achieved with their NCDs in distinct environmental water samples.[4] Additionally, CDs' optical properties provide unique widespread application in wearable optoelectronics[6], security labeling,[6] and even data encrypction[45,46].

### 1.5 Research Objective

The primary objective of this work is to optimize the QY of CDs in order to further their applicability. In doing so, synthesis methods, precursor sources (both carbon and dopant

sources), precursor carbon to dopant molar ratios, and pH media were altered, culminating in the calculation of the fluorescent QY. Particular focus was placed on pH-dependent fluorescence, as the prepared CDs have potential application as pH sensors.

# CHAPTER 2: METHODS

## 2.1 Materials and Instrumentation

Many chemicals and materials were used in the process of synthesizing, purifying, and characterizing the doped CDs. Further detail on specific applications will be provided in later sections. As is, all chemicals were used without further purification. Citric acid monohydrate was purchased from Flinn Scientific (Batavia, IL). Urea was purchased from Alfa Aesar (Haverhill, MA). D-(+)-Sucrose and quinine sulfate dihydrate were purchased from Acros Organics. Potassium phosphate monobasic, potassium chloride, and hydrochloric acid were purchased from Fisher Scientific. Sodium hydroxide was purchased from VWR International (Radnor, PA). Sodium tetraborate decahydrate, boric acid, sodium thiosulfate, 2-aminopyridine, and Corning® syringe filters (0.2 um) were purchased from Sigma Aldrich (St. Louis, MO). Sodium citrate was purchased from Spectrum Chemical (New Brunswick, NJ). Peanut oil was purchased at a local supermarket. Gold-coated silicon wafers were purchased from Ted Pella (Redding, CA). SnakeSkin™ dialysis tubing (3.5 kDa MWCO) was purchased from Thermo Scientific. All solutions were made using doubly deionized water, DDI (18.2 ohm resistivity), sourced from an in-house deionization system.

Ultraviolet-visible spectroscopy (UV-vis) was performed using an Agilent Technologies Cary 60 UV-vis spectrometer (Cary WinUV v. 5.10.1016). Fluorescence spectroscopy was conducted using a Horiba QM-8075-21-C spectrofluorometer (Felix GX v.4). Fourier transform infrared spectroscopy (FT-IR) was performed using a Bruker Alpha II fourier transform infrared spectrometer (OPUS v. 8.5(SP1)). Scanning Electron Microscopy (SEM) was conducted using a FEI Quanta 200 scanning electron microscope and a ThermoFisher Scientific Quattro S

Environmental scanning electron microscope. Transmission electron microscopy (TEM) was conducted using a JEOL 2100F scanning transmission electron microscope.

## 2.2 Synthetic Methods

Over the course of this project, various synthesis methods and purification techniques were adapted to optimize conditions for future syntheses. Many different samples were made and denoted with acronyms for dopant and carbon source compositions. All naming of CDs in this project will follow an XCD-xx format, where the first 'X' denotes the dopant source and the 'xx' after the hyphen denote the carbon source. CDs were synthesized from citric acid (ca), sodium citrate (sc), or sucrose (su) as the source of carbon. Dopant sources were either nitrogen (N), boron (B), or sulfur (S) based. The N dopant was urea, B dopants were either sodium tetraborate or boric acid, and the S dopant was sodium thiosulfate. All precursor choices were determined based on availability, literature presence, and cost.

The first major goal of this project was to determine the best synthesis method for CD formation. Of the bottom-up synthesis options presented in literature and available equipment, four methods were tested, as shown in Figure 4: oil-bath, reactor, microwave oven, and digestive microwave. Two microwave methods were utilized since microwave-assisted pyrolysis is increasingly cited for its low-cost and ease of use.[47] Microwave-assisted pyrolysis refers to the thermal decomposition of compounds at elevated temperatures due to microwave radiation.[47]

**2.2.1 Oil-Bath Synthesis**. In an anhydrous procedure proposed by Liu et al., 20 mL peanut oil in a 100 mL beaker is preheated to 250 °C on a hot plate under mechanical stirring (see Figure 5). For a synthesis of NCDs-su in a 1:1 ratio of carbon to dopant source, 30 mmol sucrose (~10 g) and 30 mmol urea (~2 g) are added to the oil. After 5 min, the resulting solution

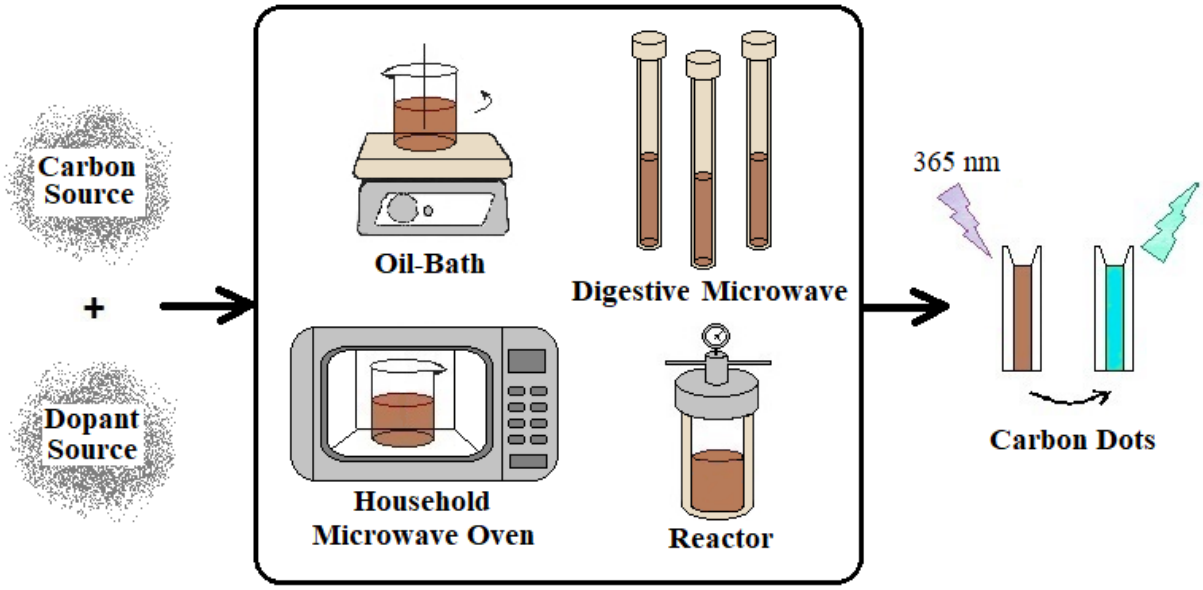


Figure 4. Schematic of doped carbon dots synthesis by multiple methods. Doped carbon dot syntheses were performed in an oil-bath, microwave, or reactor. The carbon dots then fluorescence under ultraviolet light.

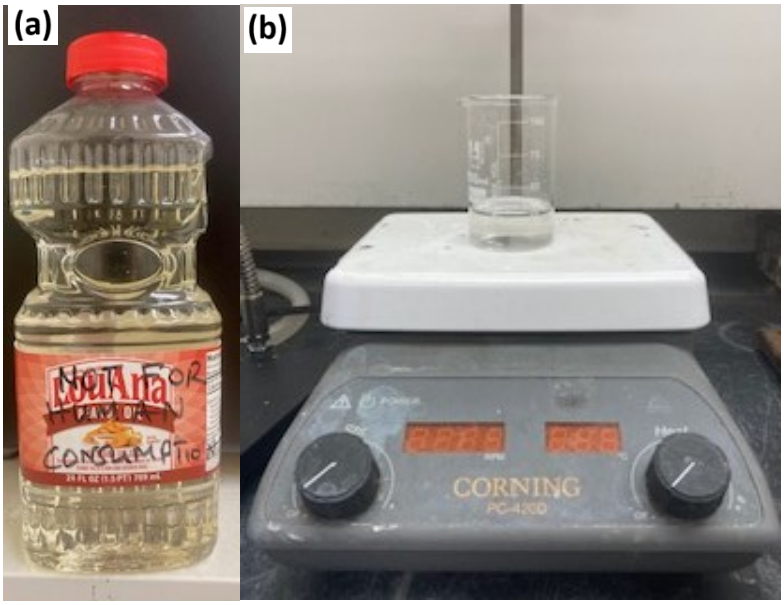


Figure 5. Oil-bath synthesis set-up. (a) Edible oil used as synthesis media, (b) typical hot-plate set-up for oil bath synthesis under mechanical stirring.

is cooled and 30 ml of water is added, stirred, and left to separate. The resulting carbon dots are very hydrophilic and are easily extracted in the aqueous layer. The oil level can then theoretically be cleaned and re-used.

**2.2.2 Autoclave Reactor Synthesis**. A Berghoff high pressure reactor with a Teflon coated inner steel autoclave was used for the reactor method of CD synthesis. For NCD-su (1:1), 30 mmol sucrose (~10 g) and 30 mmol urea (~2 g) were dissolved in 30 ml DDI water and poured into the Teflon tube. The reactor was then set to run for 3.5 hours at 200 °C under high pressure conditions. Figure 6 shows the Berghoff high pressure reactor used in this experiment.

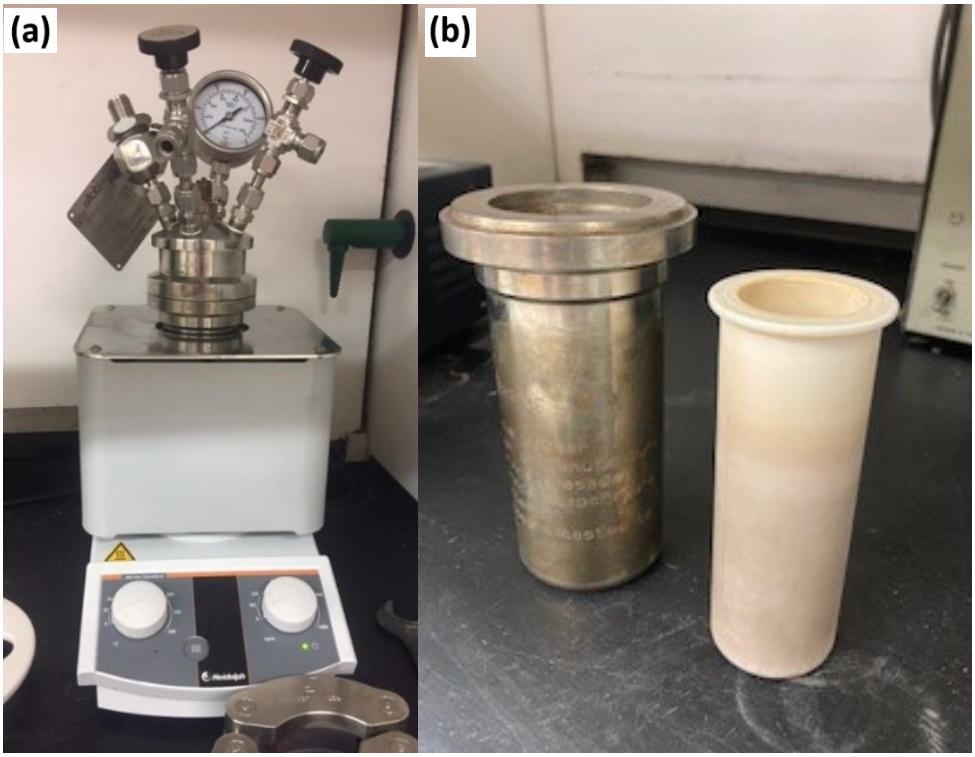


Figure 6. Berghoff autoclave. High pressure, high temperature reactor with Teflon-lined stainless-steel autoclave. (a) Berghoff reactor outside view, (b) inner steel chamber casing, left, inner Teflon chamber, right.

**2.2.3 Microwave Oven Synthesis**. Microwave-assisted pyrolysis as a method of CD synthesis was conducted using a Panasonic Inverter microwave oven (see Figure 7) with an inner glass turntable to facilitate even heating. For NCD-su (1:1), 30 mmol sucrose (~10 g) and 30 mmol urea (~2 g) were dissolved in 30 ml DDI water and placed in a 250 mL beaker. The microwave power was set to level 6 (750 W) for 5 min.

Figure 7. Panasonic Inverter microwave oven.

**2.2.4 Digestive Microwave Synthesis**. An additional microwave method was attempted using the CEM Mars 6 Digestive Microwave (see Figure 8) since it is capable of running up to 40 reactions at once. The Mars 6 Digestive Microwave has a central rotating cylinder rack which holds the Teflon vessels. For NCD-su (1:1), 30 mmol sucrose (~10 g) and 30 mmol urea (~2 g) were dissolved in 30 ml DDI water and transferred into respective Teflon tubes for sealing. Additional vials were filled with 30 mL DDI to counterweight the turntable. The samples were then microwaved for 10 minutes at 200 °C following an “organic plant material” preset. The method included a ramp time of 20-25 min to reach the chosen temperature, with a hold time of

10 min, followed by a cool-down period. The samples were fully cooled before opening the pressurized chambers.

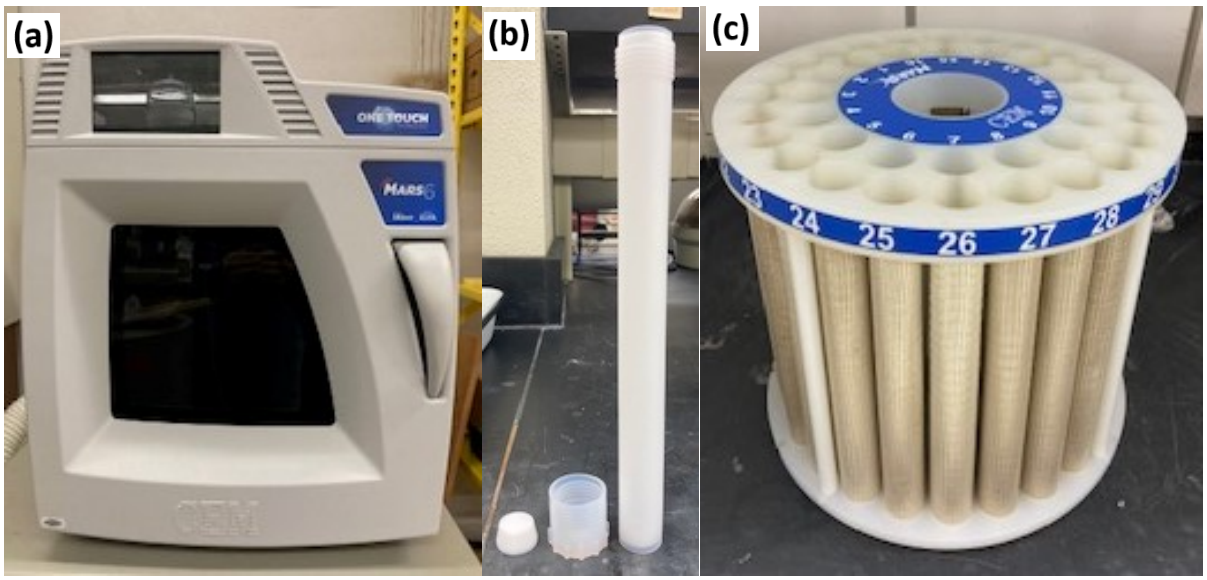


Figure 8. CEM Mars 6 Digestive Microwave. (a) Mars 6 Digestive Microwave outside view, (b) disassembled Teflon reactor tube, (c) internal turntable tube holder.

Later samples were synthesized in this same method. Table 1 shows the summary of samples prepared including their molar ratios and respective precursor amounts.

**2.2.5 Filtration and Dialysis**. Each method's resulting solutions were filtered with qualitative filtration paper to remove insoluble carbonaceous material, followed by syringe filtration with a Corning® 0.20 µm syringe filter to remove particles larger than 200 nm. Centrifugation at 3,000 rpm was attempted, but no obvious solid was present in the retentate.

For purification, dialysis with a 3.5 kDa MWCO snakeskin membrane was performed on each sample for three consecutive 24-hour periods, replacing the exchange liquid after each 24-hour cycle. The dialysate was kept for further optical testing. Figure 9 depicts a typical dialysis

set-up where the CD sample is placed in a snap cap vial with a membrane secured across a hole in the cap. The vial is inverted into a 500 mL beaker filled with about 550 mL DDI.

Table 1. Digestive microwave CD sample compositions

| Sample name | Carbon source | Amount of carbon source in mmol (g) | Dopant source | Amount of dopant source in mmol (g) |
|---|---|---|---|---|
| NCD-su (1:1) | Sucrose | 29.24 (10.01) | Urea | 33.35 (2.00) |
| NCD-ca (2:1) | Citric acid | 58.83 (11.30) | Urea | 33.37 (2.00) |
| BCD-su (2:1) | Sucrose | 14.83 (5.08) | Sodium tetraborate | 8.33 (3.18) |
| BCD-ca (1:1) | Citric acid | 32.95 (6.33) | Boric acid | 32.30 (2.00) |
| SCD-su (1:1) | Sucrose | 29.28 (10.02) | Sodium thiosulfate | 33.30 (5.26) |
| SCD-sc (1:1) | Sodium citrate | 32.89 (8.49) | Sodium thiosulfate | 32.88 (5.20) |
| NCD-ca (6:1) | Citric acid | 52.43 (10.07) | Urea | 8.69 (0.52) |
| NCD-ca (1:1) | Citric acid | 34.27 (6.58) | Urea | 33.91 (2.04) |
| NCD-ca (1:3) | Citric acid | 15.00 (2.88) | Urea | 45.00 (2.70) |
| NCD-ca (1:6) | Citric acid | 8.66 (1.66) | Urea | 50.59 (3.04) |
| NCD-ca (1:10) | Citric acid | 5.45 (1.05) | Urea | 54.55 (3.28) |

**2.2.6 Lyophilization**. To produce solutions with known concentrations, CD samples were lyophilized. Lyophilization is the practice of removing solvents from a solute via sublimation. Liquid samples are frozen via liquid nitrogen or freezer and are loaded onto the freeze-dryer under vacuum. This allows the frozen DDI to be evaporated directly via sublimation, leaving only the solid CDs behind. CD samples were transferred into plastic test tubes, covered with a secured Kimwipe, and frozen at -80 °C. Once frozen, the CD samples were

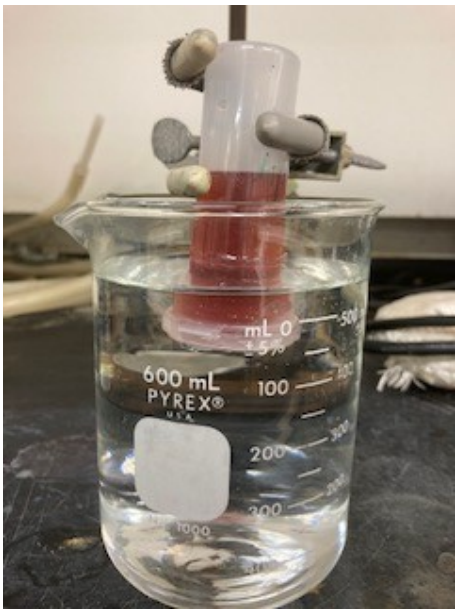


Figure 9. Dialysis set-up. Tube containing NCD-ca (6:1) with dialysis membrane adhered to a hole in the cap is suspended upside down in exchange water. As pictured, the dialysis is at the beginning of the first 24-hour cycle.

loaded onto the Flexi-Dry™ Microprocessor Control Corrosion Resistant Freeze-Dryer (see Figure 10) for lyophilization over a three-day period with a vacuum at less than 70 mTorr. The resulting solids were transferred to vials and stored in room temperature.

## 2.3 Characterization

The prepared CDs were characterized with Ultraviolet-visible Spectroscopy (UV-vis) and fluorescence spectroscopy for optical properties, fourier-transform infrared spectroscopy (FT-IR) for functional group identification, scanning electron microscopy (SEM) and transmission electron microscopy (TEM) for sizing, and energy-dispersive X-ray spectroscopy (EDS) for elemental composition.

**2.3.1 Optical Characterization**. The optical properties of the CDs were measured using UV-vis and fluorescence spectroscopy. UV-vis is a spectroscopic technique determine the

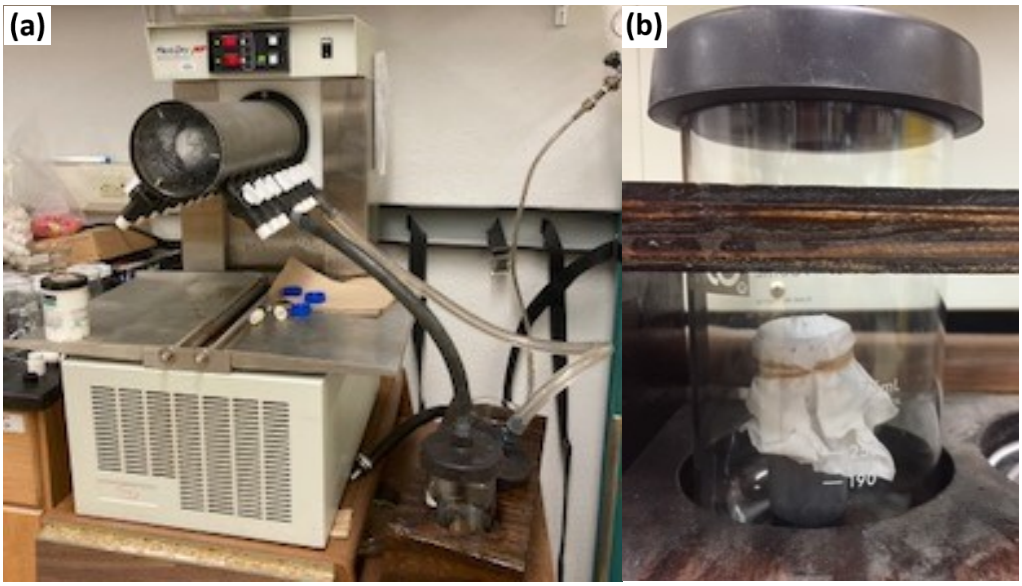


Figure 10. Freeze-dryer for lyophilization of CDs. (a) Flexi-Dry™ Microprocessor Control Corrosion Resistant Freeze-Dryer, (b) NCD-ca (1:1) loaded into sealed beaker in sample rack.

molecular absorbance profile of a species in the ultra-violet and visible range. The maximum absorbance wavelength is often chosen for the excitation wavelength in fluorescence spectroscopy. Fluorescence spectroscopy, then, measures the emission of light from a sample upon excitation by an incident photon, yielding an emission spectrum. Additionally, the integration of emission spectra can be used in calculating the fluorescent QY. All optical measurements were conducted using a 10 mm quartz crystal UV-vis and fluorescence cuvettes. For fluorescence, the maximum absorbance wavelength from the absorbance spectra were chosen for the excitation wavelength. All emission and excitation slit widths were set to 5 nm.

Because of the nature of the functional groups on the CD surface, doped CDs exhibit fluorescence dependence on pH. In this study, the pH-dependent fluorescence from pH 1-13 (pH 6 and 8 omitted) were measured for the following microwave digestor samples: BCD-su (2:1), NCD-ca (2:1), NCD-su (1:1), and NCD-ca (6:1) through (1:10). Again, the samples are denoted with the carbon to dopant molar ratios in parentheses. All pH solutions were buffered.

### 2.3.2 Scanning Electron Microscopy and Energy Dispersive X-Ray Spectroscopy.

SEM is a nondestructive method which uses an electron beam to scan the surface of a sample to yield sizing and morphology information. EDS is an add-on to the instrument, allowing for qualitative and limited quantitative information about elemental composition.

Since the CD samples are hygroscopic, all samples were redissolved and lyophilized prior to stub preparation to ensure dryness of the particles. Prior sample preparation by drop-casting CD samples in water led to aggregated rings and poor imageability. Therefore, a few milligrams of solid samples were placed in a 1 mL aliquot of ethanol and sonicated to disperse the particles. Gold-coated silicon wafers were rinsed with isopropanol and dried via nitrogen stream until clean. Copper tape was used to mount the wafers onto pre-cleaned aluminum stubs. Then, 5 μL aliquots of the samples were drop-casted onto the wafers and dried in an oven at 85 °C. Drops were repeated until sufficient sample was dispersed on the surface. All stubs were mounted in a makeshift desiccator streamed with nitrogen and sealed for transport to the SEM to prevent water intake. An example of samples drop cast onto gold-coated silicon wafers on aluminum stubs is shown in Figure 11.

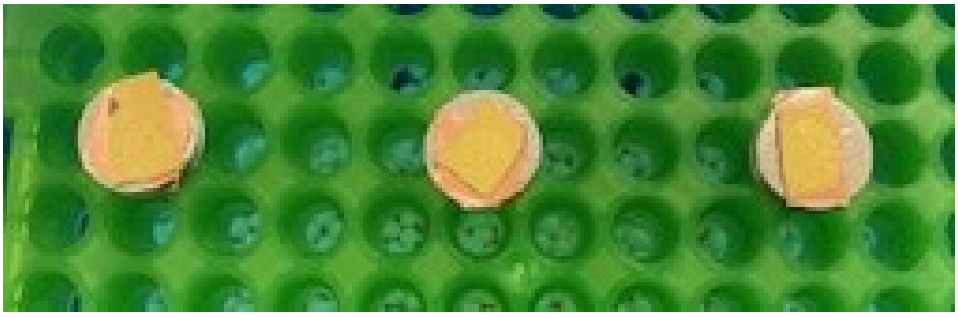

Figure 11. CD samples for SEM-EDS analysis. CD samples are dropcast onto gold-coated silicon wafers attached to aluminum stubs with copper tape.

**2.3.3 Infrared Spectroscopy**. Fourier-transform infrared spectroscopy (FT-IR) was used to confirm the presence of functional groups through the vibrational stretches and bends associated with C=O, C=C, O-H, N-H, C-N, etc. vibrations. Solid samples were directly loaded onto an Alpha II FT-IR spectrometer.

**2.3.4 Quantum Yield**. A cross-calibration of fluorescent standards was performed prior to the sample QYs, using quinine sulfate and 2-aminopyridine in 0.1 M $H_2SO_4$. Both of those standards were chosen based on their overlapping emission with the CD samples. The QY of the doped CDs were determined using 2-aminopyridine for NCD-su and BCD-su, while quinine sulfate was used for all NCD-ca samples. The other samples were not fluorescent enough to warrant calculating the QY.

All CD samples were prepared in buffered pH solutions at varying concentrations corresponding to absorbances around 0.00 (blank), 0.02, 0.04, 0.06, 0.08, 0.10. It is important to only use sample concentrations that are at or below the 0.1 absorbance value at or above the excitation wavelength to avoid inner filter effects that alter an accurate QY measurement.[24] The same UV-vis 10 mm quarts cuvette was used for all UV-vis measurements, as was the same fluorescence 10 mm quarts cuvette for all fluorescence measurements. For each UV-vis measurement, the absorbance at the excitation wavelength was recorded, with no background correction. For fluorescence, each measurement utilized 2 nm slit widths for all emission and excitation slits. The same excitation wavelength was kept for each respective sample and blanks. No background correction was utilized. Each spectrum was integrated in the same respective region. All data was corrected in analysis to account for blanks, and the integrated fluorescence of the standards and samples were plotted against the absorbances for each, producing gradient values for use in equation 1 in calculating the QY.

# CHAPTER 3: RESULTS AND DISCUSSION

## 3.1 Evaluation of Synthetic Method

**3.1.1 Oil-bath Method**. The oil-bath method using sucrose as the carbon source caused an immediate buildup of carbonaceous material within the oil that clung to the beaker sides and stirring rod. Stirring was made near impossible. Even after the addition of water after cooling the mixture and the extraction of the soluble carbon dots into the aqueous phase, the leftover oil was filled with insoluble carbonized material that was difficult to filter out (see Figure 12). Though Liu et al. marketed their method as a "green" synthesis, the oil had limited reuse as the filtration process required numerous paper filtrations to fully filter off the insoluble carbonaceous product.[4] The paper filters kept getting clogged with carbonized material, requiring the use of several filters. Once the 0.22 μm syringe filter was used, excessive force was needed to expel the solution through the filter due to the remaining large particle sizes.

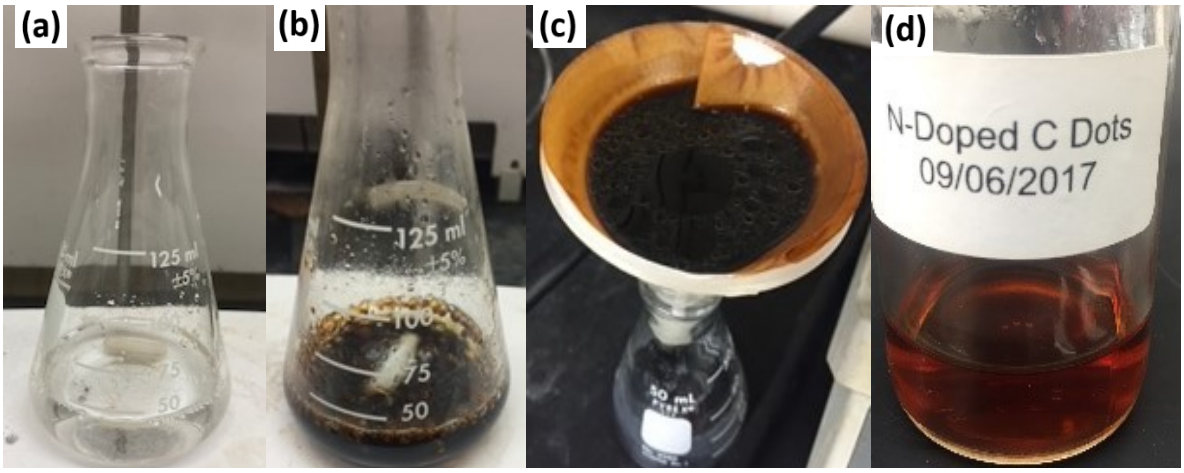


Figure 12. Oil-bath synthesis before and after results. (a) Oil-bath synthesis set-up prior to addition of solid precursors, (b) post-synthesis brown NCD-su (1:1), (c) depiction of filtration where the remaining oil is still present in aqueous layer, and (d) red NCD-su (1:1) stock.

**3.1.2 Reactor Method**. The reactor method required a much longer reaction time in comparison to the other methods, as the synthesis required multiple hours. Likewise, the larger Teflon reactor required significant cleaning post-synthesis due to the larger degree of non-soluble carbonization of sucrose. The resulting NCD-su (1:1) were brown in color, shown in Figure 13, and yellow upon dilution, just as with the oil-bath method.

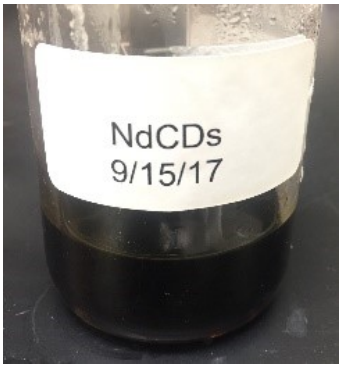


Figure 13. NCD-su (1:1) from reactor method.

**3.1.3 Microwave Oven**. The microwave oven method suffered the same degree of carbonization products as the reactor and oil-bath method, however, because no stirring was involved in the synthesis, the reaction was easier than either the reactor or oil-bath methods. Figure 14 shows the bulk NCD-su (1:1) synthesized via microwave oven. The CDs are brown and yellow on dilution.

**3.1.4 Microwave Digestor**. While the conventional microwave method seemed to be the best performing, it still lacked the ability to synthesize multiple samples at once in the same conditions. Therefore, a Mars 6 microwave digestor was utilized. This way, multiple samples could be synthesized at once in repeatable, standardized methods. Likewise, Teflon tubes allowed for easy clean-up in comparison to the previous convention microwave method.

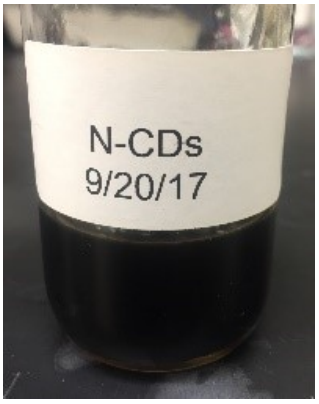


Figure 14. NCD-su (1:1) from microwave oven method.

The microwave method seemed to be the most hassle-free synthesis route, utilizing Teflon tubes as reaction chambers which could have several samples running at once. Therefore, the microwave method was determined to be the best method since multiple samples could be run at once using the microwave digestor under the same conditions. This way multiple carbon dot samples could be produced at once with different dopants, more quickly, and with less clean-up than the other two methods. The carbonization of sucrose was still a problem in the digestive microwave method (as can be seen by the overflow of carbonaceous material in the N-, B-, SCD-su Teflon tubes in Figure 15a), therefore an alternative carbon source, citric acid, was chosen for future syntheses. Figure 15b shows the Teflon tubes from N-, B-, SCD-ca, which did not result in any significant carbonaceous material as the sucrose-based CDs did. At this point, the dopant source was varied, as can be seen in Figure 15. However, that will be discussed in later sections.

Overall, Figure 16 shows a comparison of the methods in UV-vis and fluorescence spectroscopy. The maximum absorbance occurs at about 280 nm for all three methods, though the oil bath method was closer to 290 nm. The fluorescence results, however, indicate a greater similarity between the oil-bath method and reactor method than with the microwave method, as evidenced by their double peaks. The microwave has a solitary peak around 400 nm, though its

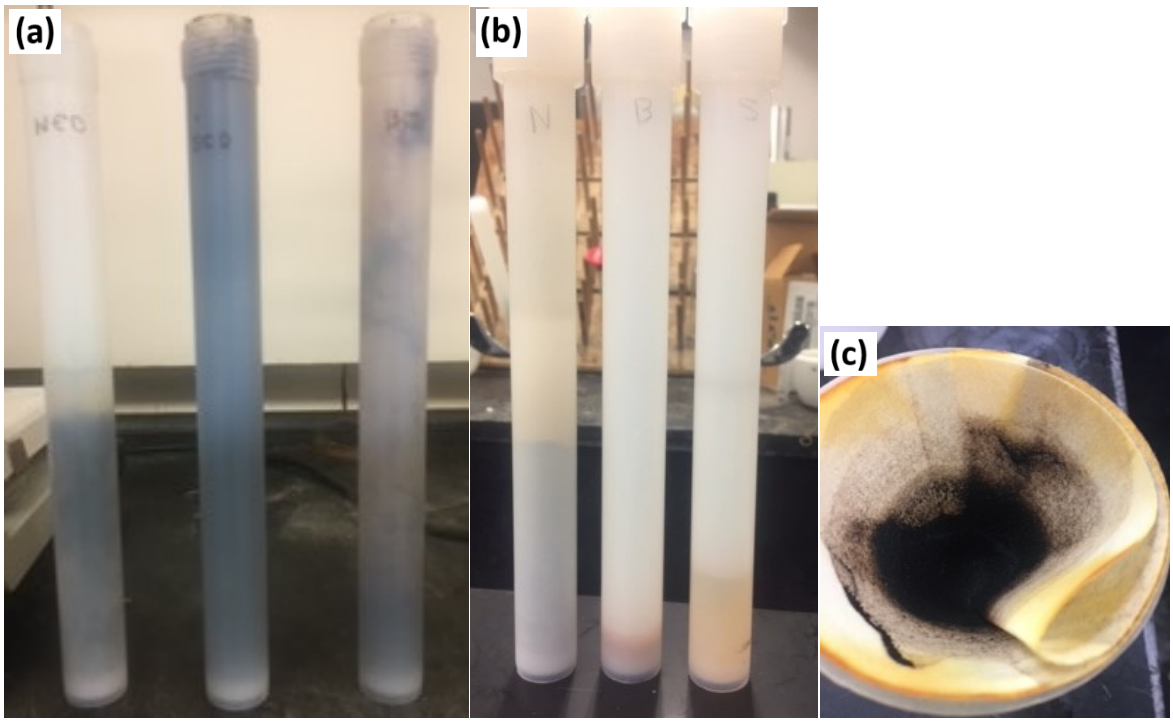


Figure 15. Teflon tubes from digestive microwave method of CD synthesis. (a) Teflon tubes from sucrose-based CDs of N, S, or B dopants, (b) Teflon tubes from citric-acid (or sodium citrate) based CDs of N, S, or B dopants, (c) paper filter from NCD-su (1:1) showing insoluble carbonaceous material that is removed by filtration.

fluorescence largely shares the same region for the other two methods. These results indicate blue-green fluorescence under UV-light excitation.

### 3.2 Comparison of Carbon and Dopant Sources

While the digestive microwave was selected as the best synthesis method, the effect of altering the heteroatom dopant (N, B, or S) and carbon precursors (sucrose, citric acid, or sodium citrate) were the next steps in optimizing CD synthesis. CD samples of each dopant source and carbon source were synthesized in the digestive microwave method in order to determine the best dopant-carbon source combination for maximum fluorescence. The dopant choice for the S dopant was sodium thiosulfate, used for both the citric acid and sucrose-based CDs. However,

because of the precipitate formed from the combination of sodium thiosulfate and citric acid, sodium citrate was used with citric acid to form sulfur-doped carbon dots (SCDs). Sodium tetraborate was initially used for sucrose-based CDs as the B dopant, but because the microwave method employed a hydrothermal approach, boric acid was used to form boron-doped carbon dots (BCDs) since it was more soluble. For the N dopant, urea was used again.

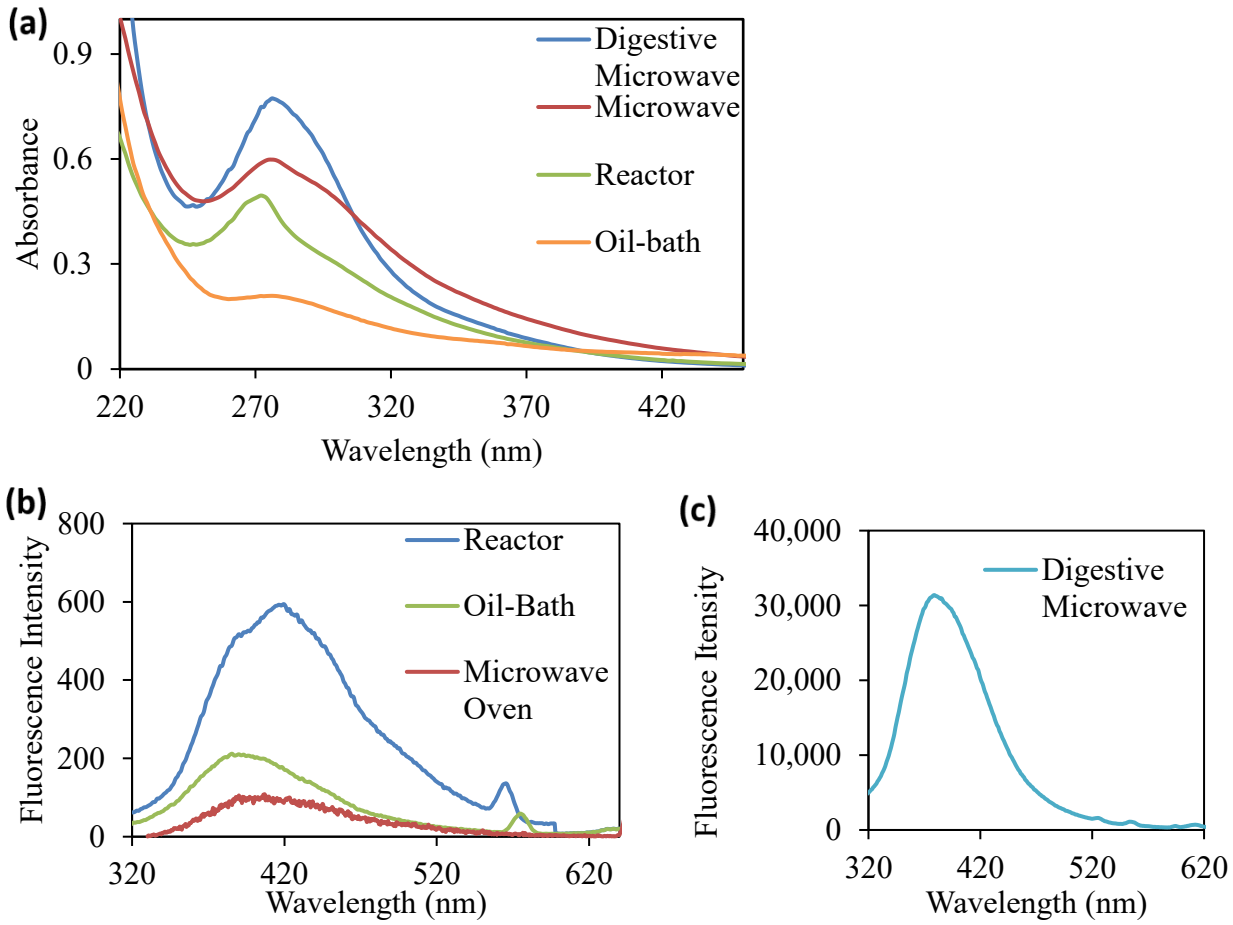


Figure 16. Absorption and emission spectra of NCD-su (1:1) comparing synthetic method. (a) Absorption spectrum of NCD-su (1:1) by synthetic method and (b) comparison of emission spectra of NCD-su (1:1) by synthetic method: reactor ($\lambda_{ex}$= 270 nm), oil-bath ($\lambda_{ex}$= 280 nm), microwave oven ($\lambda_{ex}$= 280 nm), (c) emission spectra of NCD-su (1:1) digestive microwave method isolated for larger scale from other spectra ($\lambda_{ex}$= 280 nm).

**3.2.1 Purification and Lyophilization**. Purification measures began with the paper-filtering of samples directly after synthesis to remove any large particles. Syringe filtration was performed next, which ensured all the NCD withing the final solution would be less than 200 nm. Centrifugation was attempted, but no solid came out of solution.

Purification was then conducted on each microwave-produced sample through dialysis to expel fluorescent byproducts that would otherwise falsely increase the QY of the doped CDs in the retentate. The membrane MWCO was chosen to be 3.5 kDa, as that was the minimum dialysis membrane suggested in the purification methods in Essner et. al.[14] With a 3.5 kDa membrane, smaller fluorophores were removed that would have made up the bulk of fluorescence produced in the CD samples.[14] Three 24-hour dialysis cycles were run on each microwave sample producing light yellow dialysate at each dialysis cycle. A comparison of the UV-vis spectra for NCD-su and NCD-ca to their dialysates are shown in Figure 17. Both samples show similar absorption to their first set of dialysates indicating that either the CDs are permeating the membrane, that some fluorophore byproducts may have similar absorption profiles as the CDs, or that dialysis is inadequate in removing smaller species since they are also present in the retentate. The latter theory is the most likely. Further dialysis with a larger MWCO would benefit this study.

After dialysis, the samples were frozen at -8 °C and lyophilized over a three-day period to produce the solid samples shown in Figure 18. The original solutions were a red brown. Now as solids, the red color dominates the granular NCD-su sample. The NCD-ca sample was much darker brown and lustrous with low density.

**3.2.2 Optical Characterization**. The NCD-su (1:1) and NCD-ca (1:1) samples were characterized via UV-vis spectroscopy and fluorescence spectroscopy. Figure 19a shows the UV-

vis spectra of NCD-su compared to its precursors. The absorption peak at ~280 nm indicates that the NCD-su absorption is solely due to the formation of carbon dots, as the peak is absent in both precursor spectra. These results are consistent with Liu et al. who formed NCD-su from sucrose and urea, attributing this peak to the n-π* transition of C=O.[4] The NCD-su are yellow in more dilute solutions at pH 7, as shown in the inset image in Figure 19a. The NCD-su fluoresce bright blue under UV-light, exhibiting maximum fluorescence intensity from 300-500 nm (Figure 18b).

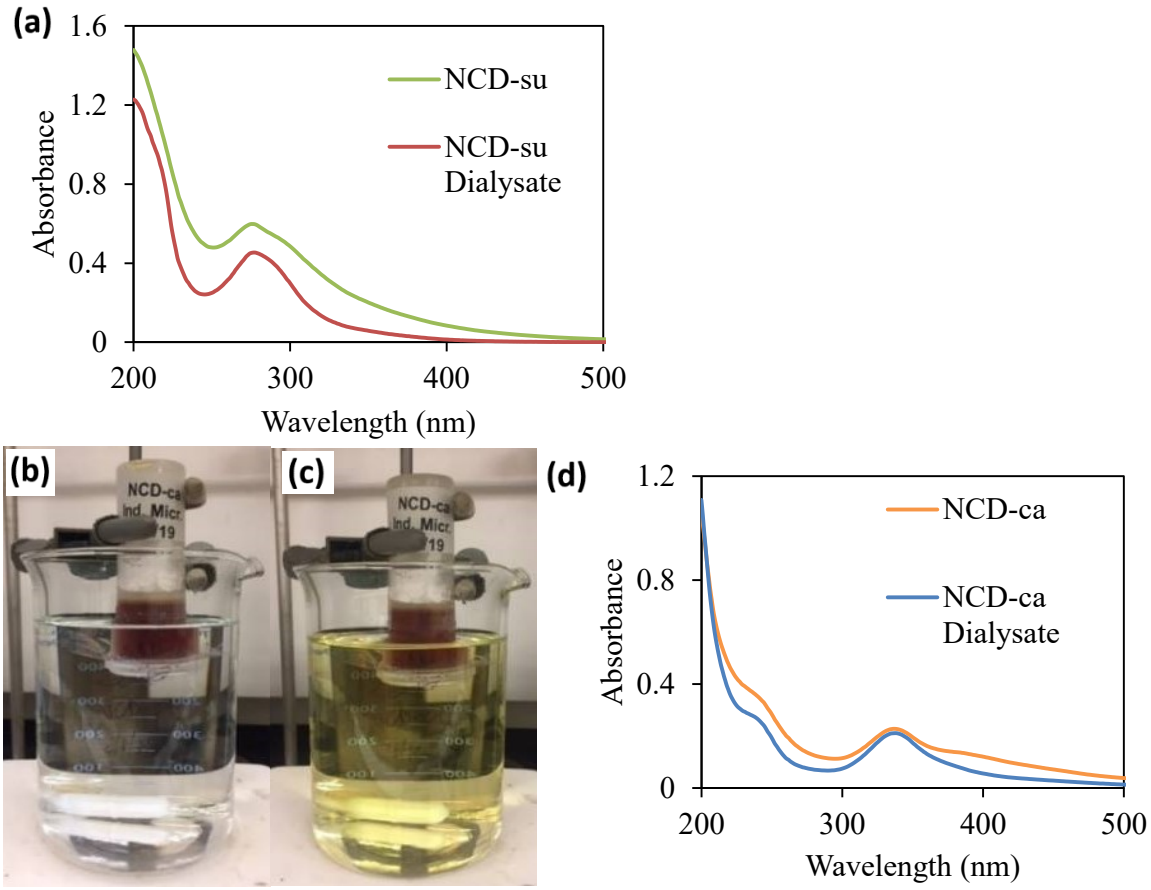


Figure 17. Absorbance spectra comparing dialysate liquids of NCD-su and NCD-ca. (a) Absorbance spectra comparison of NCD-su (1:1) and its dialysate. NCD-ca (1:1) at the (a) start and (b) end of a 24-hour dialysis cycle, (d) absorbance spectra comparison of NCD-ca (1:1) and its dialysate.

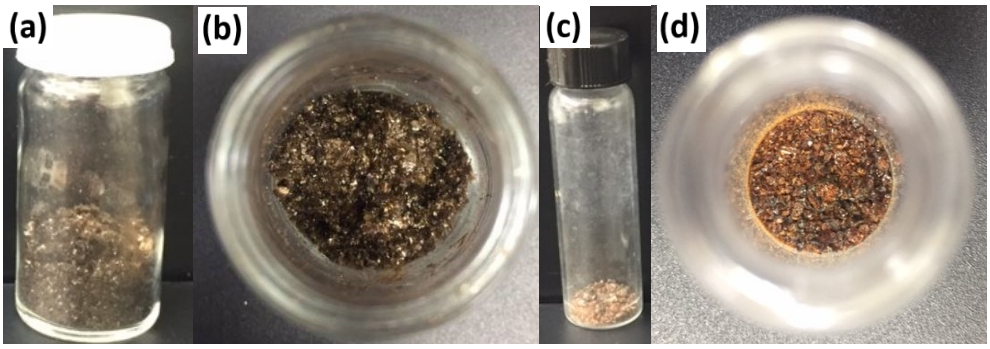


Figure 18. Solid NCD-ca (1:1) and NCD-su (1:1). (a) Side view and (b) top view of post-lyophilized NCD-ca (1:1). (c) Side view and (d) top view of post-lyophilized NCD-su (1:1).

The NCD-ca alternatively has two absorbance peaks in Figure 19c: a narrow shoulder band at 240 nm and a broad peak at 340 nm. These results are similar to reports by Zhang et al. who attributed the shoulder peak to π-π* transitions of C=C bond and the broader peak to be the n-π* transition of C=O (this is the same transition attributed to NCD-su).[36] The NCD-ca fluoresce blue when excited at 340 nm, as shown in the fluorescence spectra in Figure 19d. Though, not shown, the fluorescence when excited at 240 nm is quite low.

**3.2.3 Infrared Spectroscopy**. A comparison of FT-IR spectra of NCD-ca (1:1) and NCD-su (1:1) are shown in Figure 20. Both spectra have broad bands at 2500-3300 $cm^{-1}$ corresponding with the O-H and N-H asymmetric stretches of carboxylic acids, alcohols, and amines. These overlap slightly with C-H stretch at about 2900 $cm^{-1}$. Both spectra also exhibit peaks at ~1650 $cm^{-1}$ which correspond to C=O stretches. The strong peak at 1022 $cm^{-1}$ in NCD-su is attributed to C-O stretches and 1180 $cm^{-1}$ in NCD-ca (1:1) and NCD-su (1:1) correspond to C-N stretches. All these groups indicate the presence of surface functional groups like -COOH, -$NH_2$, and -OH, which are characteristic of NCDs.[4] Likewise these results closely resemble similar reports.[4,36]

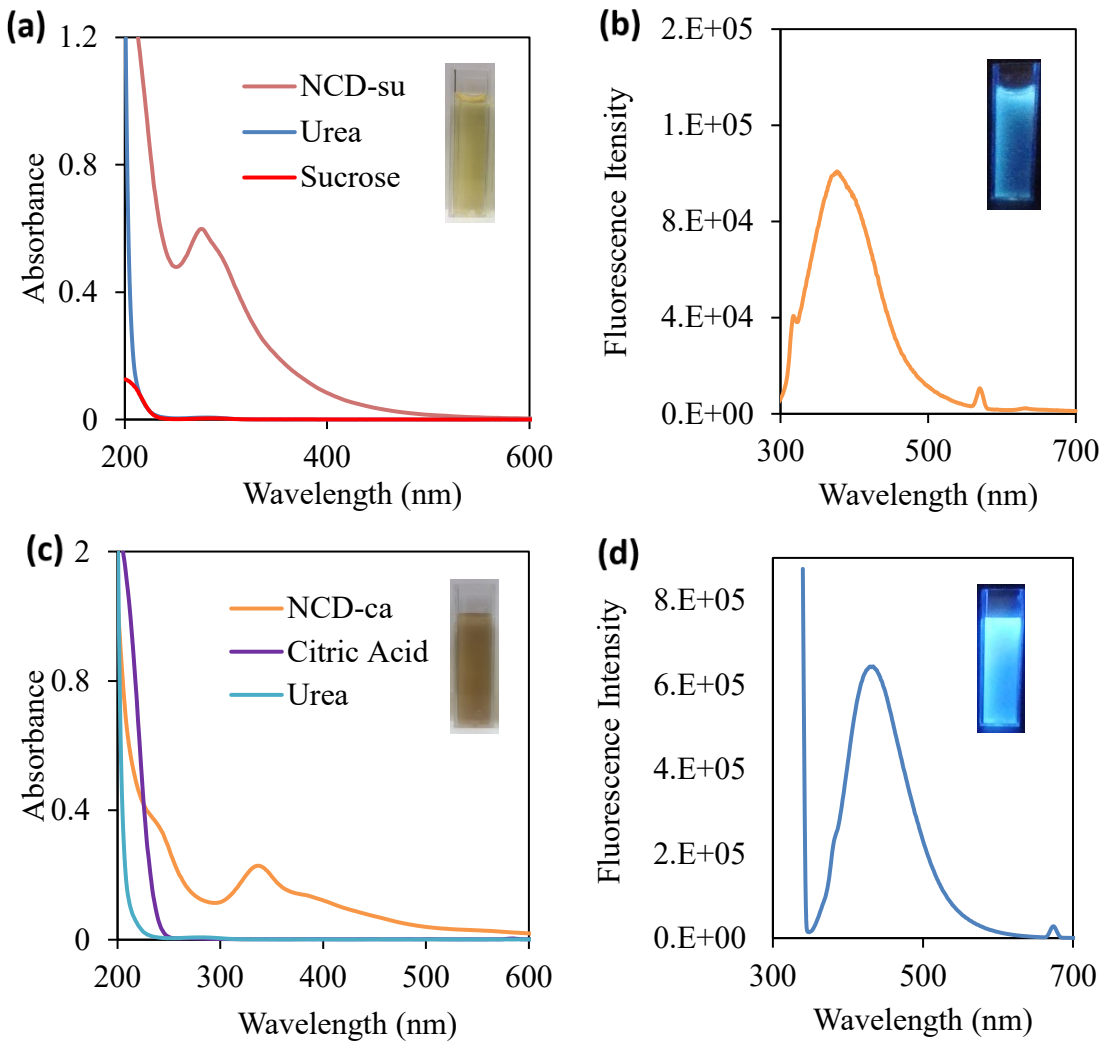


Figure 19. Comparison of nitrogen doped carbon dots by carbon source. (a) is the comparison of the UV-vis spectrum for NCD-su to its precursors with an inset image of NCD-su in white light. (b) Emission spectrum of NCD-su at 13 ppm ($\lambda_{ex}$= 280 nm) with an inset of the sample under 365 nm light. (c) Comparison of the UV-vis spectrum for NCD-ca against its precursors, with an inset image of NCD-ca in white light. (d) Emission spectrum of NCD-ca at 2 ppm ($\lambda_{ex}$= 340 nm) with an inset image of the sample under 365 nm light.

The absorption and emission spectra of the previously synthesized NCD-ca (1:1) and NCD-su (1:1) samples were compared to the SCD-sc (1:1), SCD-su (1:1), BCD-ca (1:1), and BCD-su (1:1) in Figure 21.

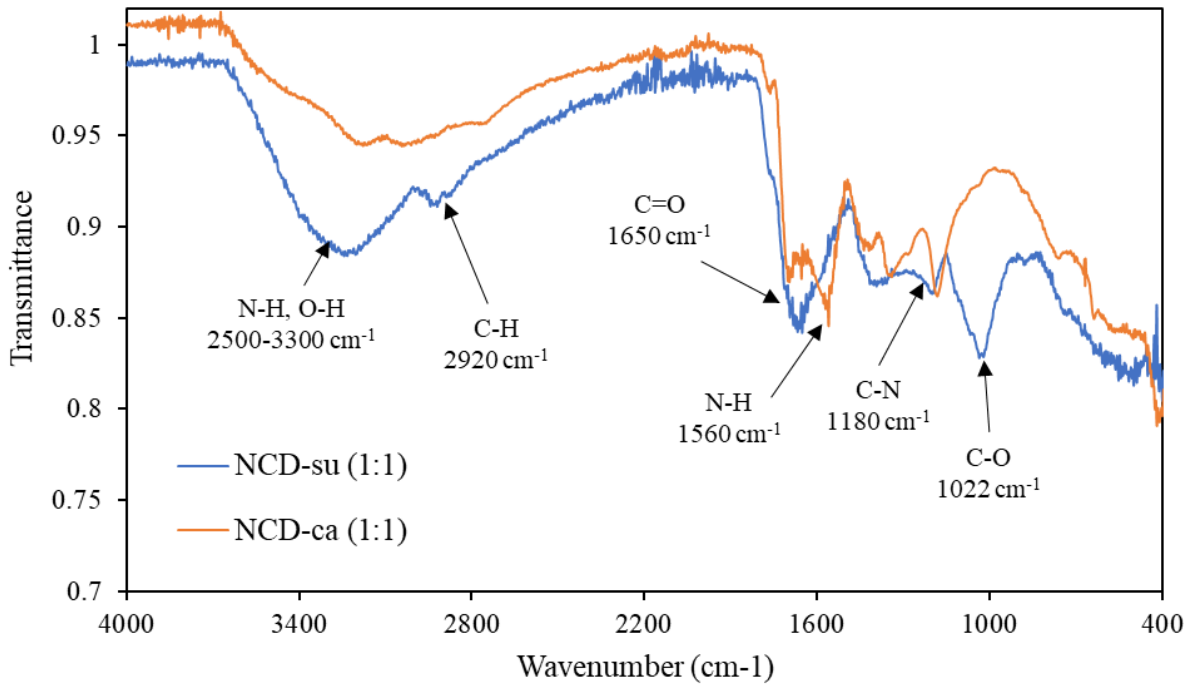


Figure 20. Comparison of NCD-su (1:1) and NCD-ca (1:1) FT-IR spectra.

Unlike the other citric acid or sodium citrate-based CDs, NCD-ca (1:1) has two maximum absorbances at 240 nm and 340 nm in the UV-vis spectra in Figure 21a, while the SCD-sc (1:1) and BCD-ca (1:1) samples has only one maximum visible at their concentrations. SCD-sc (1:1) has a maximum absorbance at 218 nm while BCD-ca (1:1) has a maximum absorbance at 220 nm. Though the sample concentrations are not identical, the similar absorbance of each CD sample indicate that the fluorescence intensities shown in Figure 21b are partially comparative. The NCD-ca (1:1) sample, with a maximum intensity at 440 nm when excited at 340 nm, has a significantly higher intensity than either the SCD-sc (1:1) sample at 420 nm, or the BCD-ca (1:1) sample at 450 nm. When NCD-ca (1:1) is excited at 218 nm, the fluorescence is much less intense. This indicates an expected low QY for both dopant sources when used with citric acid-based CDs. This could be improved through co-doping with a higher fluorescing urea dopant.

The UV-vis spectra in Figure 21c compares the N, S, and B dopants for sucrose-based CDs. NCD-su (1:1) has a strong absorption band at 280 nm while SCD-su (1:1) has a weaker absorption at 250 nm and BCD-su (1:1) has a maximum absorption at 270 nm. Like the citric acid-based CDs, the concentrations of the samples were non-comparative. However, the fluorescence of the NCD-su (1:1) sample is much greater than the other dopant samples in Figure 21d, with a maximum fluorescence intensity at 380 nm. The SCD-su (1:1) sample has the least fluorescence intensity. However, both the citric acid or sodium citrate-based and sucrose-based CDs fluoresced at some quantity above a blank sample, indicating the positive presence of fluorescent material, though in extremely low quantities.

**3.2.4 Fluorescence Dependence on pH**. Of the prepared samples, the fluorescence dependence on pH was conducted for the two highest fluorescing species, NCD-ca (2:1) and NCD-su (1:1) and the lowest fluorescing species, BCD-su (2:1) at pH 1-13. The emission spectra for NCD-ca (2:1) is shown in Figure 22 where the fluorescence intensity is highest at pH 5 and lowest at pH 13. The fluorescence spectra for NCD-su (1:1) is shown in Figure 23 with the highest fluorescence intensity at pH 3 or 4 and the lowest at pH 13. The BCD-su (2:1) sample, though lower in fluorescence intensity than either NCD-ca (2:1) or NCD-su (1:1), still demonstrates fluorescence dependence on pH, as shown in Figure 24. The sample is highest fluorescing at pH 4 and lowest at pH 13.

The dynamic range of fluorescence intensities based on changing pH for NCD-su (1:1) would make it a great potential pH-sensor. BCD-su (2:1) is less desirable since it has a lesser spread of pH-dependent fluorescence. Interestingly, NCD-ca (2:1) exhibited a less clear trend in pH-dependent fluorescence, whereas later NCD-ca samples of different molar ratios showed a clearer trend toward increased fluorescence at basic pHs. This may be due to potential buffer

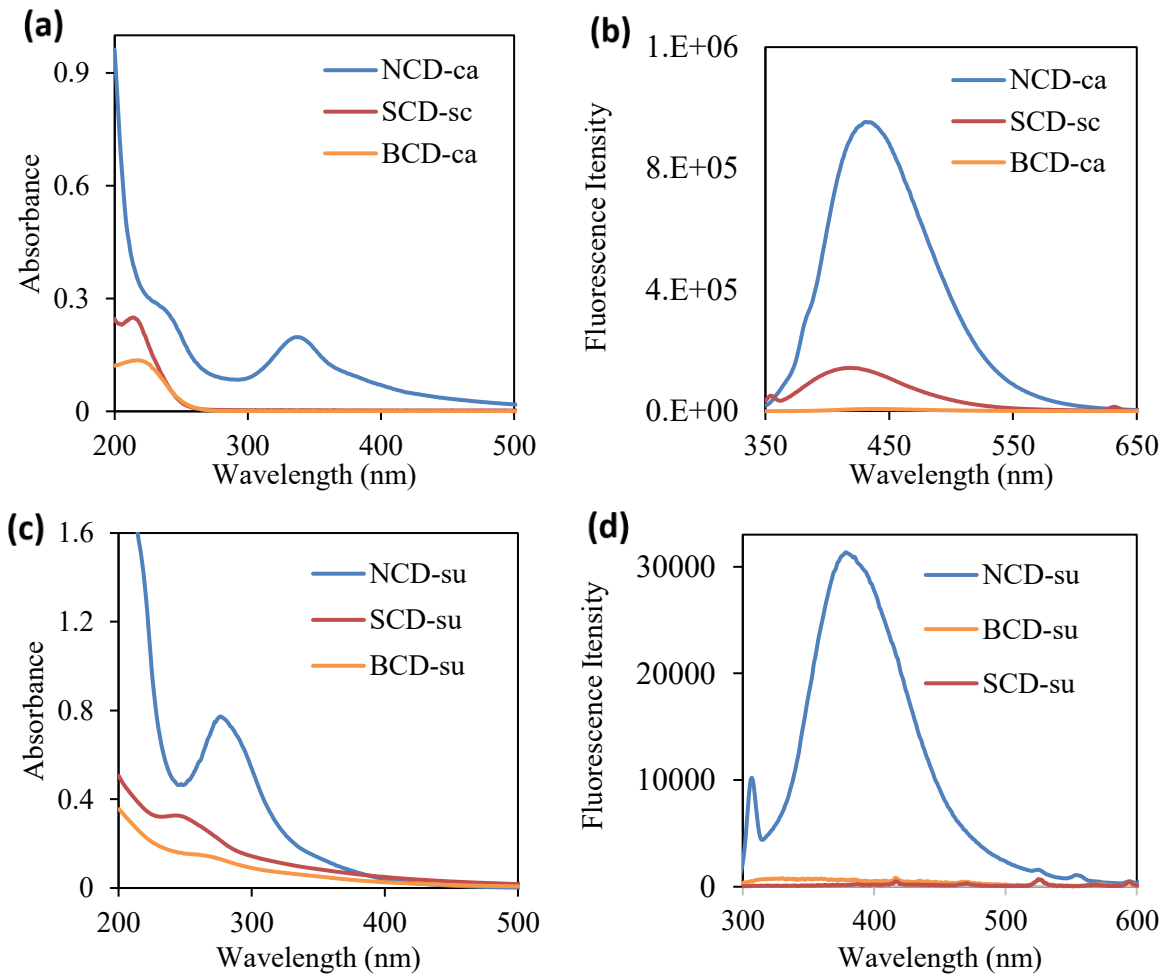


Figure 21. Microwave method synthesized CDs compared by dopant. All samples are 1:1 mol ratios with dopants: N (blue), S (orange), and B (orange). (a) UV-vis spectra and (b) emission spectra of citric acid/ sodium citrate-based CDs ($\lambda_{ex}$= 340 nm); (c) UV-vis spectra and (d) emission spectra of sucrose-based CDs ($\lambda_{ex}$= 250 nm for S, = 270 nm for B, = 280 nm for N).

degradation as the higher concentration species (pH 1, pH 13, etc.) showed the least fluorescence. Alternatively, the NCD-ca (2:1) sample as prepared may have less carboxyl or amine groups on its surface, making it less able to form a negative protective shell at basic pHs to prevent high non-radiative recombination rates.[4]

**3.2.5 Quantum Yield**. The QYs of NCD-ca (2:1), NCD-su (1:1) and BCD-su (2:1), were calculated based on the comparison to the 2-aminopyridine (60%) standard in 0.1 M $H_2SO_4$ for

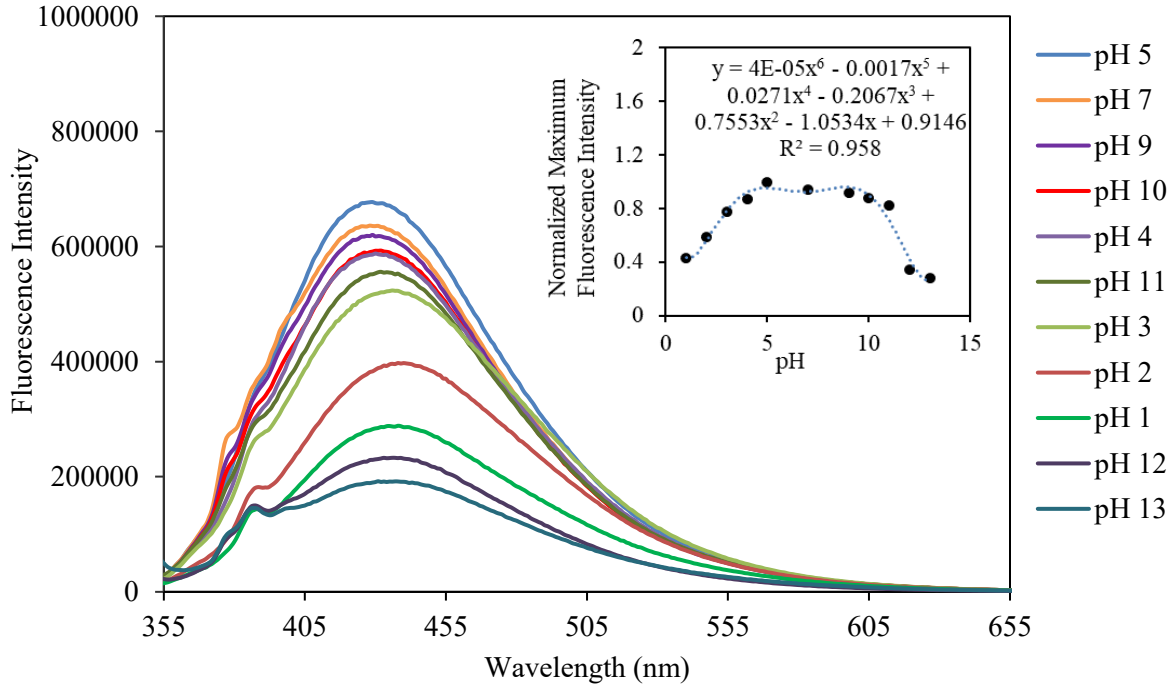


Figure 22. Emission spectra of NCD-ca (2:1) at pH 1-13; inset image: pH-dependent fluorescence polynomic trend plot.

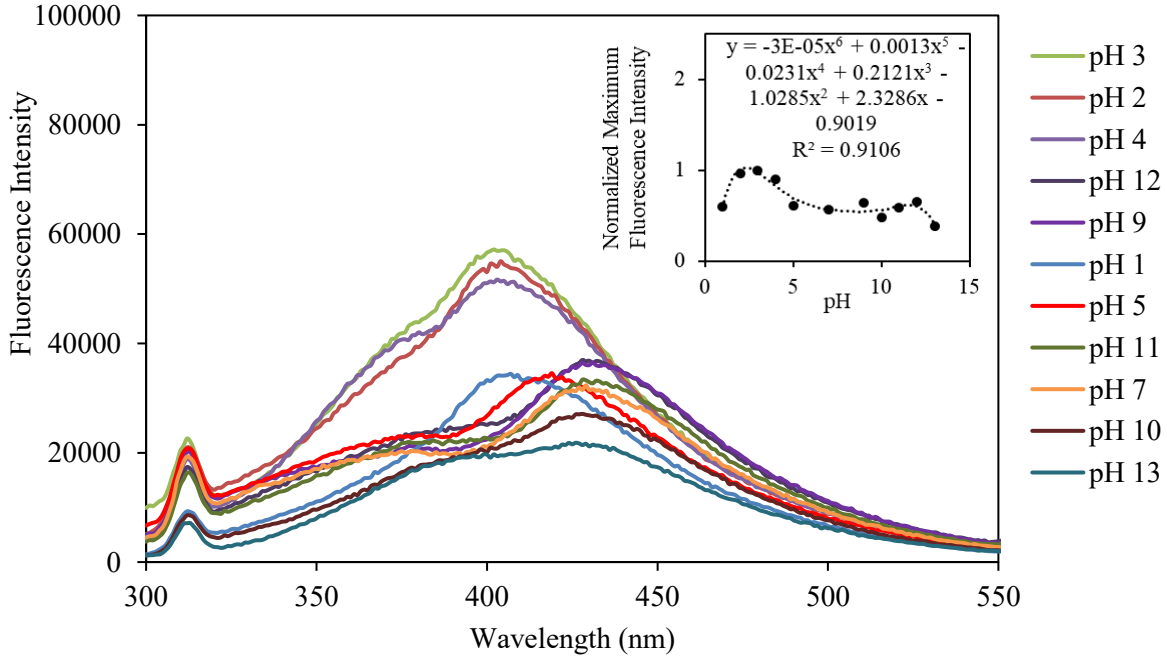


Figure 23. Emission spectra of NCD-su (1:1) at pH 1-13; inset image: pH-dependent fluorescence polynomic trend plot.

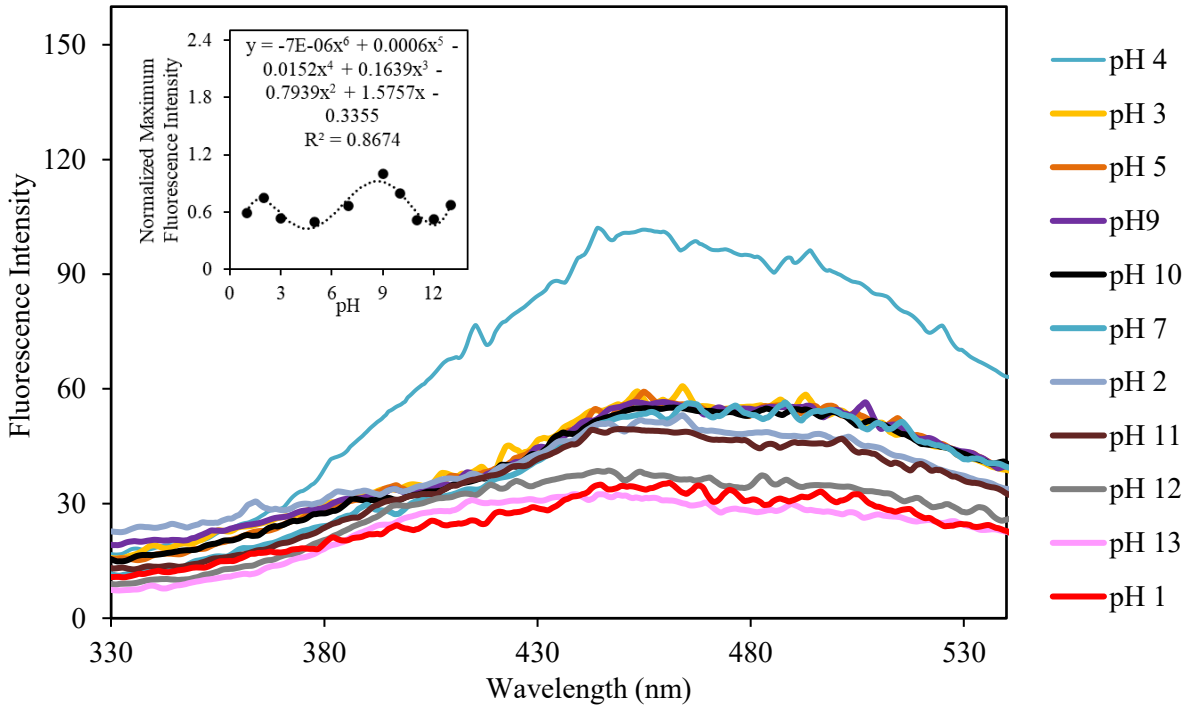


Figure 24. Emission spectra of BCD-su (2:1) at pH 1-13; inset image: pH-dependent fluorescence polynomic trend plot.

the sucrose-based samples and compared to quinine sulfate (54%) in 0.1 M $H_2SO_4$ for the citric-acid-based samples. Plots of integrated fluorescence intensity versus absorbance for increasing concentrations of the sample and standard yielded comparative gradients to be used in equation 1 (see Figure 25 for an example plot).[24] Likewise, the refractive indexes for each sample were used in equation 1 to calculate the QY.

Each sample's QY was conducted at their highest fluorescing pH: pH 3 for NCD-su (1:1), pH 4 for BCD-su (2:1), and pH 5 for NCD-ca (2:1). Each sample's gradients were significantly lower than the fluorescent standards indicating lower QYs such as with NCD-ca in Figure 25 that had a much smaller slope than quinine sulfate.

Figure 26 shows the QY results. NCD-ca (2:1) had the highest QY of 6.23% which was about twelve times the QY of NCD-su (1:1) at 0.65%. The NCD-su (1:1) QY was lower than

anticipated as a similar composition from Liu et al. produced QYs of 1.57% in pH 6 and 11.03% in pH 11. As expected, BCD-su (2:1) had the lowest QY at 0.22%. These results indicate sodium tetraborate and boric acid are not suitable dopants for boron because of their low QY when compared to urea (N) doped CD samples, unless used as a co-dopant. Likewise, though urea made a good dopant source of N for both the NCD-ca and NCD-su samples, the NCD-ca sample had the significantly better QY, indicating citric acid is a superior carbon source to sucrose.

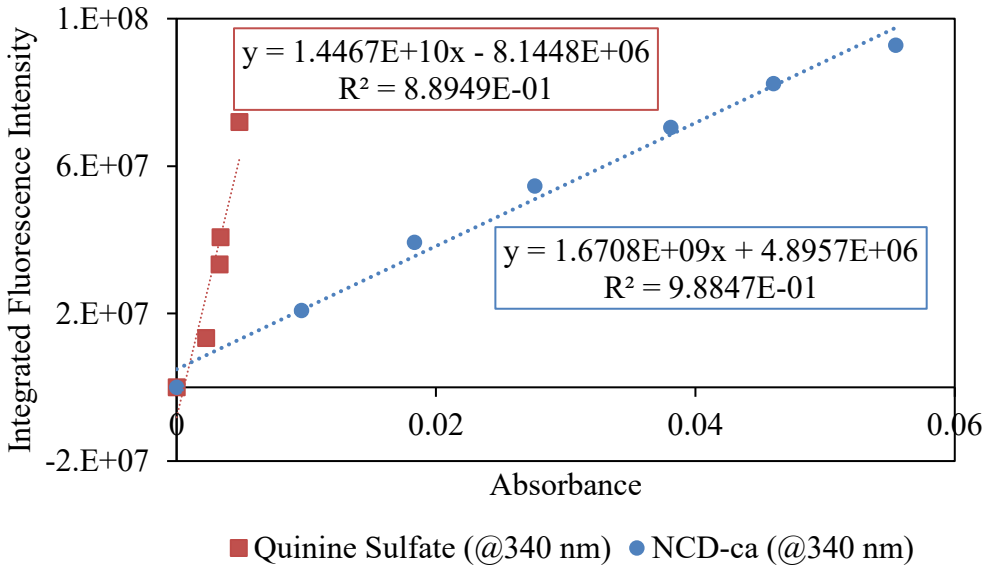


Figure 25. Integrated fluorescence intensity vs absorbance plot for QY calculation. Compares the integrated fluorescence intensities vs. absorbance for NCD-ca in pH 5 at an excitation wavelength of 340 nm (blue) versus quinine sulfate fluorescent standard in 0.1 M H2SO4 at 340 nm (red).

### 3.3 Increasing Molar Dopant Ratios of NCD-ca

Now that it has been established that CDs composed of citric acid and urea were the best combination, altering the molar dopant to carbon source ratios was investigated to optimize the QY. Initially, three samples were prepared in the following citric acid to urea ratios (mol carbon source: mol dopant source): NCD-ca (6:1), NCD-ca (1:1), and NCD-ca (1:6) based on

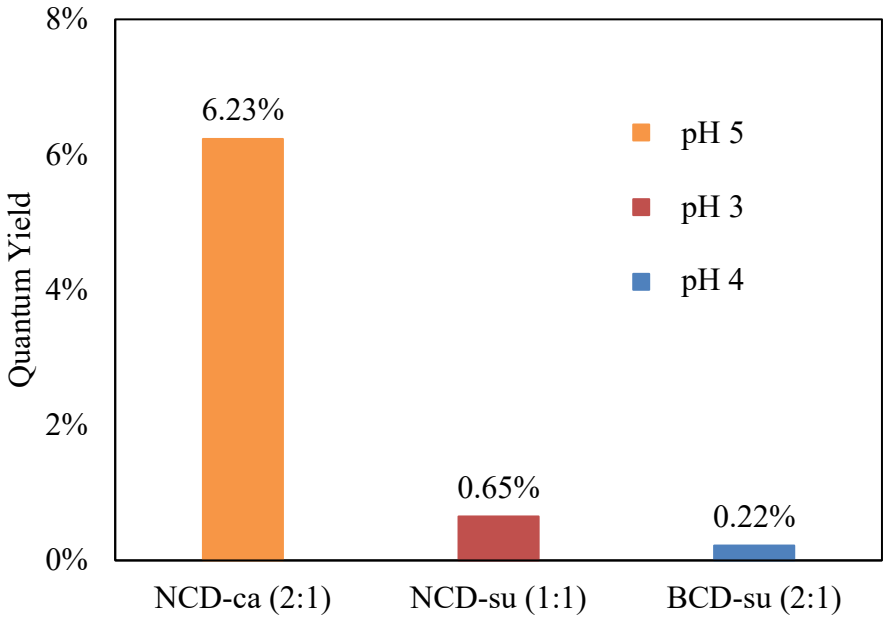


Figure 26. Comparison of NCD-ca (2:1), NCD-su (1:1), and BCD-su (2:1) QYs. NCD-ca (2:1) at pH 5 (orange), NCD-su (1:1) at pH 3 (red), BCD-su (2:1) at pH 4 (blue).

similar methods by Zhang et al. so comparisons could easily be made with literature.[36] Since NCD-ca (1:6) seemed to be the highest fluorescing, two further samples (NCD-ca (1:3) and NCD-ca (1:10)) were added later to bookend NCD-ca (1:6) to determine if greater fluorescence was above or below its composition. Along with characterization, the pH-dependent fluorescence for each sample was investigated as well as a comparison of corresponding QYs for select pHs.

**3.3.1 Sizing and Characterization**. SEM was used to image each NCD-ca sample to estimate dry nanoparticle size and morphology. Sample preparation was conducted in one of two ways depending on the degree of hygroscopic behavior in each sample. As the molar dopant amount increased, from a carbon to dopant ratio of (6:1) to (1:10), increased hygroscopic behavior was observed. This made SEM images substantially more complicated. For NCD-ca (6:1), (1:1) and (1:3), solid samples were applied directly onto aluminum stubs. Previous attempts to drop cast water-based NCD-ca solutions onto the gold-coated silicon wafers resulted

in clustered masses of CDs that did not produce very good images. Similarly, the use of ethanol as an alternative solvent also did not yield significant results as all the NCDs clustered together in solution due to the small presence of pre-absorbed water because of their hygroscopicity. Therefore, the images shown are what was able to be gathered for NCD-ca (6:1), (1:1), and (1:3).

NCD-ca (1:6) and (1:10) were the least hygroscopic and the highest fluorescing, therefore greater focus was given to them. These samples were suspended in ethanol and were successfully drop cast on wafers for SEM analysis. Additionally, EDS was performed for both samples yielding elemental population graphs of C, N, and O layered on the SEM image.

Figure 27 shows the SEM image of NCD-ca (6:1). This sample was the most hygroscopic, having absorbed moisture over time, despite a sealed containment. The sample rapidly gained additional moisture during SEM sample preparation, evident by the large 1 mm width of the particles and their smooth globular appearance. Despite redissolving the NCD-ca (6:1) sample in DDI, freezing, and re-lyophilizing to a solid, the sample remained gummy and hygroscopic. Therefore, no additional SEM images were taken. Early desiccator storage of these samples is imperative.

Figure 28 shows SEM images of NCD-ca (1:1), with Figure 28a showing a deposit of the solid directly on the stubs and Figure 28b showing the dropcast sample of water as the solvent. As seen in Figure 28a, the method of "dusting" the solid directly onto the surface did yield a clear image at a 2 mm scale. However, the hygroscopic behavior of NCD-ca (1:1) is evident from the globular cluster and large size. Figure 28b, then shows a smaller 500 μm scaled image, though the particles are clustered together, and no smaller size particle is discernable. The increased hygroscopic behavior is likely influenced by the age of these samples, as they were not imaged within weeks of synthesis.

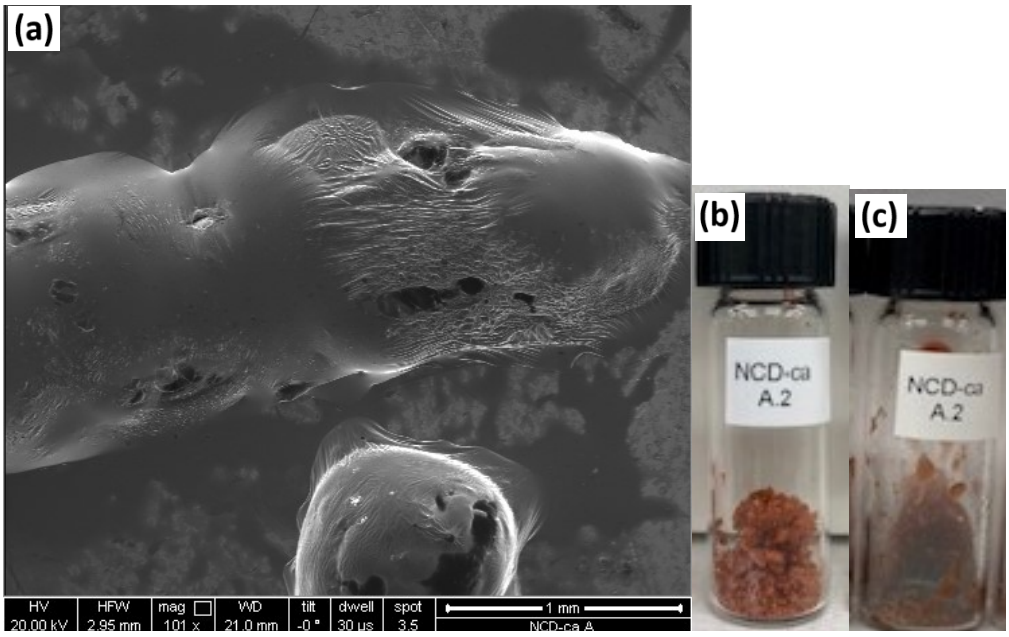


Figure 27. SEM image of NCD-ca (6:1) at (a) 1 mm scale, (b) solid stored immediately after initial lyophilization, (c) solid after several weeks exhibiting hygroscopic behavior despite seal.

Figure 29 shows SEM images of NCD-ca (1:3) at 50 µm and 300 µm scales, where the hygroscopic nature of the CDs is obvious due to the globular conglomerates shown. These images were taken from samples prepared by dusting the aluminum stubs with the solids. Since the CDs were highly soluble in water, previous attempts using drop casts of NCD-ca (1:3) in water led to unusable SEM images due to clustering when water evaporated. Of the prepared NCD-ca samples, NCD-ca (1:3) was less hygroscopic than NCD-ca (6:1) and (1:1), though that could also be attributed to it being a comparatively newer sample.

An SEM image for NCD-ca (1:6) is shown in Figure 30, along with pictures of bulk solid NCD-ca (1:6) to show hygroscopic behavior. Though some smaller clusters were present, most of the particles from depositing the NCD-ca (1:6) solid directly onto the stub were around 100 µm in diameter as shown in Figure 30a. The particle appears to be a cluster of smaller particles, with a flaky ridge-like morphology. Though not as hygroscopic as NCD-ca (6:1) or (1:1), its

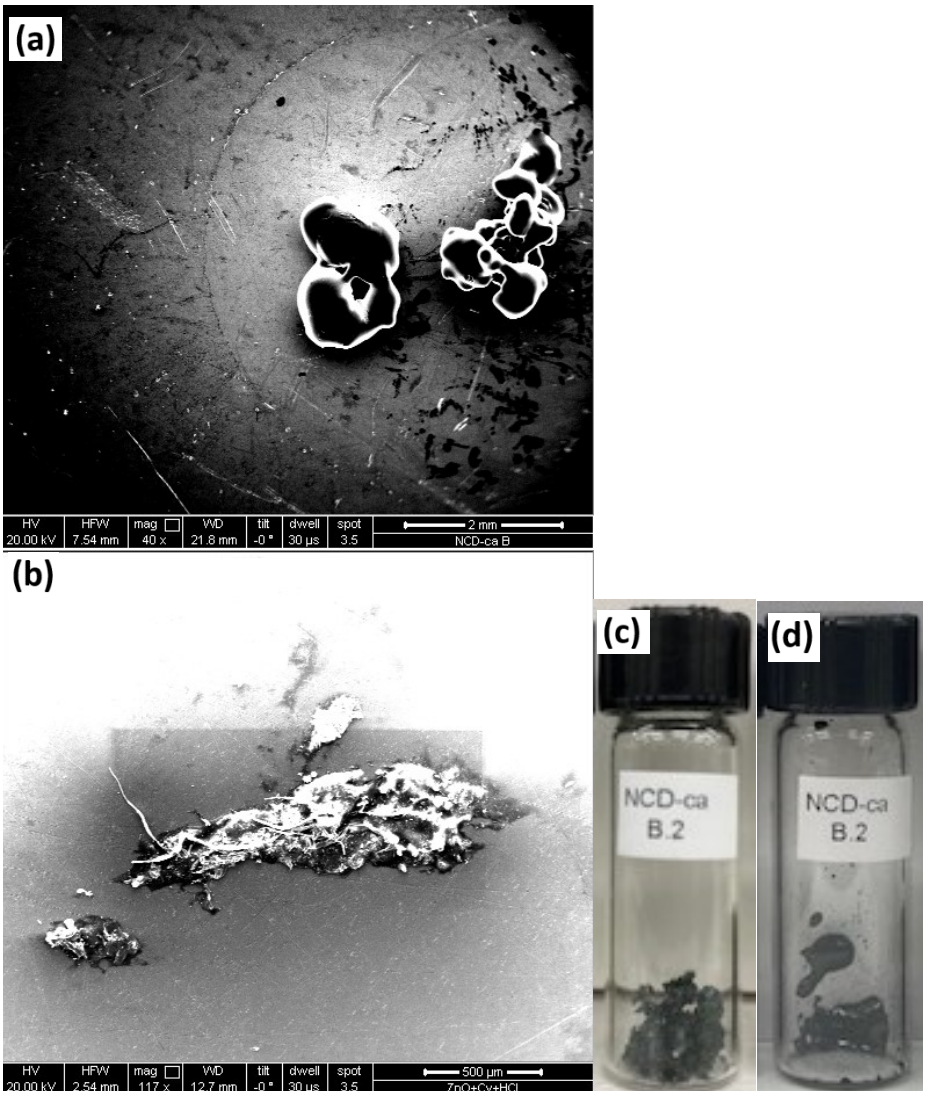


Figure 28. SEM images of NCD-ca (1:1) from (a) solid casting at 2 mm scale, (b) solution in water drop casting at a 500 µm scale, (c) solid stored immediately after initial lyophilization, and (d) solid after several weeks exhibiting hygroscopic behavior despite seal.

hygroscopic behavior is still evident in comparison of the freshly stored solid in Figure 30b from the more clustered solid pictured weeks after synthesis in Figure 30c.

When NCD-ca (1:6) was re-lyophilized and suspended in ethanol for drop casting, the resulting SEM image in Figure 31a shows distinct clusters of NCDs colored black in the image. Further EDS elemental composition overlays in Figures 31b-d show clear C, O, and N content,

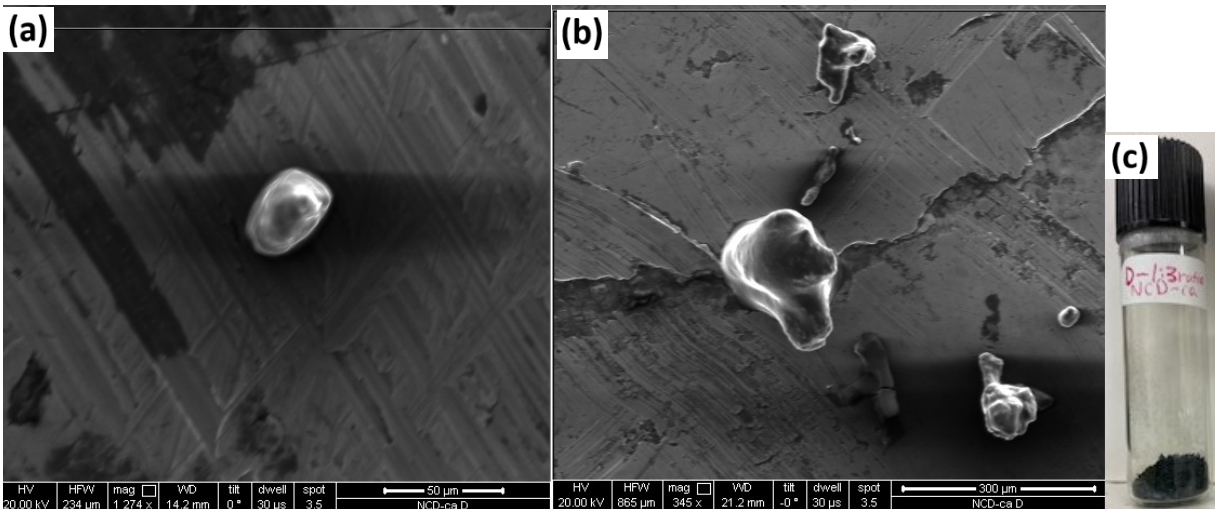


Figure 29. SEM images of NCD-ca (1:3) at (a) 50 µm and (b) 300 µm, (c) solid freshly prepared with notably no obvious difference in hygroscopic nature over several weeks.

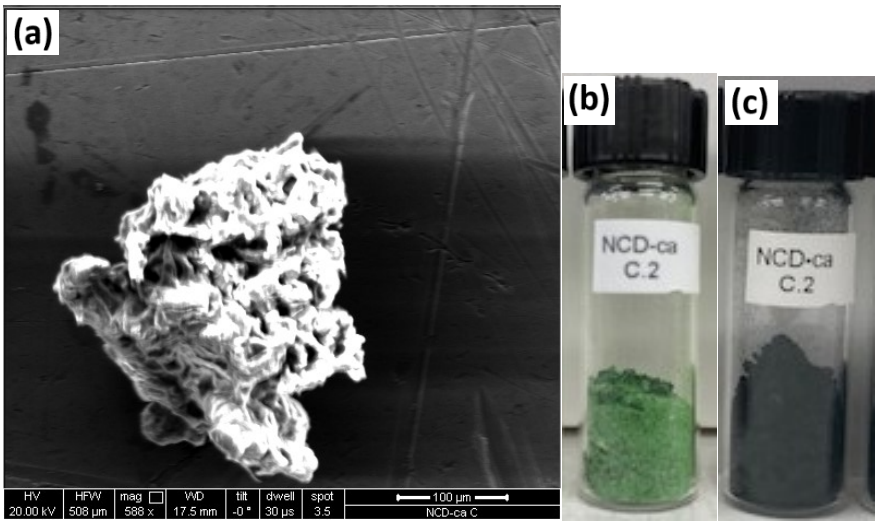


Figure 30. SEM and EDS images of NCD-ca (1:6**)** with (a) SEM image from direct solid casting at 100 µm scale, (b) solid stored immediately after synthesis, (c) solid after several weeks exhibiting slight hygroscopic behavior.

largely in the black clusters imaged in Figure 31a. A live count per second spectrum showing approximate weight percentages of each observed element is shown in Figure 31e. Silicon and gold make up the bulk of the content, as expected, since the CDs are drop casted on gold coated

silicon wafers. The small chromium spike is attributed to the chromium adhesive used in the manufacturing of the wafers. The Rb peak is anomalous and is likely attributed to impurities in the wafer. Additional peaks are present for C and O, though the N is likely too small to appear on this plot in comparison to the magnitude of the Si peak. All three elements are shown in lesser concentrations across the overlay EDS images in Figures 31b-d, suggesting the CDs are much smaller than the 100 μm scale of Figure 31a can depict. Further dilutions of the same sample preparation could yield images with even clearer sized particles.

An SEM image of NCD-ca (1:10) is shown in Figure 32, along with an image of bulk NCD-ca (1:10) solid. The SEM image in Figure 32a depicts flaky clusters of NCDs in a 100 μm scale from the direct application of solid NCD-ca (1:10) on the stub. Of all NCD samples, this is the least hygroscopic, showing no visible hygroscopic behavior after weeks of the solid sample sitting post-synthesis as shown in Figure 32b.

EDS analysis of the SEM image of NCD-ca (1:10) is shown in Figure 33a-e. The SEM image in Figure 33a is from the drop cast samples with ethanol, showing small groupings of black clusters. The black clusters are confirmed to be NCDs based on the C, O, and N elemental overlays from EDS images in Figures 33b-d. Notably, the N overlay has less resolution than O or C overlays, possibly suggesting more diffuse N within the sample due to urea oligomers potentially still present in addition to NCDs. As NCD-ca (1:10) has the highest mole ratio of urea to citric acid, it is not all unlikely to see a higher N composition. The summary of elemental composition population by count per second plot in Figure 33e shows similar results to NCD-ca (1:6). The largest peaks are from Au and Si from the wafer substrates, while C, O, and N peaks are also present. Notably, the N peak is present in this plot unlike that of NCD-ca (1:6) possibly due to the larger N character of NCD-ca (1:10).

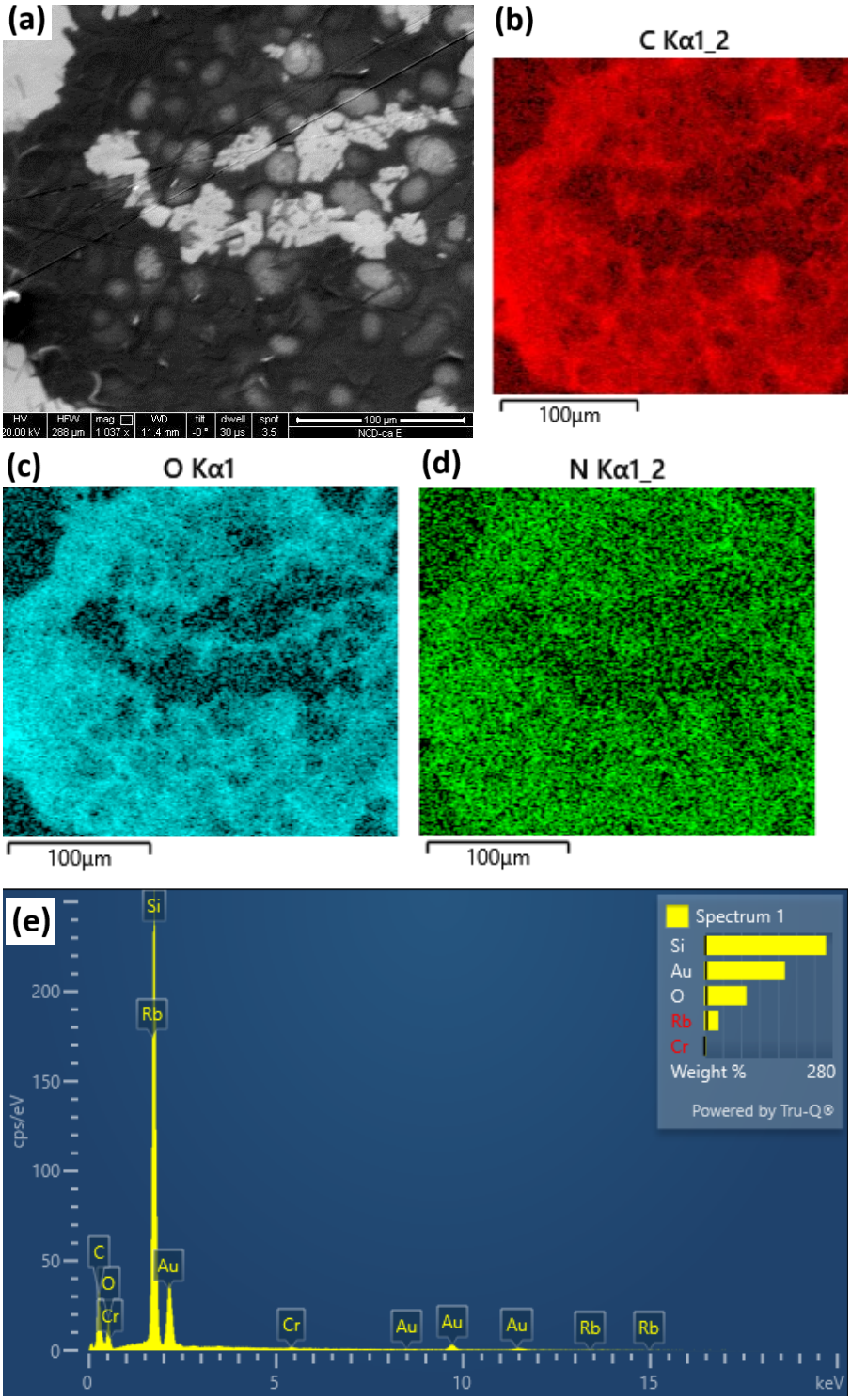


Figure 31. SEM and EDS of NCD-ca (1:6) with (a) SEM image from ethanol solution drop cast after re-lyophilization at 100 µm scale, EDS composition overlays of (b) carbon, (c) oxygen, (d) nitrogen, and (e) summary of elemental compositions by count per second and inset image of elemental composition by approximate weight percent.

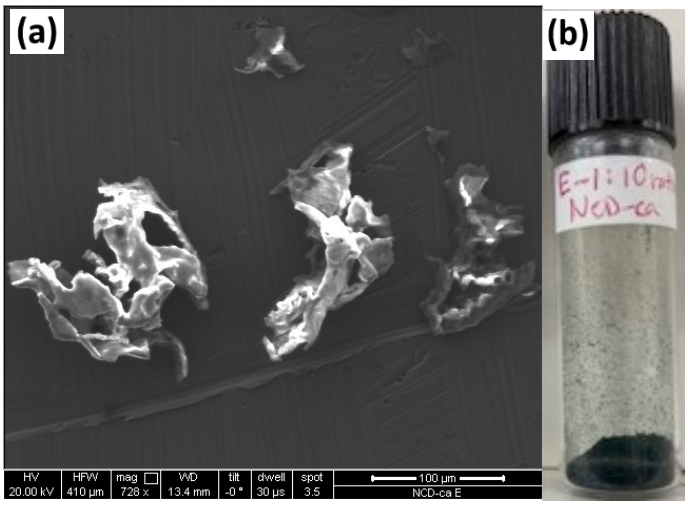


Figure 32. SEM and EDS images of NCD-ca (1:10) with (a) SEM image from direct solid casting at 100 µm scale, (b) solid stored immediately after synthesis with no notable hygroscopic clustering after several weeks post-synthesis.

An additional SEM image of NCD-ca (1:6), shown in Figure 34a, displays disperse, spherical particles. Figure 34b shows a frequency plot prepared from the SEM image using Image J software. These particles range from 3-120 nm, with over 60% of the particles being less than 20 nm. The inset in Figure 34a shows the distribution under 15 nm with a mean size of 8.1 ± 3.3 nm. This size confirms the synthesis of carbon dots which must be less than 10 nm to be considered carbon dots. The populations of larger particles are likely due to aggregation as the sample run was the dry, bulk solid.

TEM results confirm the sizing found by SEM (see Figure 35a-b). The NCD-ca (1:6) have an average size of 10.7 ± 2.8 nm and is spherical. Obtaining the TEM results was a major milestone in this project because dynamic light scattering (a sizing technique) was unsuccessful in sizing the CDs due to their fluorescence.

**3.3.2 Infrared Spectroscopy**. Each NCD-ca (6:1) through (1:6) samples were characterized by FT-IR spectroscopy for functional group identification. NCDs have excellent

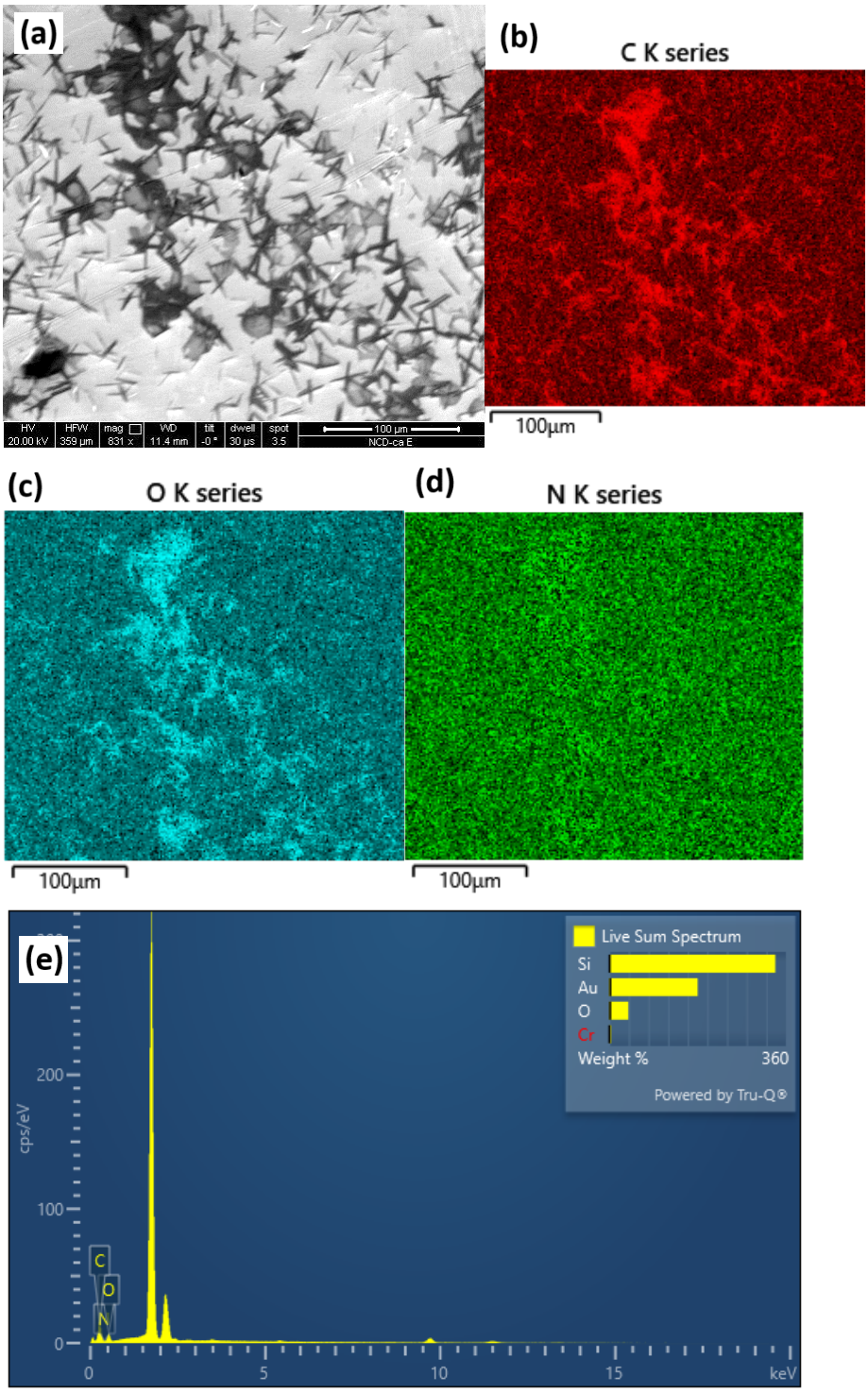


Figure 33. SEM and EDS of NCD-ca (1:10) with (a) SEM image from ethanol solution drop cast after re-lyophilization at 100 µm scale, EDS composition overlays of (b) carbon, (c) oxygen, (d) nitrogen, and (e) summary of elemental compositions by count per second and inset image of elemental composition by approximate weight percent.

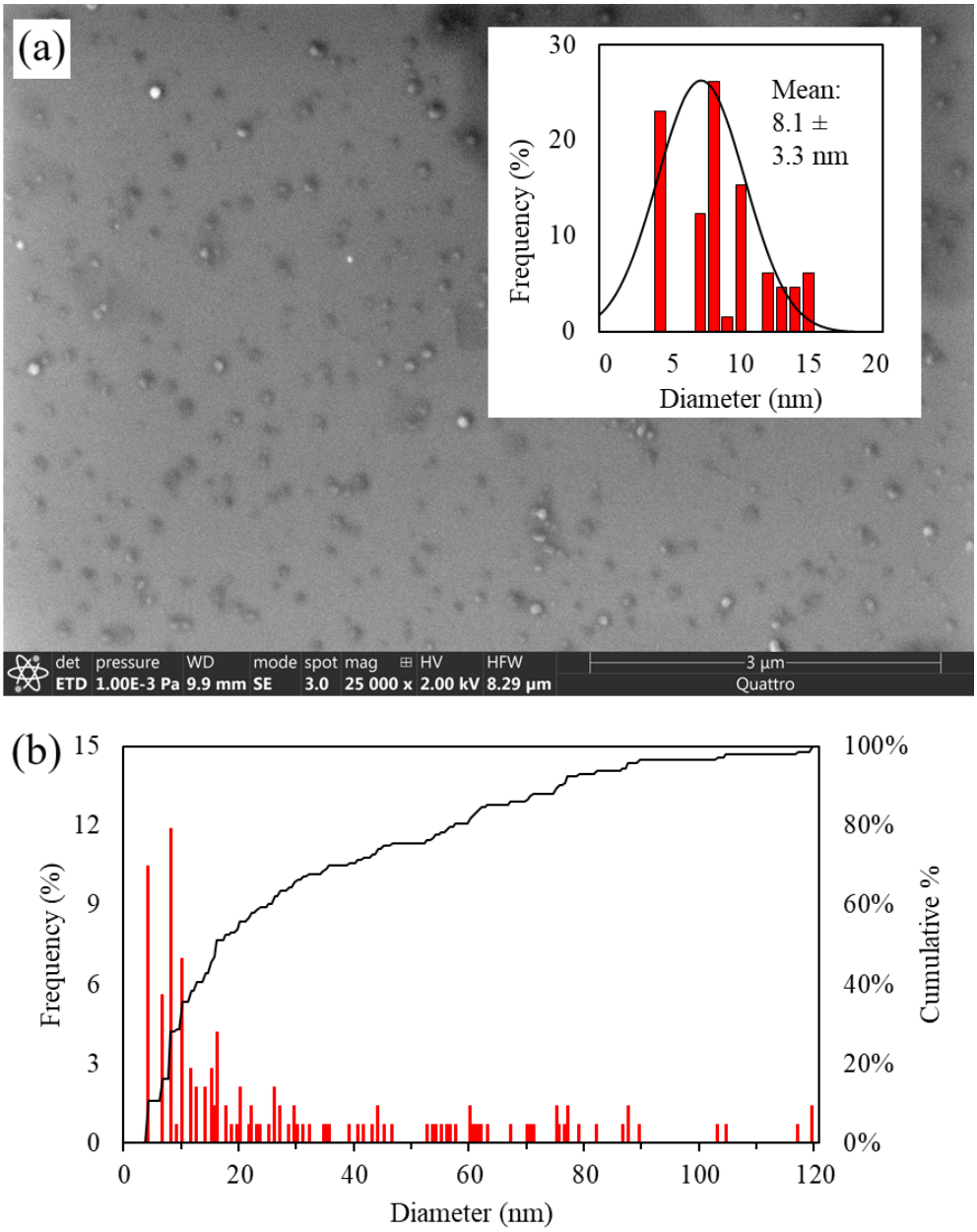


Figure 34. SEM image with size distribution of NCD-ca (1:6). (a) SEM image of NCD-ca (1:6) with inset of size distribution showing an average size of 8.1 nm and (b) frequency plot of NCD-ca (1:6) showing full sizing distribution and percent cumulation.

water solubility and exhibit pH-dependent fluorescence largely due to the myriad of functional groups on their surface including -COOH, -$NH_2$, -OH, =O, etc. The stacked IR spectra for NCD-ca (6:1) through (1:10) as well as urea and citric acid precursors are depicted in Figure 36. Broad

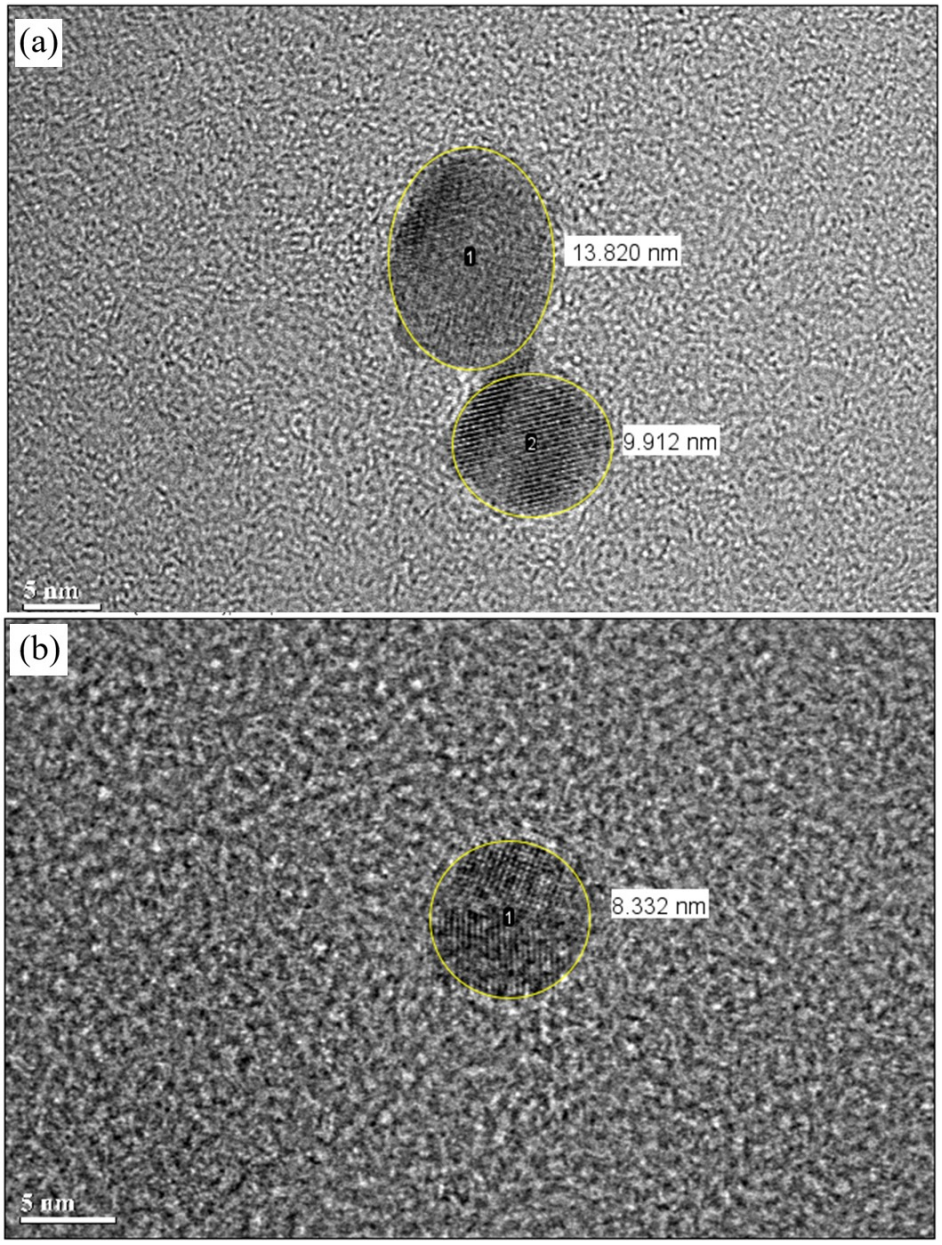


Figure 35. TEM images of NCD-ca (1:6). Both (a) and (b) are TEM of NCD-ca (1:6), showing different sizes.

absorption bands from 2500-3300 $cm^{-1}$ demonstrate clear O-H and N-H stretches in all NCD samples. The N-H stretching modes are also found in urea at 3422 and 3324 $cm^{-1}$. All NCD samples as well as urea and citric acid exhibit C=O stretches around ~1680 $cm^{-1}$, and C-O stretches around ~1150 $cm^{-1}$. Absent from citric acid, but present in all NCD samples and urea

are C=N stretches at ~1550 $cm^{-1}$and C-N stretches at ~1400 $cm^{-1}$. These results were similar to previous synthesis of NCDs from urea and citric acid by Zhang et al.[36]

**3.3.3 Optical Characterization**. Altering the carbon to dopant ratios was shown to have little effect on maximum absorbance or emission wavelengths. Zhang et al. reported this as well.[36] The following Figures 37-41 show the absorbance spectra and emission spectra at increasing excitation wavelengths of NCD-ca (6:1), (1:1), (1:3), (1:6) and (1:10). Inset images show increasingly dilute concentrations of CDs from left to right in both visible and UV light (365 nm).

NCD-ca (6:1) has a peak absorbance at ~330 nm in Figure 37a, characteristic of citric acid-based carbon dots.[36] Of interest, NCD-ca (6:1) exhibits almost no color at 1000 ppm or below as the inset image shows in Figure 37a. At higher concentrations (~2000 ppm), a slight red-orange color is exhibited at pH 7. NCD-ca (6:1) exhibits excitation-dependent fluorescence with a maximum intensity when excited at 340 nm. The emission gradually red-shifts as the excitation wavelength increases. Similar results are shown in literature.[36] NCD-ca (6:1), despite little-to-no visible color in white light at or below 1000 ppm, fluoresces blue under 365 nm UV-light (see Figure 37b). Of the prepared NCDs, NCD-ca (6:1) exhibits the least fluorescence intensity per same concentration, likely due to lesser degree of doping via urea and therefore, less fluorescence.

NCD-ca (1:1) interestingly was a green solution straight from synthesis, but over time, became increasingly darker and more purple. The color change is discussed in further sections. At present, the NCD-ca (1:1) pictured in Figure 38 is dark purple at 1000 ppm, becoming increasingly lighter purple upon dilution. Despite visual absorbance changes, at the dilute 500

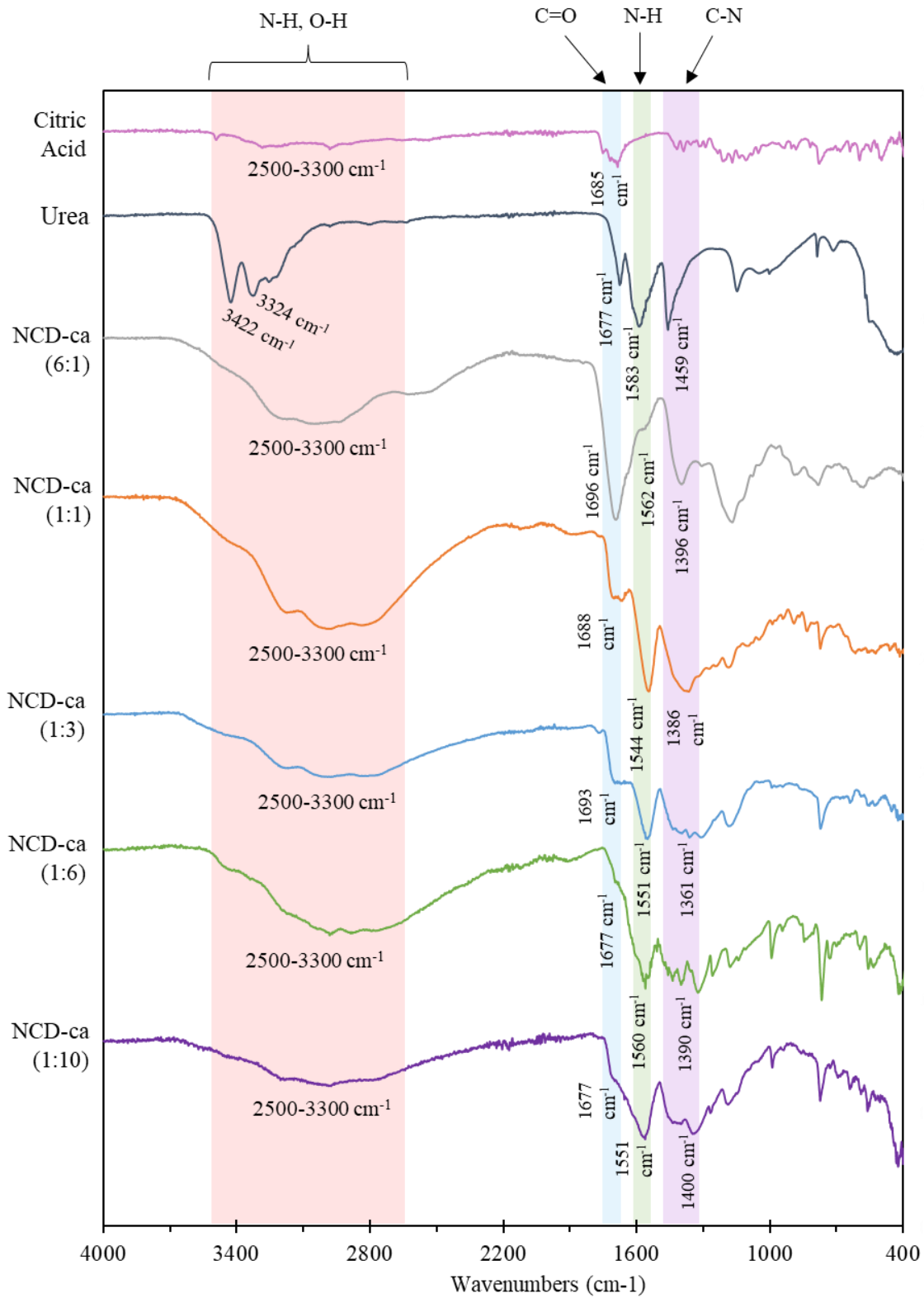


Figure 36. FT-IR of NCD-ca (6:1) through (1:10) compared to citric acid and urea.

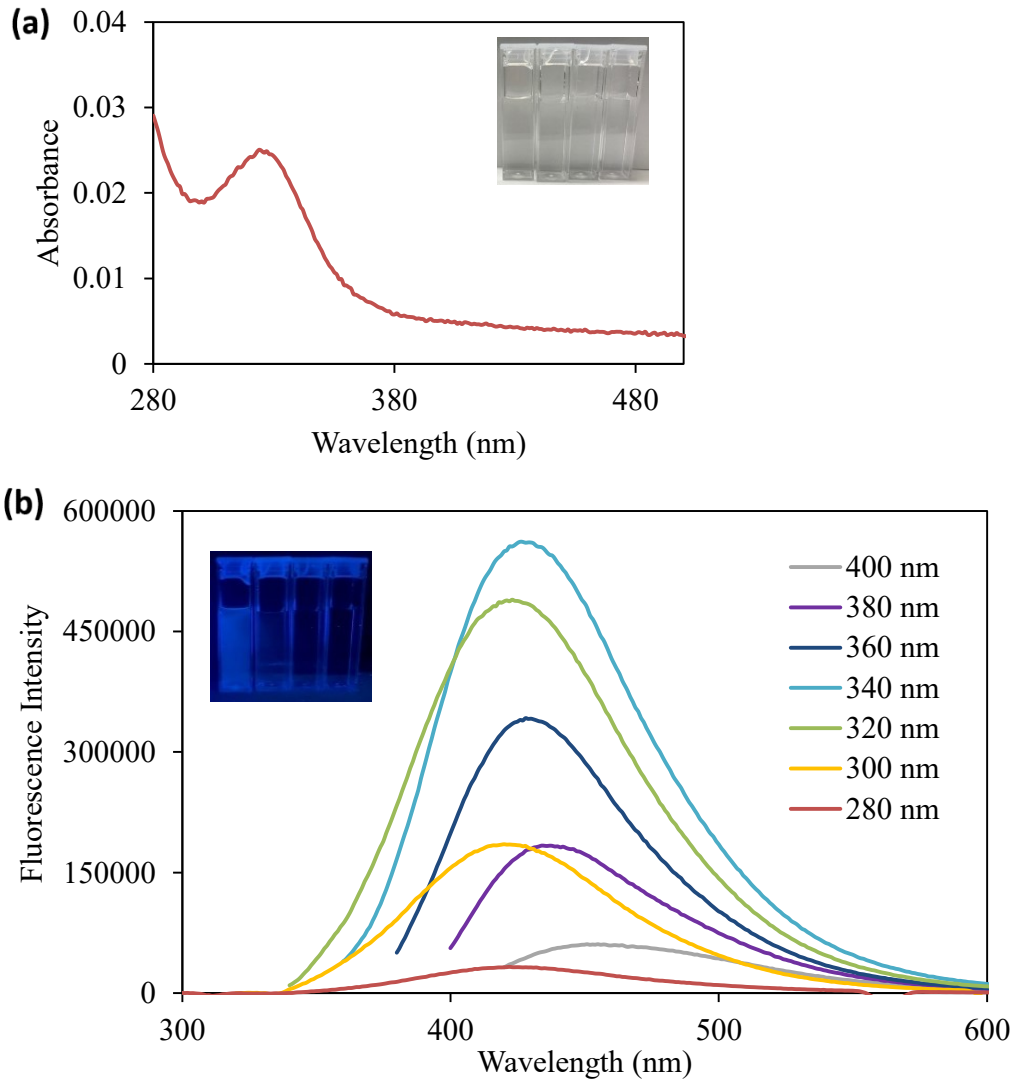


Figure 37. Absorbance and emission spectra for NCD-ca (6:1). (a) Absorbance spectrum of NCD-ca (6:1) at 50 ppm in pH 7 buffer, (b) emission spectrum of NCD-ca (6:1) in pH 7 buffer excited from 280-400 nm; inset images depict NCD-ca (6:1) at decreasing concentrations (left to right: 1000 ppm, 500 ppm, 100 ppm, 1 ppm) in (a) visible light and (b) 365 nm light.

ppb concentration used in the absorbance spectra in Figure 38a, the strong peak at 330 nm is characteristic of NCD-ca.[36] Interestingly, Zhang et al. reported brown colored CDs.

There is not much difference between the excitation-dependent emission of NCD-ca (1:1) in Figure 38b and that of NCD-ca (6:1). The excitation wavelength of 340 nm is still the highest fluorescing, with red-shifting occurring at increased excitation wavelengths. Under UV-light

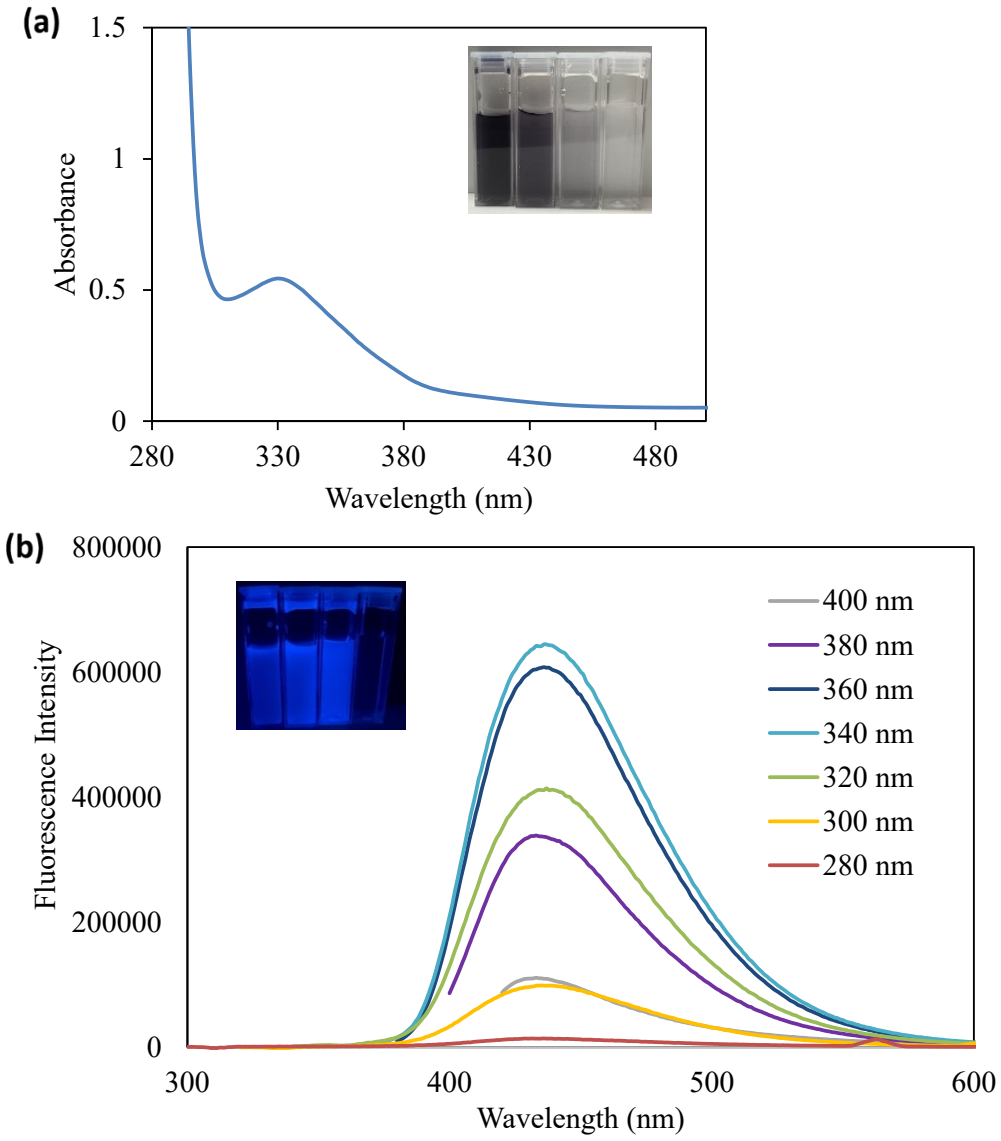


Figure 38. Absorbance and emission spectra for NCD-ca (1:1). (a) Absorbance spectrum of NCD-ca (1:1) at 500 ppb in pH 7 buffer, (b) emission spectrum of NCD-ca (1:1) in pH 7 buffer excited from 280-400 nm; inset images depict NCD-ca (1:1) at decreasing concentrations (left to right: 1000 ppm, 500 ppm, 100 ppm, 1 ppm) in (a) visible light and (b) 365 nm light.

(365 nm), NCD-ca (1:1) exhibit blue fluorescence, becoming increasingly fluorescent from 1000 ppm to 100 ppm, as the higher concentrations likely exhibit inner filter effects at such high concentrations. At 1 ppm, little to no fluorescence is apparent.

NCD-ca (1:3) showed a characteristic 330 nm absorption peak with brown colored particles (Figure 39a). Like other CD counterparts, NCD-ca (1:3) exhibits highest fluorescence when excited at 340 nm and red-shifting as the excitation wavelength is increased.

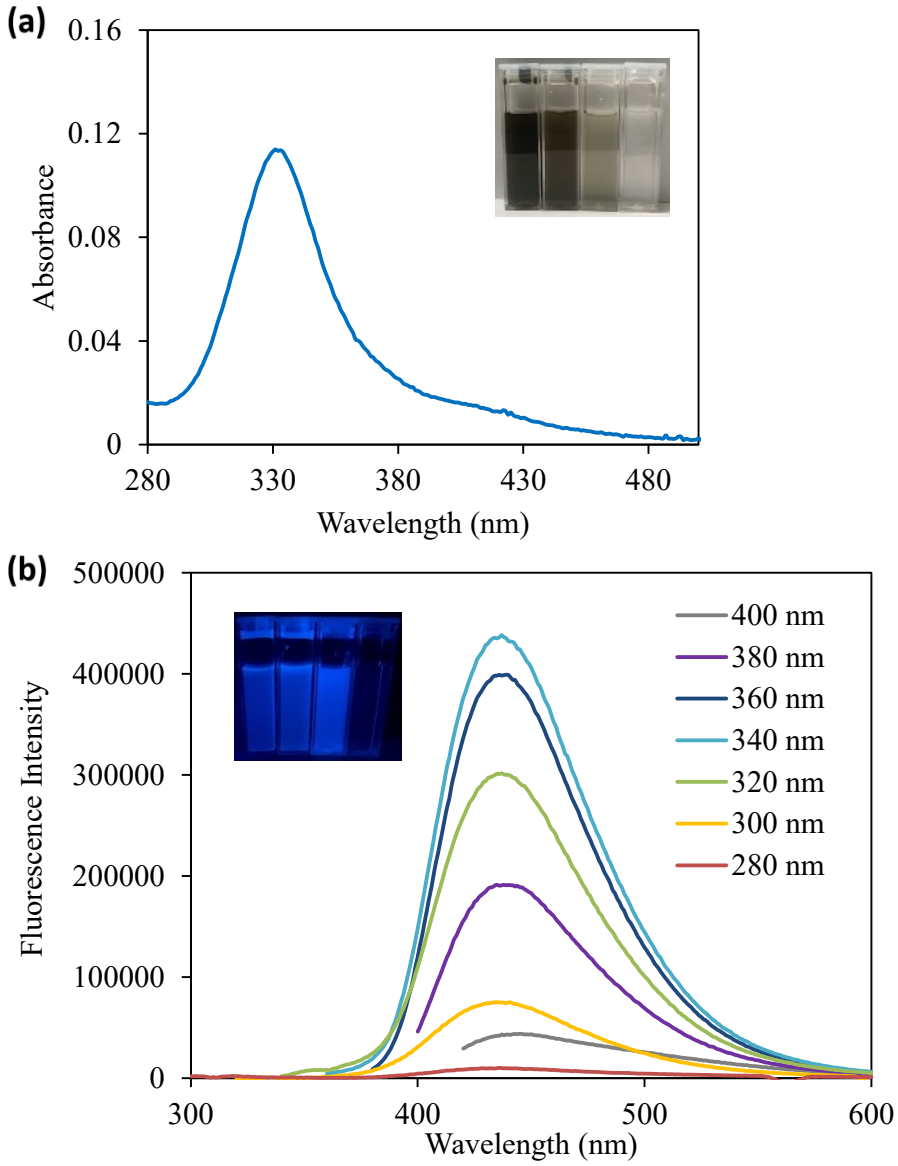


Figure 39. Absorbance and emission spectra for NCD-ca (1:3). (a) Absorbance spectrum of NCD-ca (1:3) at 5 ppm in pH 7 buffer, (b) emission spectrum of NCD-ca (1:3) in pH 7 buffer excited from 280-400 nm; inset images depict NCD-ca (1:3) at decreasing concentrations (left to right: 1000 ppm, 500 ppm, 100 ppm, 1 ppm) in (a) visible light and (b) 365 nm light.

At pH 7, the CDs fluoresce blue with the greatest observed fluorescence at 100 ppm (Figure 39b), where 500 ppm and 1000 ppm equivalents show less fluorescence likely due to inner filter effects.

NCD-ca (1:6) are orange brown colored particles with characteristic absorption near 330 nm. In comparison to lower dopant ratio counterparts, NCD-ca (1:6) has slightly higher absorbance at 340 nm (Figure 40a). The excitation-dependent emission shown in Figure 40b follows previous synthesis and reported results.[36] The CDs fluoresce highest when excited at 340 nm. As with previous CDs, the NCD-ca (1:6) has the most observed fluorescence at 100 ppm, with little to no fluorescence at 1 ppm.

Finally, NCD-ca (1:10) exhibited a brown colored solution at 1000 ppm which became more yellow upon dilution (Figure 41a). NCD-ca (1:10) have strong absorbance at 340 nm, as with the previous NCD-ca (1:6) result. This is consistent with similar reported syntheses.[36] Additionally, the observed fluorescence appears highest at 100 ppm, though the 1 ppm still shows some fluorescence indicating the potential larger fluorescent QY of NCD-ca (1:10) than NCD-ca (1:6). And although there are slight differences in the excitation-dependent emission in Figure 41b from that of other CD counterparts, the maximum fluorescence is still close at 360 or 340 nm. Similarly, red-shifting still occurs at increased excitation wavelengths.

**3.3.4 Observed Change in Absorbance in Visible Range**. After stock solutions of NCD-ca (6:1), (1:1) and (1:6) were left in room temperature storage instead of a fridge for a period of 16 days, a distinct color change was observed. The stock solutions were at pH 7, so the only factors altering the CDs were temperature and time. Since other stock solutions kept in the fridge retained their original color, and even the solid stock samples exhibited a color change, the CDs as prepared must possess temperature-dependent visible range absorbance. What, if any,

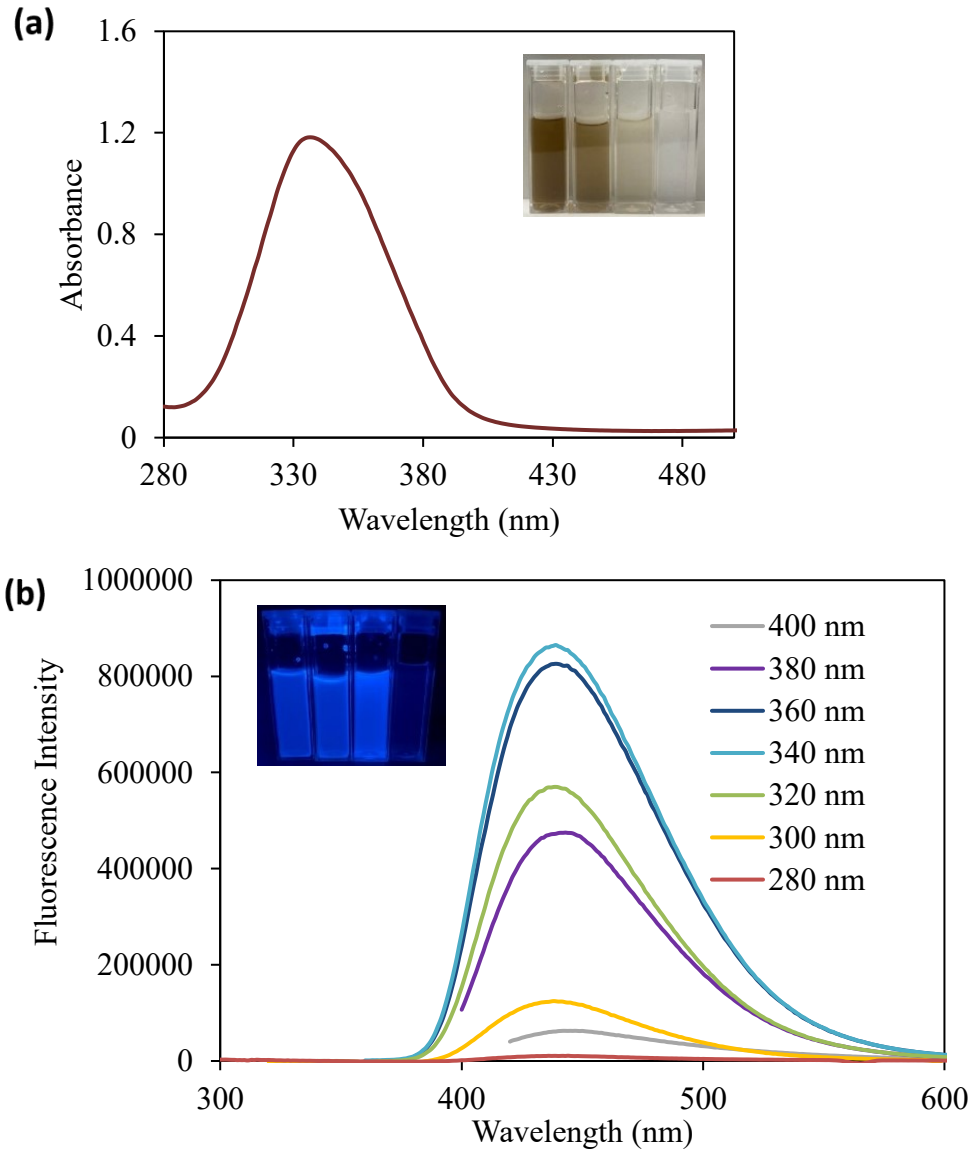


Figure 40. Absorbance and emission spectra for NCD-ca (1:6). (a) Absorbance spectrum of NCD-ca (1:6) at 50 ppb in pH 7 buffer, (b) emission spectrum of NCD-ca (1:6) in pH 7 buffer excited from 280-400 nm; inset images depict NCD-ca (1:6) at decreasing concentrations (left to right: 1000 ppm, 500 ppm, 100 ppm, 1 ppm) in (a) visible light and (b) 365 nm light.

effect this unexpected property had on QY had to be investigated. Data was limited to absorbance spectra collected from initial syntheses. Therefore, although calculating the QY of the original versus color changed species would definitively confirm if the color change would affect fluorescence, a more qualitative approach was taken. In this way, previously collected

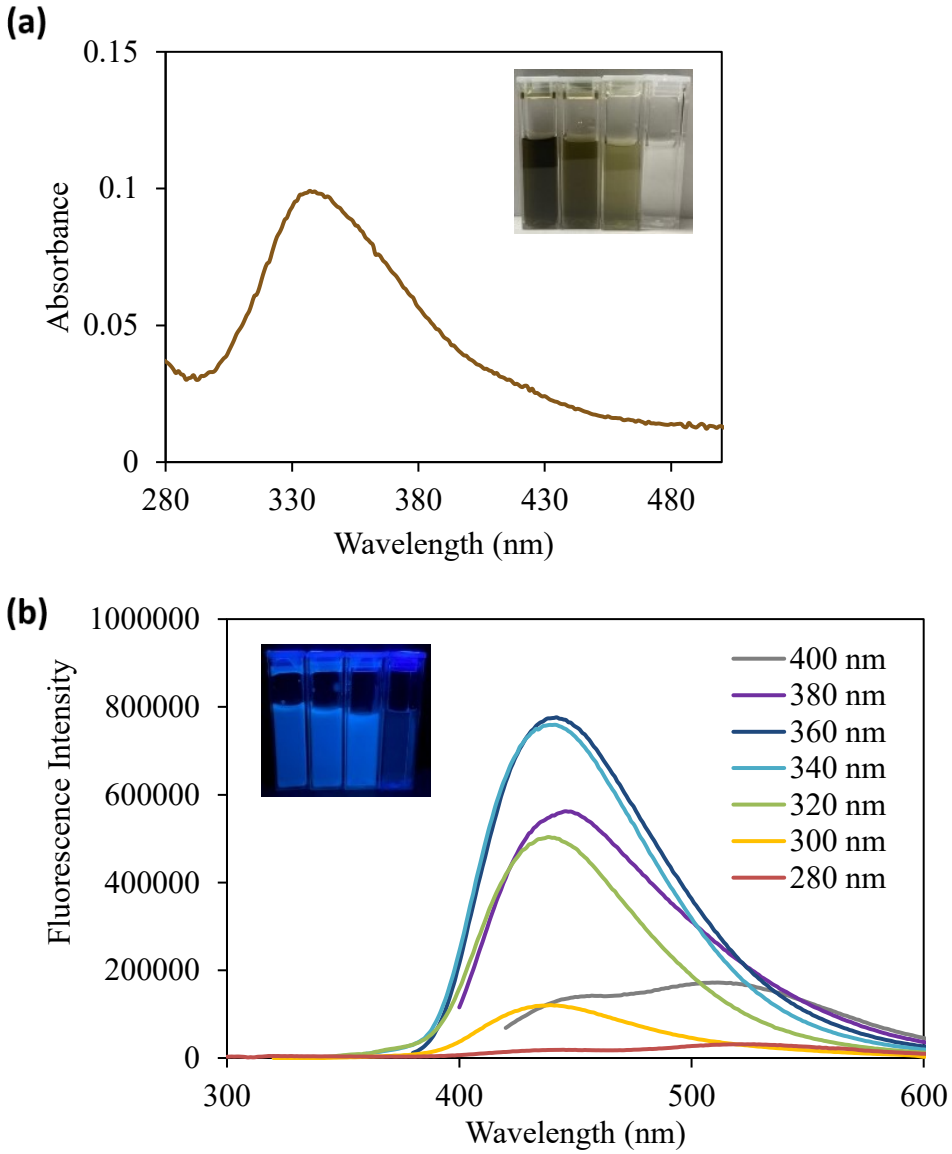


Figure 41. Absorbance and emission spectra for NCD-ca (1:10). (a) Absorbance spectrum of NCD-ca (1:10) at 5 ppm in pH 7 buffer, (b) emission spectrum of NCD-ca (1:10) in pH 7 buffer excited from 280-400 nm; inset images depict NCD-ca (1:10) at decreasing concentrations (left to right: 1000 ppm, 500 ppm, 100 ppm, 1 ppm) in (a) visible light and (b) 365 nm light.

absorbance in the visible and UV range and emission spectra were gathered and additional measurements were procured for the color change species.

NCD-ca (6:1) originally exhibited a slight red color in pH 7 as a stock solution. Upon sitting for 16 days in room temperature, the solution became more of a yellow brown. Figure 42b

depicts the color change in the inset images. There is a distinct drop in absorbance in the visible range from the original to the color change. Most importantly, however, the absorbance

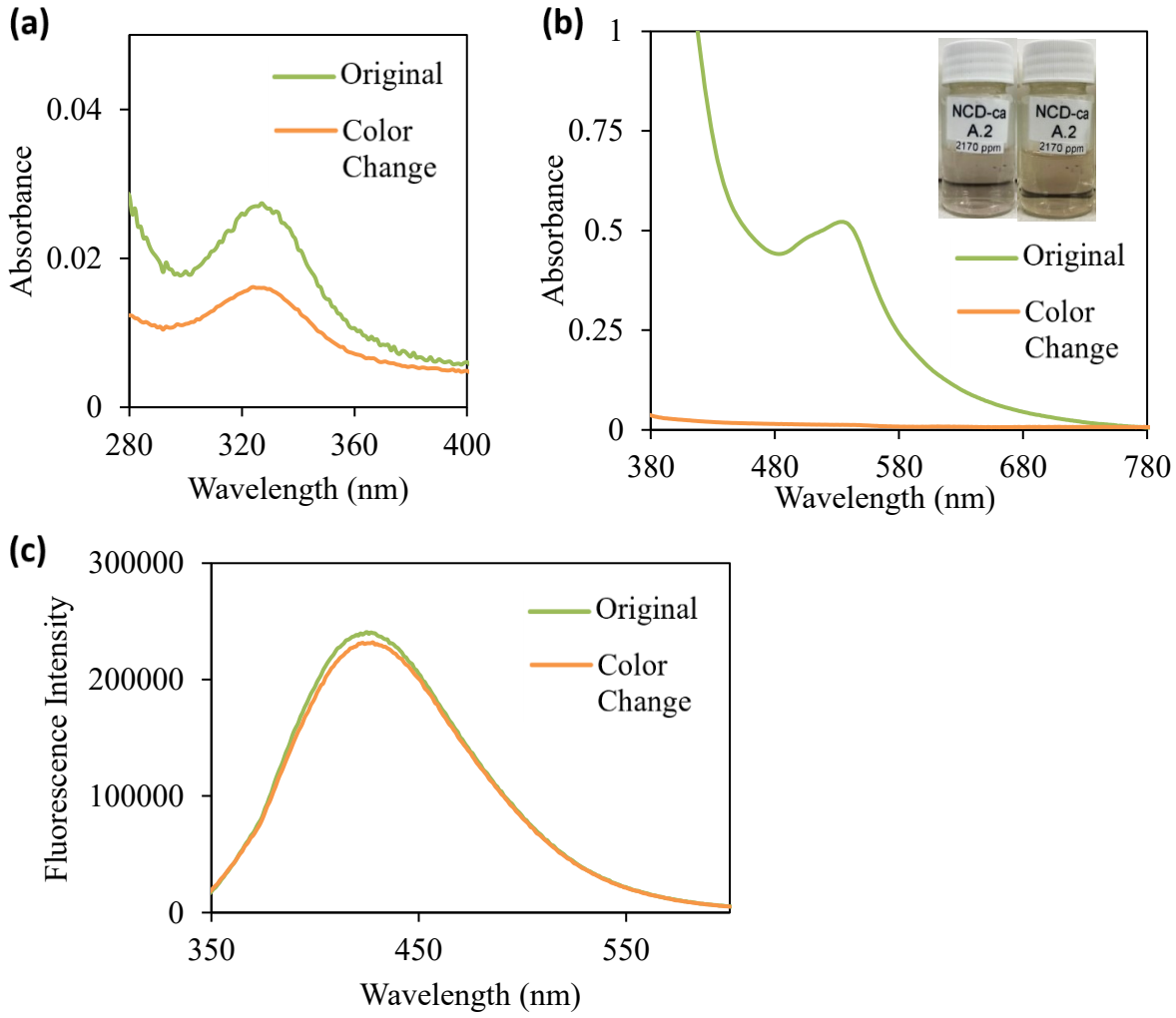


Figure 42. Color change in visible absorbance spectra of NCD-ca (6:1). Absorbance spectra of NCD-ca (6:1) in pH 7 in the (a) UV region, (b) visible region (inset images of 2170 ppm NCD-ca (6:1) in pH 7 freshly prepared, left, and after 16 days in room temperature, right), and (c) fluorescence spectra (excited at 330 nm). Green lines indicate the original samples freshly dissolved from lyophilized solids (at 50 ppm for (a) and (c) and 2170 ppm for (b)), orange lines indicate the samples that changed color after 16 days in room temperature (50 ppb for (a) and (c) and 2170 ppm for (b)).

maximum in the ultra-violet range did not change and still had a 330 nm peak despite a color

change. Similarly, the fluorescence is largely the same when excited at that maximum absorbance, suggesting visible range absorbance may be the only affected behavior from prolonged temperature change. Additionally, because the fluorescence properties of the NCD-ca are due to excitation in the UV-range, any alteration in visible range does not directly affect the fluorescence, and therefore does not directly affect the QY.

NCD-ca (1:1), which originally exhibited a bright green colored solution, turned a dark purple colored solution upon exposure to room temperature for 16 days as shown in the inset images in Figure 43. The original CD solution has absorbance peaks around 600 nm (red) and 400 nm (violet) which confirms its green color. Similarly, the color change CDs have strong absorbance around 550 nm (green) which confirms their purple color.

Most importantly, although there is a distinct color change, the absorbance peak within the UV range and the resulting emission spectra are unchanged between NCD-ca (1:1) samples. Just as with NCD-ca (6:1), this indicates the color change due to exposure to prolonged higher temperatures does not affect the UV-vis range, and therefore does not likely affect the QY.

Finally, the color change of NCD-ca (1:6) was investigated after exposure to warmer temperatures (see Figure 44). The original CDs were strongly green, as evidenced by the large absorbance around 400 nm (violet) and at 650 nm (red). The color change is clearly expressed as the absorbance at 650 nm and 400 nm all but disappears.

Just as with the previous CD equivalents, the distinct lack of change in UV range absorbance between the original and color change NCD-ca (1:6) likely means the QY is unaffected by exposure to long term warmer temperatures at pH 7.

**3.3.5 Fluorescence Dependence on pH**. As NCD-ca have myriad surface functional groups, they are sensitive to pH environment. Herein, the pH-dependent fluorescence is

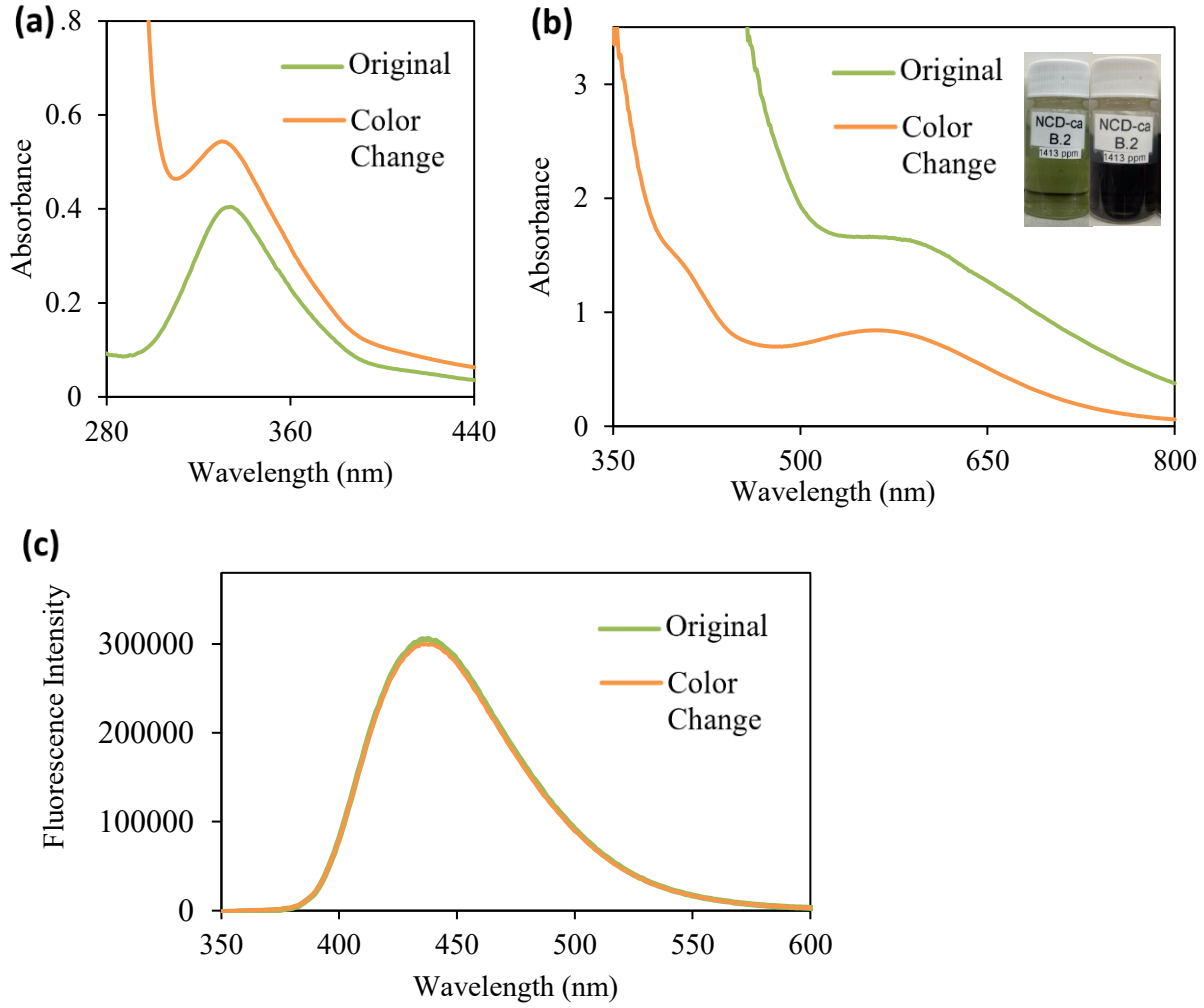


Figure 43. Color change in visible absorbance spectra of NCD-ca (1:1). Absorbance spectra of NCD-ca (1:1) in pH 7 in the (a) UV region, (b) visible region (inset images of 1413 ppm NCD-ca (1:1) in pH 7 freshly prepared, left, and after 16 days in room temperature, right), and (c) fluorescence spectra (excited at 335 nm). Green lines indicate the original samples freshly dissolved from lyophilized solids (at 50 ppm for (a) and (c) and 1413 ppm for (b)), orange lines indicate the samples that changed color after 16 days in room temperature (50 ppb for (a) and (c) and 1413 ppm for (b)).

presented for NCD-ca (6:1) through (1:10) at pH 1-13. Of note, inset images show the same concentration equivalents of each NCD-ca sample in pH 2, 7, and 13 under visible and UV-light.

NCD-ca (6:1) exhibits absorbances around 300 nm, with no clear change in color in visible light (Figure 45a). Its fluorescence is greatly increased from acidic to basic pHs, with pH 11 being the highest fluorescing pH media for NCD-ca (6:1). This follows the expected trend of

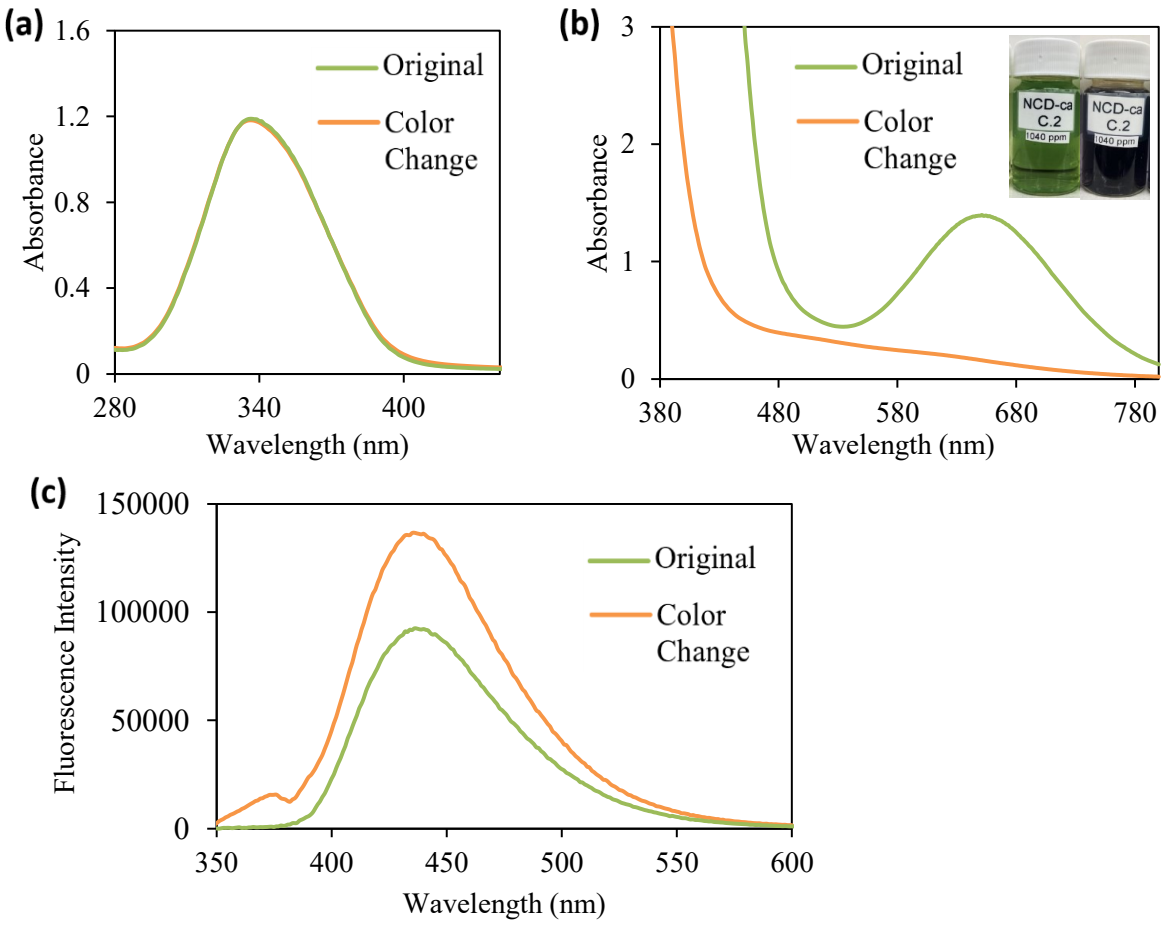


Figure 44. Color change in visible absorbance spectra of NCD-ca (1:6). Absorbance spectra of NCD-ca (1:6) in pH 7 in the (a) UV region, (b) visible region (inset images of 1040 ppm NCD-ca (1:6) in pH 7 freshly prepared, left, and after 16 days in room temperature, right), and (c) fluorescence spectra (excited at 337 nm). Green lines indicate the original samples freshly dissolved from lyophilized solids (at 50 ppm for (a) and (c) and 1040 ppm for (b)), orange lines indicate the samples that changed color after 16 days in room temperature (50 ppb for (a) and (c) and 1040 ppm for (b)).

increased fluorescence in basic media as amine groups are deprotonated from their acidic -$NH^{3+}$ forms in acidic media, and carboxylic acids are deprotonated to -$COO^-$. Similar results were shown by Liu et al. with urea doped sucrose-based carbon dots[4]. Likewise, they attributed the increase in fluorescence to a decreasing energy loss from "non-radiative recombination" made possible by the negative surface shell formed from the deprotonation of carboxylic acids in

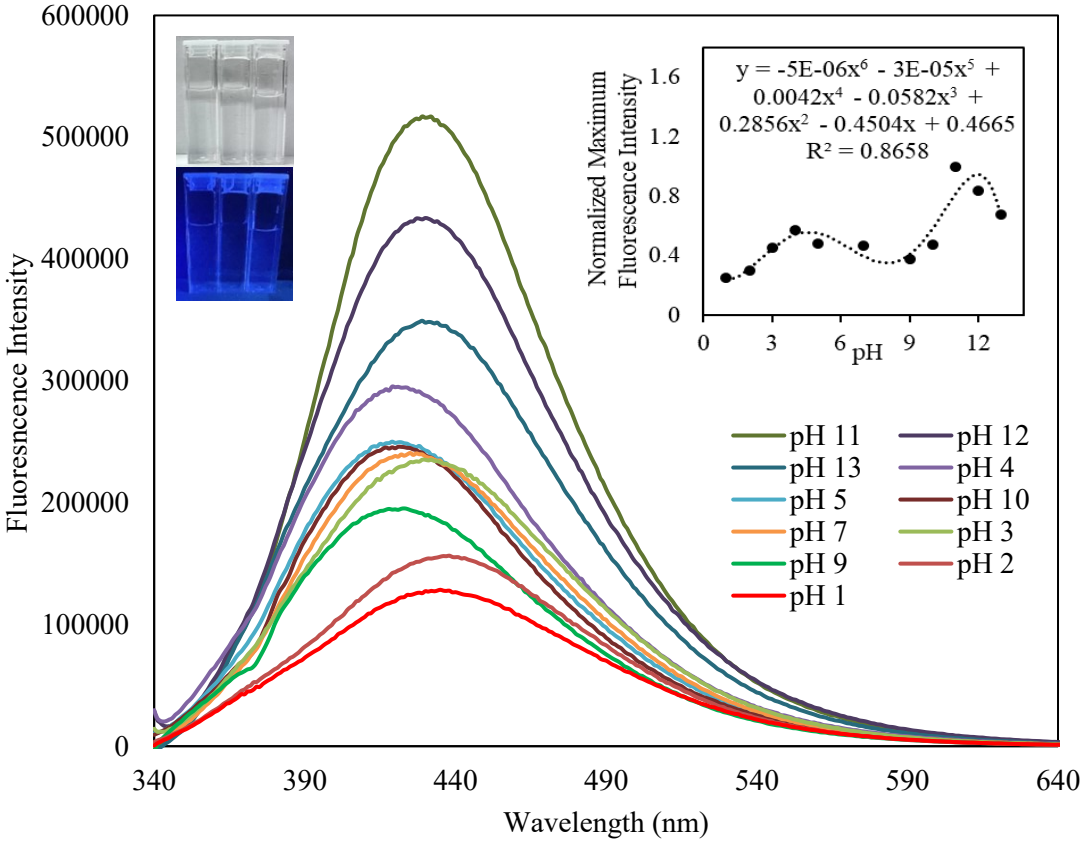


Figure 45. Emission spectra of NCD-ca (6:1) at pH 1-13 at 50 ppm. Inset images: NCD-ca (6:1) at 100 ppm (left to right: pH 2, pH 7, pH 13), in visible light, and 365 nm light; pH-dependent fluorescence polynomic trend plot.

basic media.[4] The observed fluorescence in the inset image in Figure 45b shows only slight fluorescence at 100 ppm in pH 11. Both pH 2 and 7 are largely non-fluorescent at that low of a concentration.

NCD-ca (1:1) had largely increased absorbances from pH 5-13, though the wavelength of maximum absorbance was largely unchanged in Figure 46. Notably, the purple color of NCD-ca (1:1) in exposed to room temperature for 16 days is only purple at pH 7. At pH 11, the color is light yellow, and at pH 2, a light orange. Emission spectra largely follow a trend toward

increased fluorescence with basic media. This is visually confirmed by the larger fluorescence intensity in pH 7 and pH 11 of Figure 46 inset images than that of pH 2.

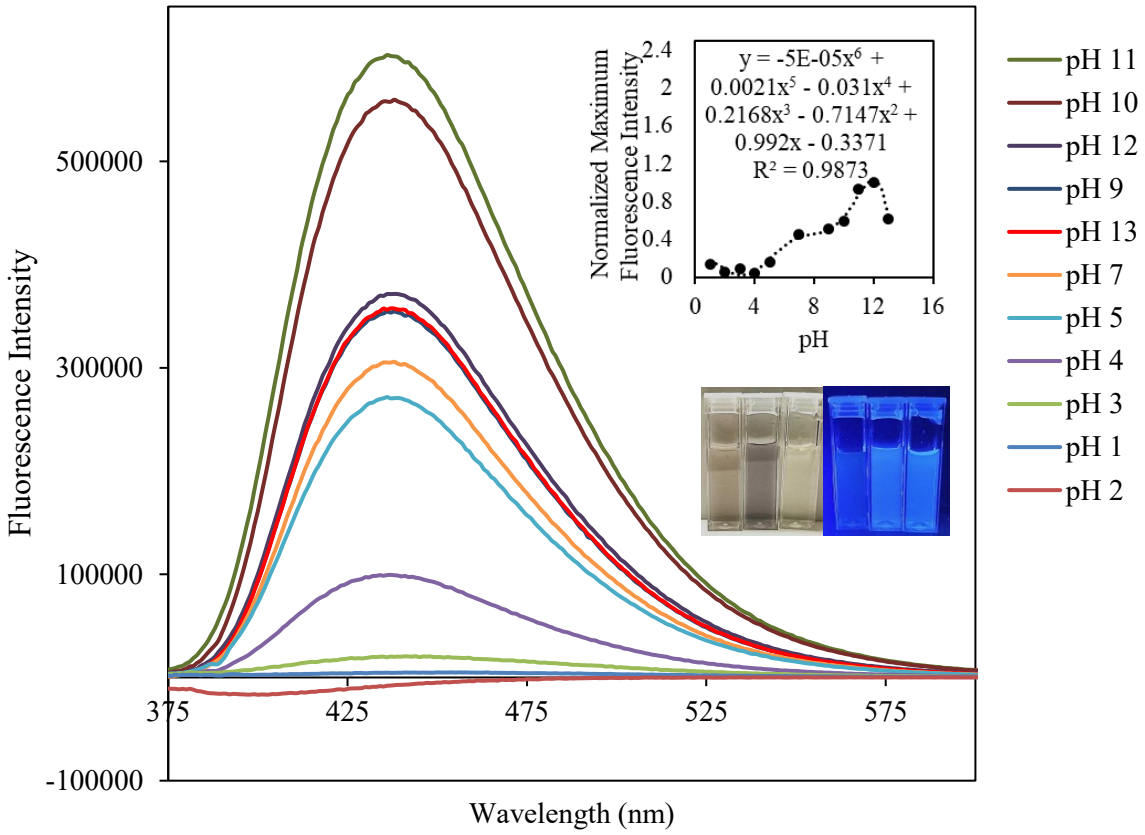


Figure 46. Emission spectra of NCD-ca (1:1) at pH 1-13 at 500 ppb. Inset images: NCD-ca (1:1) at 100 ppm (left to right: pH 2, pH 7, pH 13), in visible light, and 365 nm light; pH-dependent fluorescence polynomic trend plot.

NCD-ca (1:3), largely follows an increased absorbance and fluorescence intensity from pH 1-13 (Figure 47) with the highest fluorescence as pH 10. Slightly lower fluorescence was about equal for pH 11, 12 and 13, indicating NCD-ca (1:3) like other NCDs fluoresce best in basic media. The inset images in Figure 47a show a brown color in pH 2, gray color in pH 7, and yellow in pH 2. Similarly, the fluorescence at pH 7 and pH 11 look largely the same in the inset

image in Figure 47b, though unlike previous NCD counterparts, the pH 2 NCD-ca (1:6) shows some fluorescence despite comparative concentrations. This demonstrates the stark fluorescent capability of higher doped carbon dots in comparison to lower dopant CDs. Based on these results, the QY is expected to increase as the dopant ratio increases.

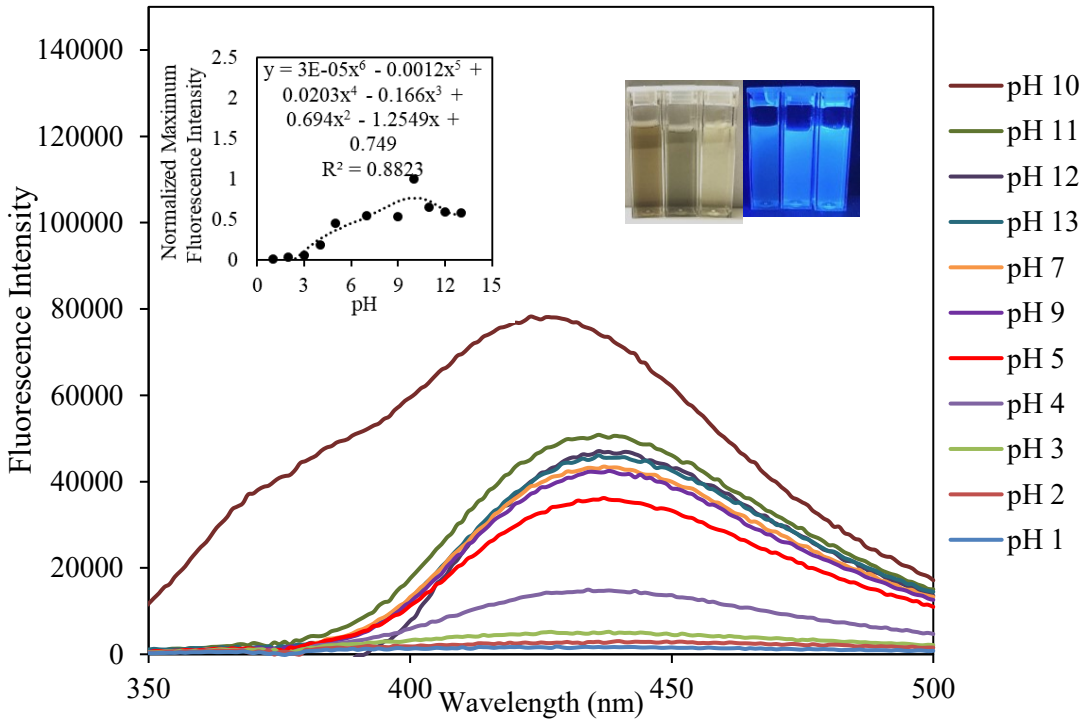


Figure 47. Emission spectra of NCD-ca (1:3) at pH 1-13 at 50 ppb. Inset images: NCD-ca (1:3) at 100 ppm (left to right: pH 2, pH 7, pH 13), in visible light, and 365 nm light; pH-dependent fluorescence polynomic trend plot.

NCD-ca (1:6) also demonstrated increased absorbance from pH 5-13, as shown in the inset image in Figure 48. The other inset images in Figure 48 show a slight change in color from pH 7 (yellow) to pH 2 (orange). The pH 11 closely resembled pH 7 in color under white light. As with previous NCDs, fluorescence intensity was largely dependent on pH, whereby the fluorescence is highest in basic media from pH 7-11.

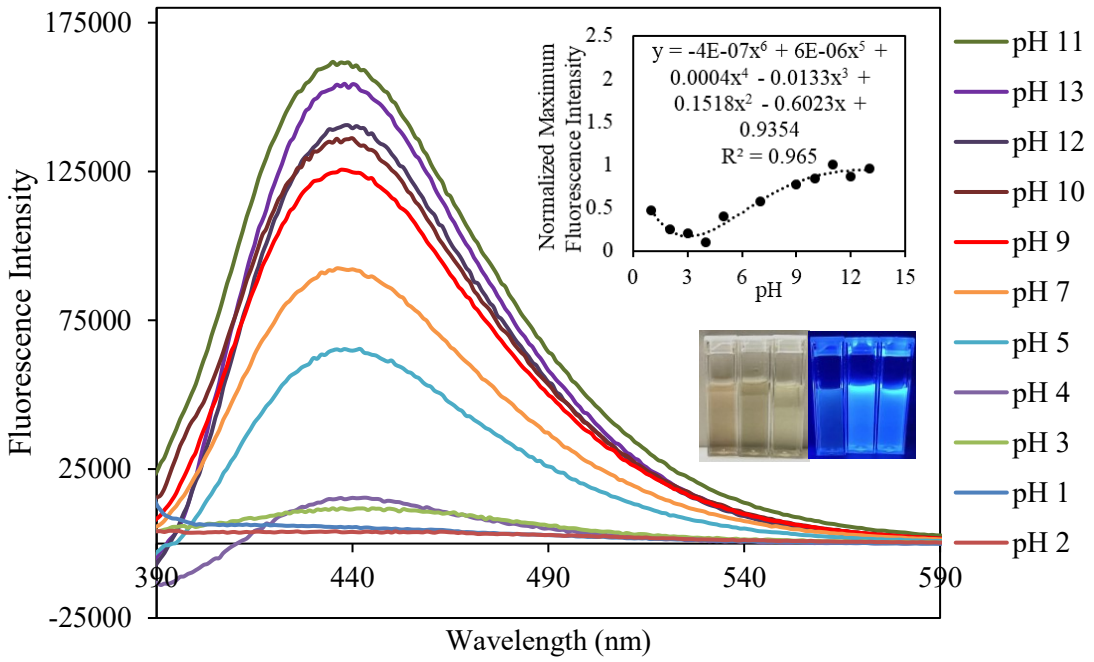


Figure 48. Emission spectra of NCD-ca (1:6) at pH 1-13**;** inset images: NCD-ca (1:6) at 100 ppm (left to right: pH 2, pH 7, pH 13), in visible light and 365 nm light.

Finally, NCD-ca (1:10) likewise exhibits increased absorbance and fluorescence intensity in increasingly basic media. However, the maximum emission wavelengths are largely unchanged. The pH 13 in Figure 49b does not visually match all other iterations and can likely be attributed to possible sample contamination for that pH. Most notably, the color of fluorescence emission in Figure 48 is green in pH 2, and blue in pH 7 and 13. Though blue fluorescence is largely expected for the CDs, green fluorescence at low pHs is of interest.

**3.3.6 Quantum Yield**. The culmination of this project is the calculation of QY for the varying carbon to dopant molar ratio CDs. With these numbers, the definitive CD composition can be chosen for optimized fluorescence intensity. Likewise, as QY is a quantitative character that allows researchers to be easily compare fluorescent species, it is a vital step in communicating advances in fluorescent materials.

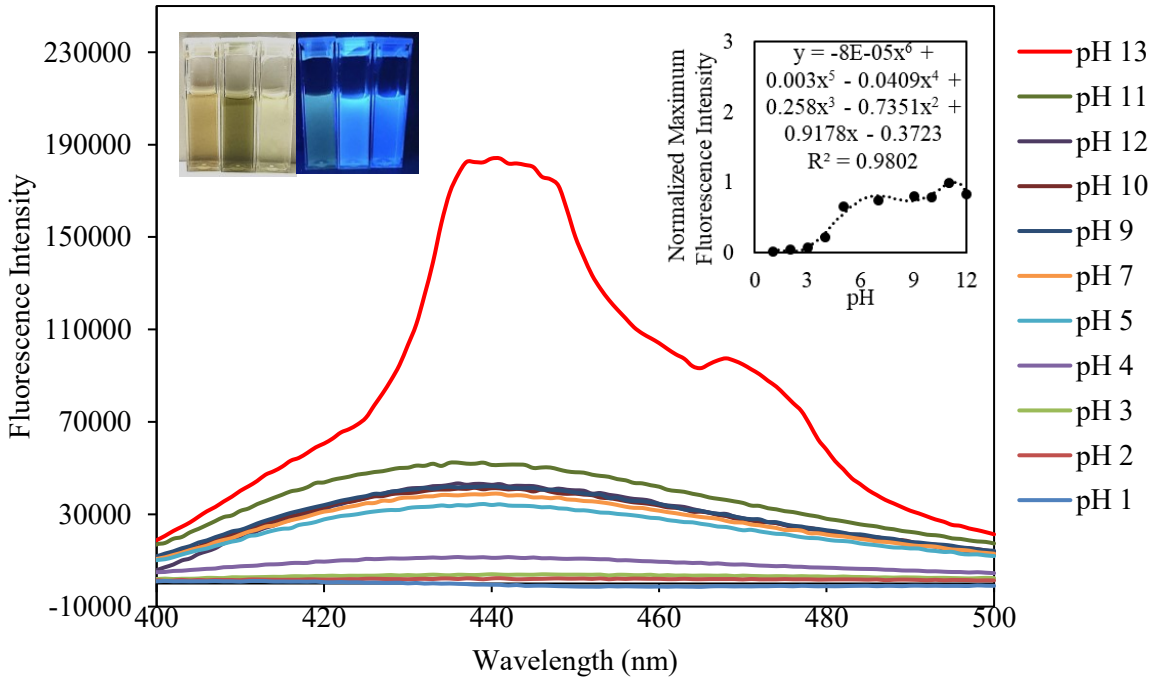


Figure 49. Emission spectra of NCD-ca (1:10) at pH 1-13 at 50 ppb. Inset images: NCD-ca (1:10) at 100 ppm (left to right: pH 2, pH 7, pH 13), in visible light and 365 nm light; pH-dependent fluorescence polynomic trend plot.

In the final portion of this project, the QY of NCD-ca (6:1) through (1:10) were calculated for buffered pH 2, 5, 7, 11, and 13 solutions without further purification. The QYs were calculated in reference to quinine sulfate and the results are tabulated in Figure 50.

Of the five CD samples, NCD-ca (6:1) has the lowest molar ratio of urea dopant. Likewise, it also has the lowest overall QYs, exhibiting a general decrease in QY with increases in pH from 2-13. It's highest QY is in pH 2 (4.22%) and lowest in pH 7 (1.40%). These results are lower than the 8.9% reported for a NCD-ca (6:1) by Zhang et al.[36]

Unsurprisingly, NCD-ca (1:1) had an overall increased QY from that of NCD-ca (6:1), largely due to increased $NH_2$ groups from an increased urea dopant ratio. The highest QY was in

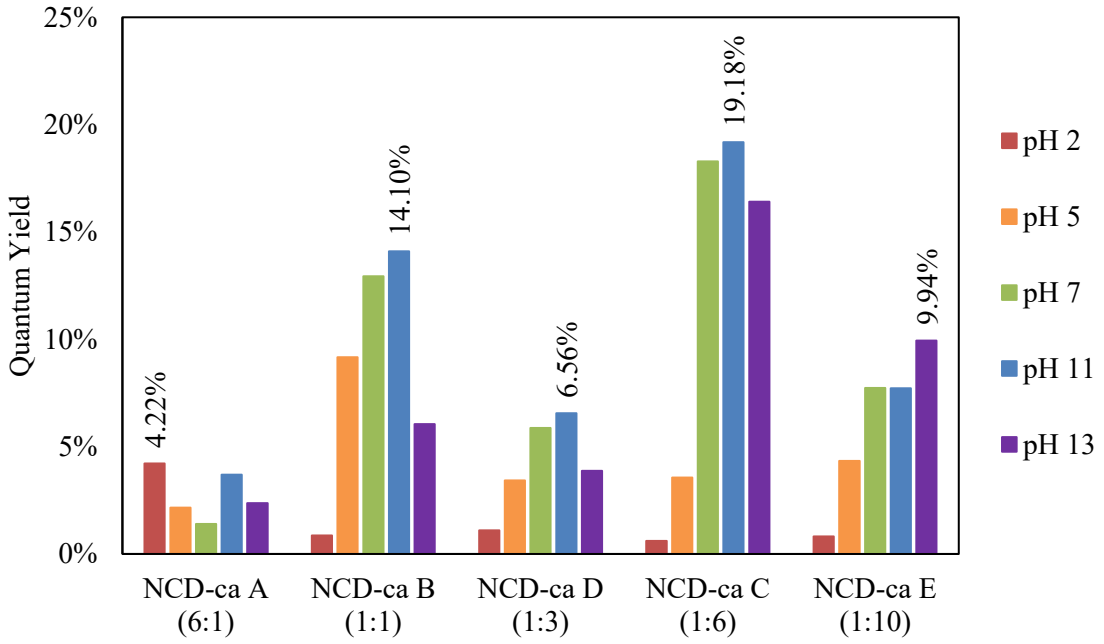


Figure 50. Quantum yield of NCD-ca (6:1) through (1:10) at pH 2, 5, 7, 11, 13. All samples in respective pH buffers and highest QY labeled for each sample.

pH 11 (14.10%) while the lowest was in pH 2 (0.89%). Though pH 13 should have been more fluorescent, its lower QY may be attributed to the harsher environment of a pH 13 medium.

An unexpected drop in overall QY was observed in NCD-ca (1:3), though it should have theoretically been higher in QY since it had more N dopant. One consideration that may account for the decreased QY is that both NCD-ca (1:3) and NCD-ca (1:10) were synthesized months after the other three CD samples. Therefore, if QY is not as stable as expressed in literature with CDs photostability, the QYs may be too low for the newer samples or too high for the older samples. Further studies in photostability are needed to elucidate that theory. NCD-ca (1:3) has the highest QY in pH 11 (6.56%) and the lowest in pH 2 (1.10%).

NCD-ca (1:6) has the highest QY of all prepared CDs, making its composition, the best choice. The highest QY is at pH 11 (19.18%) and the lowest QY at pH 2 (0.60%). Zhang et al.

reported a QY of 20% for their NCD-ca (1:6), which aligns with these results.

Finally, though the NCD-ca (1:10) was theorized to have an even higher overall QY due to the largest amount of urea dopant, it is only slightly above NCD-ca (1:3). The highest QY is at pH 13 (9.94%) and lowest at pH 2 (0.81%).

Overall, NCDs exhibit lowest lower QYs in acidic media and higher QYs in basic media. Except for NCD-ca (6:1), NCDs exhibit only slightly lower fluorescence in pH 7 than in basic media. Therefore, to avoid harsher chemicals required for higher alkaline environments, a small decrease in QY can be traded for mild, neutral conditions.

# CHAPTER 4: CONCLUSION

Through this project, the quantum yield of carbon dots was optimized. First, the best synthetic method was determined to be the digestive microwave because it could rapidly produce CDs in a facile and easily reproducible method. Next, the starting materials, both carbon source and dopant, were chosen with consideration for tuning electronic properties of CDs. Though sucrose was used in the successful synthesis of NCDs, the NCD-ca was the superior choice as less carbonization occurred at same temperatures, allowing for more facile purification. Likewise, the resulting CD-ca had higher QYs. Therefore, citric acid was the best carbon source. Additionally, by doping with the heteroatomic impurities, N, B, and S, the synthesized doped CDs exhibited increased fluorescence, especially with the use of urea for the N dopant source. Consequently, the highest QY of 19.18% for microwave-produced NCD-ca demonstrates the ideal carbon to dopant source combination with a 1:6 ratio of citric acid to urea. The other dopants, sodium tetraborate, boric acid or sodium thiosulfate were inferior to the performance of urea as a dopant. As of now, the use of sodium tetraborate or boric acid are poor dopant sources for both citric acid and sucrose-based carbon dots, without co-doping. Likewise, sodium thiosulfate is a weak dopant source.

The fluorescent properties of the CDs were particularly interesting for their dependence on pH. As is, the CDs are most fluorescent in neutral and basic pHs, showing polynomic trends in pH-dependent fluorescence. CDs could then be used in biological applications where higher fluorescence in neutral pHs is desired.

Overall, the future of this project would be to run column chromatography to ensure all byproducts were removed during dialysis in order to amend the synthetic method for future syntheses. Additionally, further characterizations of the CDs including conducting X-ray

photoelectron spectroscopy (XPS), photostability tests, and biocompatibility would add to this project. Likewise, developing an application for the CDs beyond a pH-sensor would be of increased interest. Finally, the effects of co-doping or different N dopant sources as well utilizing larger MWCO during dialysis would greatly benefit this research.

## REFERENCES


(1) Nagarajan, R. Nanoparticles: Building Blocks for Nanotechnology. In *Nanoparticles: Synthesis, Stabilization, Passivation, and Functionalization*; ACS Symposium Series; American Chemical Society, 2008; Vol. 996, pp 2–14. https://doi.org/10.1021/bk-2008-0996.ch001.

(2) Khan, I.; Saeed, K.; Khan, I. Nanoparticles: Properties, Applications and Toxicities. *Arab. J. Chem.* 2019, *12* (7), 908–931. https://doi.org/10.1016/j.arabjc.2017.05.011.

(3) Sagbas, S.; Sahiner, N. 22 - Carbon Dots: Preparation, Properties, and Application. In *Nanocarbon and its Composites*; Khan, A., Jawaid, M., Inamuddin, Asiri, A. M., Eds.; Woodhead Publishing Series in Composites Science and Engineering; Woodhead Publishing, 2019; pp 651–676. https://doi.org/10.1016/B978-0-08-102509-3.00022-5.

(4) Liu, X.; Liu, J.; Zheng, B.; Yan, L.; Dai, J.; Zhuang, Z.; Du, J.; Guo, Y.; Xiao, D. N-Doped Carbon Dots: Green and Efficient Synthesis on a Large-Scale and Their Application in Fluorescent PH Sensing. *New J. Chem.* 2017, *41* (19), 10607–10612. https://doi.org/10.1039/C7NJ01889D.

(5) Sun, X.; Lei, Y. Fluorescent Carbon Dots and Their Sensing Applications. *TrAC Trends Anal. Chem.* 2017, *89*, 163–180. https://doi.org/10.1016/j.trac.2017.02.001.

(6) Wang, D.; Wang, Z.; Zhan, Q.; Pu, Y.; Wang, J.-X.; Foster, N. R.; Dai, L. Facile and Scalable Preparation of Fluorescent Carbon Dots for Multifunctional Applications. *Engineering* 2017, *3* (3), 402–408. https://doi.org/10.1016/J.ENG.2017.03.014.

(7) Shi, H.; Wei, J.; Qiang, L.; Chen, X.; Meng, X. *Fluorescent Carbon Dots for Bioimaging and Biosensing Applications*. https://doi.org/info:doi/10.1166/jbn.2014.1881.

(8) Wang, Q.; Huang, X.; Long, Y.; Wang, X.; Zhang, H.; Zhu, R.; Liang, L.; Teng, P.; Zheng, H. Hollow Luminescent Carbon Dots for Drug Delivery. *Carbon* 2013, *59*, 192–199. https://doi.org/10.1016/j.carbon.2013.03.009.

(9) Zuo, J.; Jiang, T.; Zhao, X.; Xiong, X.; Xiao, S.; Zhu, Z. Preparation and Application of Fluorescent Carbon Dots. *J. Nanomater.* 2015, *2015*, 1–13. https://doi.org/10.1155/2015/787862.

(10) Xu, X.; Ray, R.; Gu, Y.; Ploehn, H. J.; Gearheart, L.; Raker, K.; Scrivens, W. A. Electrophoretic Analysis and Purification of Fluorescent Single-Walled Carbon Nanotube Fragments. *J. Am. Chem. Soc.* 2004, *126* (40), 12736–12737. https://doi.org/10.1021/ja040082h.

(11) Sun, Y.-P.; Zhou, B.; Lin, Y.; Wang, W.; Fernando, K. A. S.; Pathak, P.; Meziani, M. J.; Harruff, B. A.; Wang, X.; Wang, H.; Luo, P. G.; Yang, H.; Kose, M. E.; Chen, B.; Veca, L.

M.; Xie, S.-Y. Quantum-Sized Carbon Dots for Bright and Colorful Photoluminescence. *J. Am. Chem. Soc.* 2006, *128* (24), 7756–7757. https://doi.org/10.1021/ja062677d.

(12) Lim, C. S.; Hola, K.; Ambrosi, A.; Zboril, R.; Pumera, M. Graphene and Carbon Quantum Dots Electrochemistry. *Electrochem. Commun.* 2015, *52*, 75–79. https://doi.org/10.1016/j.elecom.2015.01.023.

(13) Sarkar, S.; Gandla, D.; Venkatesh, Y.; Bangal, P. R.; Ghosh, S.; Yang, Y.; Misra, S. Graphene Quantum Dots from Graphite by Liquid Exfoliation Showing Excitation-Independent Emission, Fluorescence Upconversion and Delayed Fluorescence. *Phys. Chem. Chem. Phys.* 2016, *18* (31), 21278–21287. https://doi.org/10.1039/C6CP01528J.

(14) Essner, J. B.; Kist, J. A.; Polo-Parada, L.; Baker, G. A. Artifacts and Errors Associated with the Ubiquitous Presence of Fluorescent Impurities in Carbon Nanodots. *Chem. Mater.* 2018, *30* (6), 1878–1887. https://doi.org/10.1021/acs.chemmater.7b04446.

(15) Tuerhong, M.; Xu, Y.; Yin, X.-B. Review on Carbon Dots and Their Applications. *Chin. J. Anal. Chem.* 2017, *45* (1), 139–150. https://doi.org/10.1016/S1872-2040(16)60990-8.

(16) Yuan, T.; Meng, T.; He, P.; Shi, Y.; Li, Y.; Li, X.; Fan, L.; Yang, S. Carbon Quantum Dots: An Emerging Material for Optoelectronic Applications. *J. Mater. Chem. C* 2019, *7* (23), 6820–6835. https://doi.org/10.1039/C9TC01730E.

(17) Ng, S. M. 12 - Carbon Dots as Optical Nanoprobes for Biosensors. In *Nanobiosensors for Biomolecular Targeting*; Gopinath, S. C. B., Lakshmipriya, T., Eds.; Micro and Nano Technologies; Elsevier, 2019; pp 269–300. https://doi.org/10.1016/B978-0-12-813900-4.00012-9.

(18) Zhu, S.; Song, Y.; Zhao, X.; Shao, J.; Zhang, J.; Yang, B. The Photoluminescence Mechanism in Carbon Dots (Graphene Quantum Dots, Carbon Nanodots, and Polymer Dots): Current State and Future Perspective. *Nano Res.* 2015, *8* (2), 355–381. https://doi.org/10.1007/s12274-014-0644-3.

(19) Song, Y.; Zhu, S.; Zhang, S.; Fu, Y.; Wang, L.; Zhao, X.; Yang, B. Investigation from Chemical Structure to Photoluminescent Mechanism: A Type of Carbon Dots from the Pyrolysis of Citric Acid and an Amine. *J. Mater. Chem. C* 2015, *3* (23), 5976–5984. https://doi.org/10.1039/C5TC00813A.

(20) Tepliakov, N. V.; Kundelev, E. V.; Khavlyuk, P. D.; Xiong, Y.; Leonov, M. Yu.; Zhu, W.; Baranov, A. V.; Fedorov, A. V.; Rogach, A. L.; Rukhlenko, I. D. Sp2–Sp3-Hybridized Atomic Domains Determine Optical Features of Carbon Dots. *ACS Nano* 2019, *13* (9), 10737–10744. https://doi.org/10.1021/acsnano.9b05444.

(21) Lin, Z.; Xue, W.; Chen, H.; Lin, J.-M. Classical Oxidant Induced Chemiluminescence of Fluorescent Carbon Dots. *Chem. Commun.* 2012, *48* (7), 1051–1053. https://doi.org/10.1039/C1CC15290D.

(22) Synder Filtration. *Molecular Weight Cut Off*. Definition of Molecular Weight Cut Off. https://synderfiltration.com/learning-center/articles/membranes/molecular-weight-cut-off/ (accessed 2020-05-09).

(23) Strauss, V.; Wang, H.; Delacroix, S.; Ledendecker, M.; Wessig, P. Carbon Nanodots Revised: The Thermal Citric Acid/Urea Reaction. *Chem. Sci.* 2020, *11* (31), 8256–8266. https://doi.org/10.1039/D0SC01605E.

(24) HORIBA Scientific. A Guide to Recording Fluorescence Quantum Yields. 6.

(25) Liu, C.; Zhang, F.; Hu, J.; Gao, W.; Zhang, M. A Mini Review on PH-Sensitive Photoluminescence in Carbon Nanodots. *Front. Chem.* 2021, *8*.

(26) Gharat, P. M.; Chethodil, J. M.; Srivastava, A. P.; K, P. P.; Pal, H.; Choudhury, S. D. An Insight into the Molecular and Surface State Photoluminescence of Carbon Dots Revealed through Solvent-Induced Modulations in Their Excitation Wavelength Dependent Emission Properties. *Photochem. Photobiol. Sci.* 2019, *18* (1), 110–119. https://doi.org/10.1039/C8PP00373D.

(27) Zhang, J.; Yuan, Y.; Liang, G.; Yu, S.-H. Scale-Up Synthesis of Fragrant Nitrogen-Doped Carbon Dots from Bee Pollens for Bioimaging and Catalysis. *Adv. Sci.* 2015, *2* (4), 1500002. https://doi.org/10.1002/advs.201500002.

(28) Su, H.; Bi, Z.; Ni, Y.; Yan, L. One-Pot Degradation of Cellulose into Carbon Dots and Organic Acids in Its Homogeneous Aqueous Solution. *Green Energy Environ.* 2019, *4* (4), 391–399. https://doi.org/10.1016/j.gee.2019.01.009.

(29) Deka, M. J.; Dutta, P.; Sarma, S.; Medhi, O. K.; Talukdar, N. C.; Chowdhury, D. Carbon Dots Derived from Water Hyacinth and Their Application as a Sensor for Pretilachlor. *Heliyon* 2019, *5* (6), e01985. https://doi.org/10.1016/j.heliyon.2019.e01985.

(30) Sahu, S.; Behera, B.; Maiti, T. K.; Mohapatra, S. Simple One-Step Synthesis of Highly Luminescent Carbon Dots from Orange Juice: Application as Excellent Bio-Imaging Agents. *Chem. Commun.* 2012, *48* (70), 8835–8837. https://doi.org/10.1039/C2CC33796G.

(31) Wang, X.; Qu, K.; Xu, B.; Ren, J.; Qu, X. Microwave Assisted One-Step Green Synthesis of Cell-Permeable Multicolor Photoluminescent Carbon Dots without Surface Passivation Reagents. *J. Mater. Chem.* 2011, *21* (8), 2445–2450. https://doi.org/10.1039/C0JM02963G.

(32) Liu, H.; Zhang, Y.; Huang, C. Development of Nitrogen and Sulfur-Doped Carbon Dots for Cellular Imaging. *J. Pharm. Anal.* 2019, *9* (2), 127–132. https://doi.org/10.1016/j.jpha.2018.10.001.

(33) Wang, Z.-X.; Yu, X.-H.; Li, F.; Kong, F.-Y.; Lv, W.-X.; Fan, D.-H.; Wang, W. Preparation of Boron-Doped Carbon Dots for Fluorometric Determination of Pb(II), Cu(II) and Pyrophosphate Ions. *Microchim. Acta* 2017, *184* (12), 4775–4783. https://doi.org/10.1007/s00604-017-2526-3.

(34) Wang, H.; Gao, P.; Wang, Y.; Guo, J.; Zhang, K.-Q.; Du, D.; Dai, X.; Zou, G. Fluorescently Tuned Nitrogen-Doped Carbon Dots from Carbon Source with Different Content of Carboxyl Groups. *APL Mater.* 2015, *3* (8), 086102. https://doi.org/10.1063/1.4928028.

(35) Bansal, A. K.; Antolini, F.; Zhang, S.; Stroea, L.; Ortolani, L.; Lanzi, M.; Serra, E.; Allard, S.; Scherf, U.; Samuel, I. D. W. Highly Luminescent Colloidal CdS Quantum Dots with Efficient Near-Infrared Electroluminescence in Light-Emitting Diodes. *J. Phys. Chem. C* 2016, *120* (3), 1871–1880. https://doi.org/10.1021/acs.jpcc.5b09109.

(36) Zhang, Q.; Zhang, C.; Li, Z.; Ge, J.; Li, C.; Dong, C.; Shuang, S. Nitrogen-Doped Carbon Dots as Fluorescent Probe for Detection of Curcumin Based on the Inner Filter Effect. *RSC Adv.* 2015, *5* (115), 95054–95060. https://doi.org/10.1039/C5RA18176C.

(37) Krysmann, M. J.; Kelarakis, A.; Dallas, P.; Giannelis, E. P. Formation Mechanism of Carbogenic Nanoparticles with Dual Photoluminescence Emission. *J. Am. Chem. Soc.* 2012, *134* (2), 747–750. https://doi.org/10.1021/ja204661r.

(38) Huang, Y.; Cheng, Z. Simple and Green Synthesis of Boron-, Sulfur-, and Nitrogen-Co-Doped Carbon Dots as Fluorescent Probe for Selective and Sensitive Detection of Sunset Yellow. *Nano* 2017, *12* (10), 1750123. https://doi.org/10.1142/S1793292017501235.

(39) Bourlinos, A. B.; Trivizas, G.; Karakassides, M. A.; Baikousi, M.; Kouloumpis, A.; Gournis, D.; Bakandritsos, A.; Hola, K.; Kozak, O.; Zboril, R.; Papagiannouli, I.; Aloukos, P.; Couris, S. Green and Simple Route toward Boron Doped Carbon Dots with Significantly Enhanced Non-Linear Optical Properties. *Carbon* 2015, *83*, 173–179. https://doi.org/10.1016/j.carbon.2014.11.032.

(40) Yan, Y.; Li, L.; Zhang, H.; Du, F.; Meng, Y.; Shuang, S.; Wang, R.; Song, S.; Dong, C. Carbon Dots for Ratiometric Fluorescence Detection of Morin. *Spectrochim. Acta. A. Mol. Biomol. Spectrosc.* 2021, *256*, 119751. https://doi.org/10.1016/j.saa.2021.119751.

(41) Kamali, S. R.; Chen, C.-N.; Agrawal, D. C.; Wei, T.-H. Sulfur-Doped Carbon Dots Synthesis under Microwave Irradiation as Turn-off Fluorescent Sensor for Cr(III). *J. Anal. Sci. Technol.* 2021, *12* (1), 48. https://doi.org/10.1186/s40543-021-00298-y.

(42) Yue, L.; Li, H.; Sun, Q.; Zhang, J.; Luo, X.; Wu, F.; Zhu, X. Red-Emissive Ruthenium-Containing Carbon Dots for Bioimaging and Photodynamic Cancer Therapy. *ACS Appl. Nano Mater.* 2020, *3* (1), 869–876. https://doi.org/10.1021/acsanm.9b02394.

(43) Khan, W. U.; Wang, D.; Wang, Y. Highly Green Emissive Nitrogen-Doped Carbon Dots with Excellent Thermal Stability for Bioimaging and Solid-State LED. *Inorg. Chem.* 2018, *57* (24), 15229–15239. https://doi.org/10.1021/acs.inorgchem.8b02524.

(44) Song, Y.; Zhu, C.; Song, J.; Li, H.; Du, D.; Lin, Y. Drug-Derived Bright and Color-Tunable N-Doped Carbon Dots for Cell Imaging and Sensitive Detection of Fe3+ in Living Cells. *ACS Appl. Mater. Interfaces* 2017, *9* (8), 7399–7405. https://doi.org/10.1021/acsami.6b13954.

(45) Liu, J.; Li, R.; Yang, B. Carbon Dots: A New Type of Carbon-Based Nanomaterial with Wide Applications. *ACS Cent. Sci.* 2020, *6* (12), 2179–2195. https://doi.org/10.1021/acscentsci.0c01306.

(46) Chao, T.; Dong, X.; Wang, J.; Song, R.; Xie, Z.; Zhou, S. Enhanced Aggregation-Induced Phosphorescence of Carbon Dots for Information Encryption Applications. *ACS Appl. Nano Mater.* 2022. https://doi.org/10.1021/acsanm.2c03785.

(47) Kiran, S.; Misra, R. D. K. Mechanism of Intracellular Detection of Glucose through Nonenzymatic and Boronic Acid Functionalized Carbon Dots. *J. Biomed. Mater. Res. A* 2015, *103* (9), 2888–2897. https://doi.org/10.1002/jbm.a.35421.